PUBLICATIONS OF
THE UNIVERSITY OF EASTERN FINLAND

Dissertations in Health Sciences

OLLI LAHTINEN

NEW ULTRASOUND TECHNIQUES IN THE IMAGING OF THE LYMPHATIC SYSTEM

– CONTRAST-ENHANCED ULTRASOUND AND SHEAR WAVE ELASTOGRAPHY

NEW ULTRASOUND TECHNIQUES IN THE IMAGING OF THE LYMPHATIC SYSTEM

– CONTRAST-ENHANCED ULTRASOUND AND SHEAR WAVE ELASTOGRAPHY

Olli Lahtinen

NEW ULTRASOUND TECHNIQUES IN THE IMAGING OF THE LYMPHATIC SYSTEM

– CONTRAST-ENHANCED ULTRASOUND AND SHEAR WAVE ELASTOGRAPHY

To be presented by permission of the Faculty of Health Sciences, University of Eastern Finland for public examination in MS302 Auditorium, Kuopio on January 19th, 2024, at 12 o'clock noon

Publications of the University of Eastern Finland
Dissertations in Health Sciences
No 800

Department of Clinical Radiology, Institute of Clinical Medicine, School of Medicine, Faculty of Health Sciences,
University of Eastern Finland, Kuopio
2024

Punamusta Oy
Joensuu, 2024
Distributor: University of Eastern Finland
Kuopio Campus Library

ISBN: 978-952-61-5086-4 (nid.)
ISBN: 978-952-61-5087-1 (PDF)
ISSNL: 1798-5706
ISSN: 1798-5706
ISSN: 1798-5714 (PDF)

Author's address: Department of Clinical Radiology
Kuopio University Hospital
University of Eastern Finland
KUOPIO
FINLAND

Doctoral programme: Doctoral programme of Clinical Research

Supervisors: Professor Ritva Vanninen, M.D., Ph.D.
Institute of Clinical Medicine, Radiology
School of Medicine, Faculty of Health Sciences
University of Eastern Finland
KUOPIO
FINLAND

Suvi Rautiainen, M.D., Ph.D.
Department of Clinical Radiology
Kuopio University Hospital
KUOPIO
FINLAND

Reviewers:

Docent Ilkka Martikainen, M.D., Ph.D.
Department of Clinical Radiology
Tampere University Hospital
TAMPERE
FINLAND

Docent Mika Nevalainen, M.D., Ph.D.
Department of Clinical Radiology
Oulu University Hospital
OULU
FINLAND

Opponent:

Professor Jussi Hirvonen, M.D., Ph.D.
Department of Clinical Radiology
University of Tampere
TAMPERE
FINLAND

Lahtinen, Olli
New Ultrasound Techniques in the Imaging of the Lymphatic System
– Contrast-enhanced Ultrasound and Shear Wave Elastography
Kuopio: University of Eastern Finland
Publications of the University of Eastern Finland
Dissertations in Health Sciences 800. 2024, 113 p.
ISBN: 978-952-61-5086-4 (nid.)
ISSNL: 1798-5706
ISSN: 1798-5706
ISBN: 978-952-61-5087-1 (PDF)
ISSN: 1798-5714 (PDF)

ABSTRACT

Although lymphatic system and its importance has been genereally understood and recognized for a long time, it has been somewhat neglected from the imaging perspective. Lymphatic disorders and in particular, secondary lymphedema accompanying modern cancer treatments afflicts a vast number of patients and may significantly decrease quality of life. Traditional imaging of the lymphatic vessels has involved lymphography and lymphoscintigraphy; ultrasound (US) has also been used to evaluate potential malignant features of the lymph nodes (LNs) as well as in biopsy guidance. In more recent years new lymphatic imaging techniques have been introduced, such as magnetic resonance lymphangiography and indocyanine imaging. However, each of the techniques used for more accurate assessment of the lymphatic system are either time-consuming, resource intensive or are rather expensive. Thus, there is a clear need for cost-effective and widely available imaging modality and techniques for assessing the lymphatic system.

The aim of this thesis was to study new US techniques in the assessment of the lymphatic system. More precisely, the aim of study I) was to assess the feasibility of contrast-enhanced ultrasound (CEUS) as a sentinel lymph node (SLN) procedure in patients with newly diagnosed

vulvar cancer (n = 12) compared to traditional lymphoscintigraphy; study II) was designed to evaluate the reproducibility and to define the optimal orientation and region of interest (ROI) for shear wave measurements of 2D-Shear wave elastography (2D-SWE) in inguinal LNs (n = 32), while study III) investigated the suitability of CEUS for visualizing superficial lymphatic vessels in the upper limbs of healthy volunteers (n = 30). All studies were carried out at the Kuopio University Hospital between the years 2016 to 2021.

Study I showed that CEUS had a high technical success rate of 94.7 % for identifying potential enhancing SLN. The technique showed an overall sensitivity of 81.2 % compared to the conventional lymphoscintigraphy and/or methylene blue dye. Moreover, CEUS detected potential SLN in two cases where conventional methods failed to do so. The procedure correctly identified all the metastatic SLNs. Thus, US-based contrast-enhanced SLN procedure can be applied identifying SLNs in patients with vulvar cancer.

Study II revealed that the most effective way of obtaining reproducible results when using SWE in inguinal LNs is to place a 3 mm circular ROI on the cortex of the LN in the axial plane. Elastography offers an additional non-invasive tool in addition to conventional US in assessment of superficial inguinal LNs.

The third study demonstrated that CEUS with intradermal injection had a high success rate (98.3 %) and is a viable, minimally invasive method for visualizing superficial lymphatic vessels in the upper limbs of healthy volunteers. The technique proved to be fast, with a median enhancement time of 75 s for the contrast agent to reach axilla from the distal antebrachium. Further studies are needed to evaluate the method in patients with lymphatic dysfunction such as secondary lymphedema.

In conclusion, new US techniques provide added value in imaging of the lymphatic system, particularly in the assessment of superficial LNs and superficial lymphatic vessels.

Keywords: contrast-enhanced ultrasound; lymphatic imaging; sentinel lymph node; ultrasound elastography; vulvar cancer;

Lahtinen, Olli
Uudet ultraäänitekniikat lymfaattisen järjestelmän kuvantamisessa – varjoainetehosteinen ultraääni ja shear wave elastografia
Kuopio: Itä-Suomen yliopisto
Publications of the University of Eastern Finland
Dissertations in Health Sciences 800. 2024, 113 p.
ISBN: 978-952-61-5086-4 (nid.)
ISSNL: 1798-5706
ISSN: 1798-5706
ISBN: 978-952-61-5087-1 (PDF)
ISSN: 1798-5714 (PDF)

TIIVISTELMÄ

Lymfaattisen järjestelmän yleinen tehtävä ja rooli on ollut tiedossa jo pitkään, mutta siitä huolimatta tieteellinen kiinnostus tätä kohtaan on ollut varsin vähäistä kuvantamisen näkökulmasta. Lymfaattiset ongelmat ja varsinkin sekundäärinen lymfaturvotus johtuen moderneista syöpähoidoista rasittavat suurta joukkoa potilaita laskien heidän elämänlaatuaan. Perinteisesti imusuonten kuvantaminen on tapahtunut joko lymfografialla tai lymfoscintigrafialla. Lisäksi ultraääntä (UÄ) on käytetty arvioitaessa niin imusolmukkeiden mahdollista pahanlaatuisuutta kuin myös auttamaan imusolmukkeiden kuvantamisohjatussa näytteenotossa. Viime vuosien varrella uusia kuvantamistekniikoita on ilmaantunut lymfaattisen järjestelmän kuvantamiseen kuten magneettikuvantaminen ja indocyaniinivihreä-merkkiaine. Uusista menetelmistä huolimatta käytössä olevat tekniikat lymfaattisen järjestelmän tarkempaan arvioon kuvantaen ovat joko aikaa vieviä, runsaasti resurssia sitovia tai varsin kalliita. Täten on tarve edulliselle ja helposti saatavissa olevalle kuvantamismenetelmälle lymfaattisen järjestelmän kuvantamisessa.

Tämän väitöskirjatutkimuksen tarkoitus oli tutkia uusia UÄ-menetelmiä lymfaattisen järjestelmän arviossa. Tarkemmin ottaen, tarkoituksena oli

tutkimuksessa I) arvioida varjoainetehosteisen UÄ:n käyttökelpoisuutta vartijaimusolmuketutkimuksena ulkosynnytinsyöpäpotilailla (n = 12) verrattuna perinteiseen vartijaimusolmuketutkimukseen, tutkimuksessa II) tutkia 2D-shear wave elastografian (SWE) toistettavuutta nivusten imusolmukkeissa (n = 32) ja määrittää paras mahdollinen kimmoisuusmittausalueen koko, ja Tutkimuksessa III) arvioida varjoainetehosteisen UÄ:n käyttökelpoisuutta kuvannettaessa yläraajojen pinnallisia imuteitä terveiltä vapaaehtoisilta (n = 30). Tutkimukset toteutettiin Kuopion yliopistollisessa sairaalassa vuosina 2016–2021.

Tutkimus I osoitti, että varjoainetehosteisella UÄ:llä oli korkea tekninen onnistumisaste (94.7 %) löytää mahdollinen tehostuva vartijaimusolmuke. Verrattuna perinteisiin lymfoscintigrafiaan sekä metyleenisineen herkkyys oli 81.2 %. Varjoainetehosteisessa UÄ:ssä löytyi tehostuva vartijaimusolmuke kahdessa tapauksessa, joissa perinteisissä menetelmissä vartijaimusolmuke ei kuvautunut. Menetelmä onnistui löytämään kaikki metastaattiset vartijaimusolmukkeet. Täten varjoainetehosteista UÄ:tä voidaan käyttää löytämään vartijaimusolmukkeet ulkosynnytinsyöpäpotilailla.

Tutkimuksessa II nähtiin, että toistettavin tapa tehdä SWE nivusimusolmukkeisiin on käyttää 3 mm kokoista, ympyrän mallista mittausaluetta asetettuna imusolmukkeen kuorikerrokseen potilaaseen nähden poikittaisessa tasossa. Kimmoisuusmittaus tarjoaa uuden kajoamattoman menetelmän perinteisten UÄ:n rinnalle arvioitaessa imusolmukkeiden tilaa.

Kolmas tutkimus osoitti, että varjoainetehosteinen UÄ-tutkimus ihon pintakerrokseen pistetyllä varjoaineella saavutti korkean onnistumisasteen (98.3 %) ja on käyttökelpoinen sekä minimaalisesti kajoava menetelmä pinnallisten imusuonten kuvantamiseen yläraajoissa terveillä vapaaehtoisilla. Lisäksi menetelmä osoittautui nopeaksi ja keskimääräinen varjoaineen kulkeutumisaika kyynärvarren distaaliosasta kainaloon oli 75 sekuntia. Jatkotutkimuksia tarvitaan arvioimaan menetelmän käyttökelpoisuutta imuteiden poikkeavuuksissa kuten lymfaturvotuksesta kärsivillä potilailla.

Yhteenvetona voidaan todeta, että uudet UÄ-tekniikat tarjoavat lisäarvoa arvioitaessa pinnallisia imusolmukkeita sekä imuteitä lymfaattisen järjestelmän kuvantamisessa.

Avainsanat: imuteiden kuvantaminen; ulkosynnytinsyöpä; ultraääni elastografia; vartijaimusolmuke; varjoainetehosteinen ultraääni;

ACKNOWLEDGEMENTS

This thesis is based on investigations carried out in the Department of Clinical Radiology of Kuopio University Hospital during the years 2016 – 2021. I wish to express my thanks to all people in our department as well as all the patients who participated and made this study possible. Especially, I want to thank those 30 brave souls who were willing to sacrifice themselves at the altar of science as lab rats and made the third study possible.

I express my deepest gratitude to Professor Ritva Vanninen, MD, PhD, who also served as my principal supervisor, for giving me the possibility of undertaking this study and pushing me forwards during the whole journey. Her skillful guidance in scientific writing and thinking as well as encouraging support helped me throughout development of this thesis from initial scratches and jottings to a more orderly and substantial end result.

I also want to express my deep gratitude to my second supervisor Suvi Rautiainen, MD, PhD, who was always willing help me even through the darkest hours of the thesis writing and for having the energy to constantly try to improve my work. Her knowledge related to axillary sentinel studies laid the foundation for my research.

I owe my special thanks to my father Docent Tapani Lahtinen, PhD, to whom I could always turn to at any time when I needed help with my thesis and who at times seemed to have even greater enthusiasm for lymphatic imaging than I did. His vast knowledge on skin anatomy and lymphatic vessels provided me with new insights and understanding about many aspects of this field.

I wish to express my gratitude to Docent Maarit Anttila, MD, PhD, and Henna Kärkkäinen, MD, PhD as well as Marja-Liisa Eloranta, MD, for their collaboration and for making the vulvar cancer study possible. I also want to thank Docent Reijo Sironen, MD, PhD, for providing his expertise in the field of pathology involving the studies and also Mika Pulkkinen, MD, for participating in the elastography study.

I wish to thank our present head of Clinical Radiology department Docent Mikko Taina, MD, PhD, and current Professor Juhana Hakumäki, MD, PhD, for making facilities and resources available as well as the support I have been given.

This thesis was financially supported by a State Research Funding grant to prof. Ritva Vanninen and open access funding provided by grants from Wiljasalo Foundation, Cancer Association of Northern Savo, Kuopio University Hospital Research Foundation, Paavo Koistinen Foundation and the Finnish Radiology Association.

I am also grateful to the official reviewers of this thesis, Ilkka Martikainen and Mika Nevalainen for valuable comments and insights concerning the manuscript.

I wish to thank Tuomas Selander, Biostatistician, MSc, without whom I would still be struggling to apply the more complex statistical analyses, to Helena Schmidt for the illustrations in this manuscript and to Peter Sorjonen-Ward for the linguistic check.

Finally, the warmest thanks go to my loving wife Tanja Lahtinen for keeping up with me all these years for better or worse, now and always.

Kuopio, December 2023
Olli Lahtinen

LIST OF ORIGINAL PUBLICATIONS

This dissertation is based on the following original publications:

I Lahtinen O, Eloranta M, Anttila M, Kärkkäinen H, Sironen R, Vanninen R, Rautiainen S. Preoperative sentinel lymph node localization in vulvar cancer: preliminary experience with inguinal intradermal contrast-enhanced ultrasound. Eur Radiol. 2018 May;28(5): 2089-295.

II Lahtinen O, Pulkkinen M, Sironen R, Vanninen R, Rautiainen S. 2D-shear wave elastography in the evaluation of suspicious superficial inguinal lymph nodes: Reproducibility and region of interest selection. PLoS One. 2022 Mar 28;17(3):e0265802.

III Lahtinen O, Vanninen R, Rautiainen S. Contrast-enhanced ultrasound: a new tool for imaging the superficial lymphatic vessels of the upper limb. Eur Radiol Exp. 2022 Apr 12;6(1):18.

CONTENTS

ABBREVIATIONS

AUC	area under curve
ARFI	acoustic radiation force impulse
BMI	body mass Index
CA	contrast agent
CE	contrast-enhanced
CEUS	contrast-enhanced ultrasound
CNB	core needle biopsy
CTR	contrast to tissue ratio
CT	computed tomography
E	elasticity
EFSUMB	European Federation of Societies for Ultrasound in Medicine and Biology
ESGO	European Society of Gynecological Oncology
ICC	intraclass correlation coefficient
ICG	indocyanine green
IFL	inguinofemoral lymphadenectomy
LN, LNs	lymph node, lymph nodes
LND	lymph node dissection
MRI	magnetic resonance imaging
MRL	magnetic resonance lymphangiography
NIR	near-infrared
pSWE	point shear wave elastography
ROC	receiver operating characteristic
ROI	region of interest
SE	strain elastography
SLN	sentinel lymph node
SLNB	sentinel lymph node biopsy
SWE	shear wave elastography
US	ultrasound
SPECT	single positron emission computed tomography
USCA	ultrasound contrast agent
2D-SWE	2D-shear wave elastography

1 INTRODUCTION

The lymphatic system is rather poorly understood despite its important role and function in human physiology. While primary lymphatic disorders are somewhat rare, the enlarged lymph nodes (LN) are commonly encountered problem and there is a consequent need for accurate assessment and diagnosis. LN-status is an important parameter in cancer prognosis and is an essential part of cancer staging, affecting the choice of treatment options. Sentinel lymph node (SLN) procedures have been shown to be feasible in breast cancer treatment (1), while the trend towards less invasive treatments has also been investigated in other cancers, including vulvar cancer (2), in attempting to reduce the high complication rates of more radical surgeries.

Lymphatic dysfunction, particularly in the western world is associated with acquired damage or obstruction to the lymphatic system by various means such as cancer treatments, infections, systemic diseases, surgery or trauma. Impairment of the lymphatic system can lead to lymphedema and decreased quality of life (3,4). Secondary lymphedema in upper extremities is typically related to breast cancer treatments while in the lower limbs, it is commonly a consequence of treatment for gynecological cancers, melanoma, lymphoma and urologic cancers (4–7).

Amongst lymphatic imaging techniques, ultrasound (US) has served as a first line modality assessing superficial LN areas in cases of abnormal lumps, lymphadenopathy or suspected lymphoma. However, due to the development of innovative US techniques such as shear wave elastography (SWE) and contrast-enhanced ultrasound (CEUS), US is being increasingly applied to lymph node (LN) assessment (8) and in SLN studies with promising results (9–11).

Lymphatic imaging has in the past tended to focus on conventional lymphography and lymphoscintigraphy. However, during the 21st century these techniques have been superseded by other imaging modalities and innovations. Cross sectional imaging and in particular, magnetic resonance imaging (MRI) have both demonstrated their capability in lymphatic imaging. Additionally, indocyanine green (ICG)-imaging has emerged as a non-traditional radiological method for lymphatic imaging (12–14). Nevertheless, these methods are either time consuming, expensive or require substantial human resources. Thus, the field of radiology still lacks routine and efficient methods to evaluate the vast number of patients with problems in their lymphatic system.

This thesis is focused on new US techniques for imaging the lymphatic system and assessing LNs and superficial lymphatic vessels. More specifically, the study aimed to compare US SLN procedure in inguinal LNs with lymphoscintigraphy in patients with vulvar cancer, to investigate the reproducibility of SWE in inguinal LNs and to assess the feasibility of CEUS in visualizing superficial lymphatics vessels in the upper extremities in healthy volunteers.

2 REVIEW OF THE LITERATURE

2.1 IMMUNE SYSTEM

The human immune system is twofold in nature; 1) the innate immune response acts as an immediate defense system with a short-term memory, whereas 2) the adaptive immune system creates long term defense after identifying unknown antigens. The function of the immune system is to limit or prevent the effect of an infectious agent via immune response (15,16). Precursors of the immune cells are produced in the bone marrow and can undergo a series of changes before maturing. The lymphatic system as a part of the immune system is responsible for regulating the immune response by transportation of bacteria, foreign matter, antigens and immune cells to regional LNs and other lymphoid structures as well as in the production and release of the immune cells that identify and destroy foreign invaders.

2.2 LYMPHATIC SYSTEM

2.2.1 Finding the lymphatic system

The lymphatic system is still rather poorly understood despite its important role in maintaining homeostasis as well as its role in human health and diseases. Unlike the vascular system, which has been recognized and studied since ancient times, knowledge of the lymphatic system remained obscure and inaccurate for centuries. The first written references to lymphatic vessels date back to 4th century when Greeks found structures in the human body with a colorless fluid. However, it was only in the early 17th century, in 1622 that Gasparo Aselli in Italy observed “lacteal vessels” in the abdomen of a dog. Several decades later, the lymph flow from liver to thoracic duct was observed and the vast network of lymphatic vessels throughout the body was discovered. From the perspective of imaging the

lymphatic system, mercury was the first substance to be used by Nuck in 1692, followed by further experimentation with mercury by Mascagni and Sappey. The term “vasae lymphaticae”, as a precursor to the current form of “lymphatic vessels” was introduced by Thomas Bartholini in 1653. The fluid absorption function of the lymphatic system was demonstrated in 1746 and the question of lymph fluid formation was further elaborated upon in the mid-19th century by Carl Ludwig and later by Ernest Sterling. Subsequently, during the early 20th century, Drinker introduced the concept of maintaining fluid balance by returning proteins and fluids lost from blood vessels back into circulation (17–19).

2.2.2 Function and physiology of the lymphatic system

The lymphatic system serves the fundamental physiological purpose of maintaining normal fluid balance in tissues. On a daily basis, around 8 L of fluid escape from capillaries and becomes afferent lymph. Some of the water in the lymph is reabsorbed in the LNs and approximately 4 L of efferent lymph flows through the lymphatic channels per day (20). Lymph circulates through the lymphatic system along with 50 % of the protein circulating in the vascular system. The lymph fluid that escapes from the vessels is not reabsorbed by capillaries. Instead, approximately half of the lymph re-enters the circulatory system via great veins and the other half at LNs. In addition to maintaining the fluid balance, the intestinal lymphatic system has an important role in absorption and transportation of lipids in the digestive system (17–19,21). The vast network of lymphatic vessels is also responsible for quick antigen identification and presentation to LNs. For a long time Frank-Starling’s law was considered to be unwavering in governing fluid transfer between spaces. However, recent data have shown that capillaries are not in a sustained equilibrium fluid absorption state and that the lymphatic system has a more active role in clearing the excess fluid from the interstitial spaces (22).

Lymph fluid is formed by ultrafiltration during capillary microcirculation. As a result, fluids, small molecules and proteins migrate from microvessels

into the interstitium. The lymph consists of tissue metabolism products, apoptotic cells, cellular debris and circulating immune cells (23,24). Immune cells from both the innate (dendritic cells, neutrophils and monocytes) and adaptive immune systems (leukocytes such as B and T cells) migrate from tissues to LNs via lymphatic vessels. Additionally, leukocytes can enter the LNs from the bloodstream (15,16,25).

Lymphatic fluid contains high amounts of protein, although depending on the composition of the lymphatic fluid it can be classified into three categories: liver, intestinal and soft tissue lymphatic fluid. Protein concentration is highest in the liver lymph and lowest in the soft tissue lymph. Additionally, the concentration of triglycerides varies, being highest in the intestinal lymph. The composition of the lymph can therefore be useful in determining the origin of the lymph (26,27).

Movement of the lymph in the vessels is dictated by the forces responsible for the initial formation of lymphatic fluid, intrinsic pump mechanisms and the external pressure of the tissues. Additionally, unlike blood circulation, the lymph fluid does not actually circulate but rather a filtrate is delivered through the lymphatic system back into circulation.

2.2.3 Anatomy of the lymphatic vessel network

The lymphatic system is a complex network of small vessels found in almost every tissue (Figure 1.). Its structure depends on the location and the density of the lymphatic vessels, which does not always follow the vascular anatomy. Recent discoveries have revealed evidence that lymphatic structures are present in tissues normally thought to lack lymphatic vessels, including the central nervous system, bone marrow, cartilage and the cornea (19). The term ‘glymphatic system’ has been introduced in recent studies where cerebrospinal fluid (CSF) and interstitial fluid in the central nervous system exhibit continuous interchange through a complex series of mechanisms including arterial pulsatility, pressure gradients of the CSF, loose fibrous matrix of the perivascular spaces and specific water channels. Eventually the cerebral interstitial fluid is driven

into the perivenous space and drains out from the brain before entering the cervical lymphatic system (28,29). The lymphatic network can be found in the superficial parts of the entire body but also around internal surfaces of the gastrointestinal and respiratory tract. As a rough generalization, the lymphatic collectors from the intestinale tract, lower lumbar region and other peripheral lymphatic vessels in most regions of the body drain into the thoracic duct. This contrasts with, the upper right thorax, right upper limb, right side of the head and neck region, which drain into the right lymphatic duct. The thoracic duct and right lymphatic duct drain into their subclavian vein counterparts.

The structure of the lymphatic vessels varies depending on their location. Three categories can be identified, each being referred to by different names in the literature: lymphatic capillaries or initial lymphatics, precollectors or intermediary lymphatic vessels and lymph-collecting vessels or afferent lymphatic vessels.

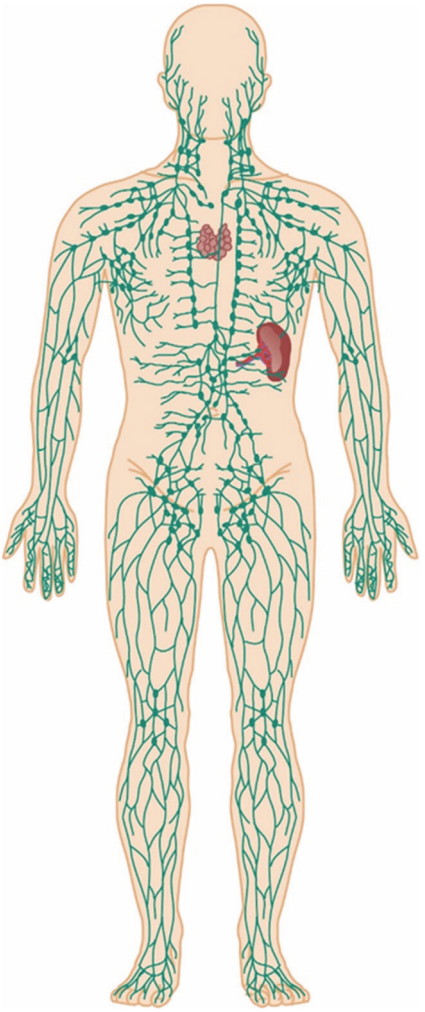

Figure 1. A graphic illustration of the extensive network of lymphatic vessels

2.2.4 Lymphatic vessels

Lymphatic capillaries are the smallest of the lymphatic vessels (20 – 70 μm in diameter), facilitating microcirculation and covering a large surface area. They often have blind terminations but can also form interconnected networks. The initial lymphatic fluid is formed in these most distal lymphatic capillaries. The single endothelial cell layer that forms the

capillaries is loosely connected and an anchoring fibrous filament connects the cells to the surrounding tissues. In the event of excess interstitial fluid accumulation, the endothelial cells are pulled outwards, opening the gaps between the cells, enabling collection of extra fluid by capillaries. Unlike larger lymph collecting vessels, lymphatic capillaries do not possess valvular structures (17–19,21,30).

Lymphatic capillaries drain into **precollectors** (ranging from 70 – 150 μm in diameter) which have one-way bicuspid valves that only permit lymphatic flow towards larger collectors. Due to the lack of a smooth muscle cell layer, the lymphatic flow in the precollectors is mostly dependent on pressure differences between individual tissue segments.

Precollectors connect and transform into larger collecting vessels, known respectively as **lymph collecting vessels** or **afferent lymphatic vessels** (150 – 500 μm in diameter). Depending on their relationship with deep fascial structures they are divided into superficial and deep vessels. In addition to the valvular structure of the precollectors, the wall of the lymph collecting vessels comprises a layer of smooth muscle cells and another layer of collagen fibers with fibroblasts. These layers allow the wall structure to contract periodically, propelling the lymphatic flow. Collecting lymphatic vessels are more organized than their smaller counterparts. Multiple afferent lymphatic vessels can lead into a single LN whereas usually, only a single efferent collecting lymphatic vessel exits from the LN.

The lymphatic system of the skin behaves according to roughly the same principles. As with the microvasculature of the skin, the lymphatic system also comprises two layers. The superficial layer with lymphatic capillaries is located immediately beneath the epidermis and drains via vertical precollectors into larger collecting vessels in the lower dermis and to some extent, into the superficial portion of the subcutaneous tissue (Figure 2.). The second layer of collectors is situated beneath the deep fascia, along with arteries and veins. Unlike the vascular system, vessels of the lymphatic system have fewer interconnections and despite the existence of perforating vessels they do not form bridges between the superficial and deep vessels (17–19,21,30).

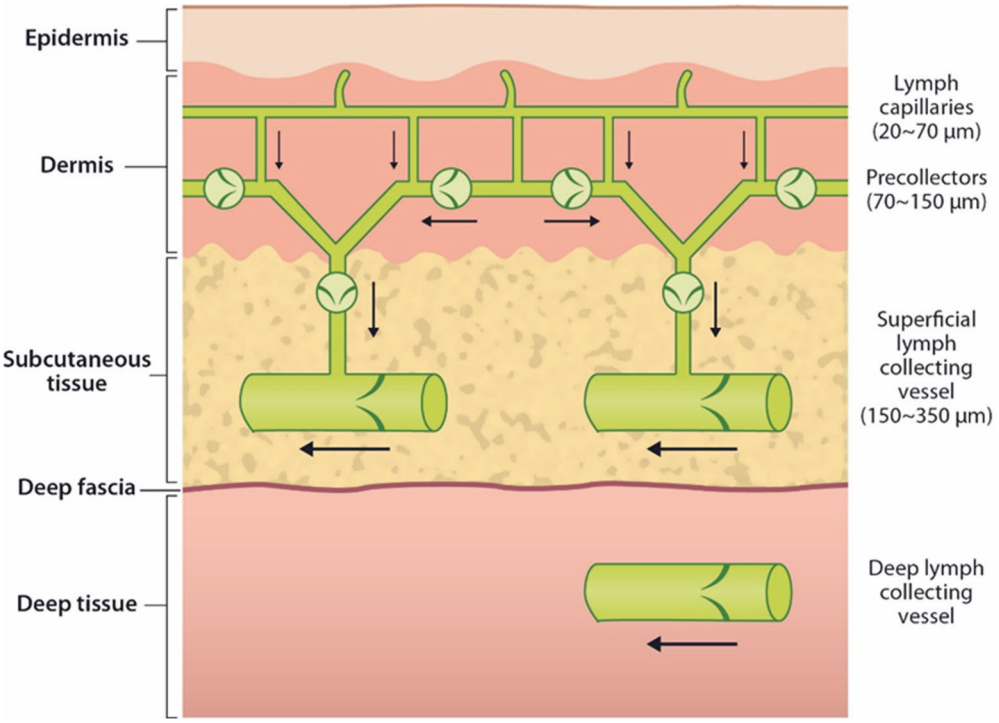

Figure 2. Layers of the lymphatic vessels in skin, according to Suami et al. (30).

2.2.5 Lymph nodes

The human body has approximately 800 LNs located at the near vicinity of large vascular vessels. Although some variation exists between individuals in the exact location of the LNs, they are generally located in axilla, groin, neck and in abdominal and thoracic regions (31). The lymphatic fluid travels through the LNs which serve as checkpoints for antigen detection and initiation response from the adaptive immune system (3).

LNs have three anatomically distinguishable areas: cortex, paracortex and medulla, each of which have different functions. LNs contain one or more lymphoid lobules depending on the size of the LN. The lymphoid lobule represents the functional unit of the LN. Lymphoid lobules are located side by side and are triangular in shape, with a narrower base and

wider apex. Subcapsular sinuses separate the lobules from the capsule and they are also surrounded by lymphatic sinuses. The lymph flows to the LNs via afferent lymphatic vessels, each of which provide lymph flow to the subcapsular sinuses within each lobule. The lymph travels towards the hilar area and medullary sinuses via transverse sinuses from the sides of the lymphoid lobules. All of the lymph flowing through the LN drains into a single efferent lymphatic vessel exiting from the hilus (32) (Figure 3.).

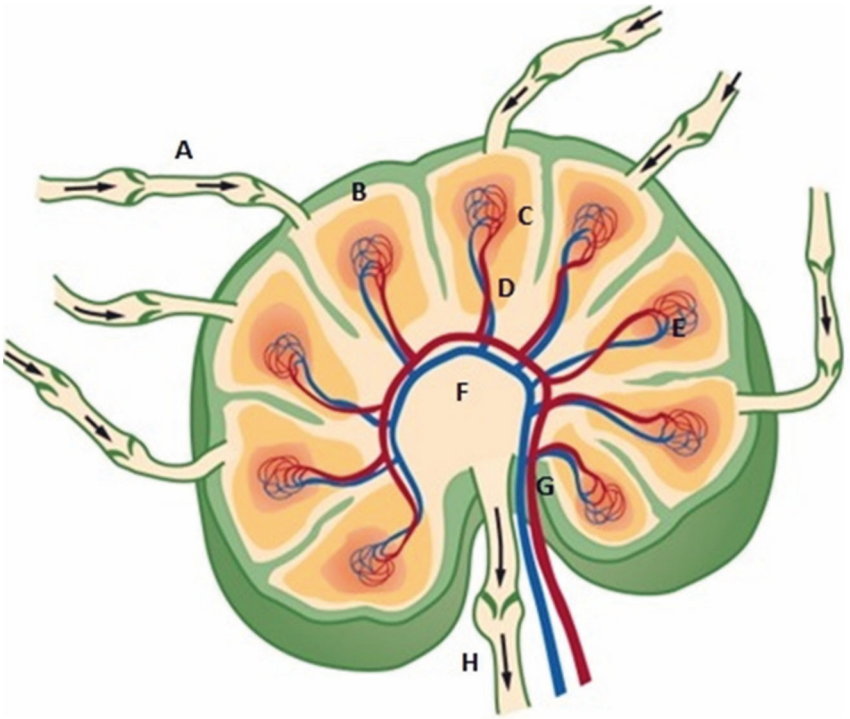

Figure 3. Schematic anatomy of a lymph node. The figure shows the anatomy of the lymph node; A = afferent lymphatic vessel, B = cortex, C = lymphoid follicles, D = paracortex, E = germinal center, F = medulla, G = artery & vein, H = efferent lymphatic vessel

Recent cadaver studies have identified a new feature of the lymphatic anatomy, namely the lymphosome. By using a microinjection technique with hydrogen peroxide and a radiocontrast medium and by observing the

course of the superficial lymphatic vessels the superficial lymphatics of the skin have been divided into domains known as lymphosomes (Figure 4). These areas are responsible for lymphatic drainage into corresponding LNs (30,33). This concept has been applied by using indocyanine green (ICG) in classifying lymphatic vessels in the lymphosomes in patients with lower limb lymphedema (34). Additionally, multilymphosome injections have been studied in lower limb lymphedema to investigate potential candidates and sites for lymphatico-venous anastomosis procedures (35).

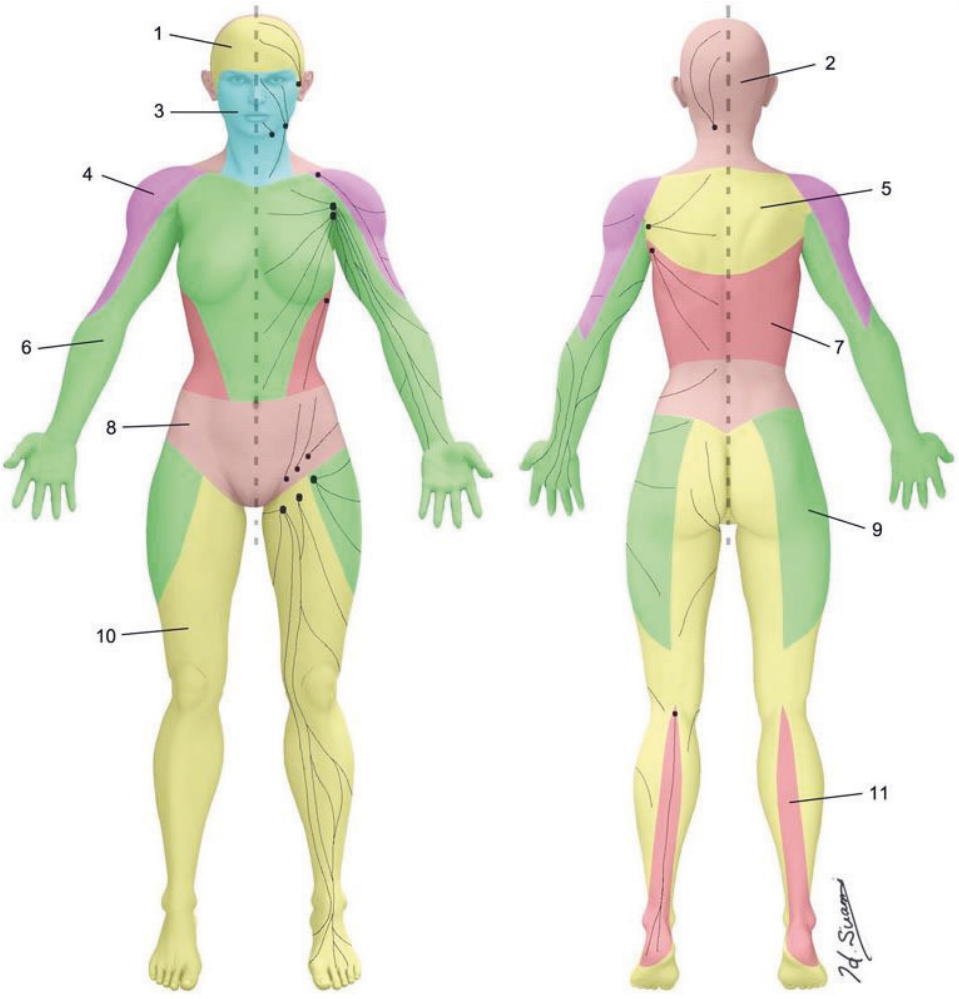

Figure 4. Illustration of the lymphomes, their territories and corresponding lymph nodes (30), reproduced with permission of Hiroo Suami, 2023.

2.2.6 Lymphatic disorders

Various causes can lead to abnormal function in the lymphatic system. Causes include congenital forms such as lymphatic malformations or inherited gene mutations. However, dysfunction is far more commonly associated with acquired damage or obstruction to the lymphatic system by trauma, vascular disorders, infection, systemic diseases, cancer or alternatively, is iatrogenic in nature as a result of surgery or treatments. These factors can result in impaired lymphatic drainage and may eventually lead to lymphedema and lowered quality of life (3,4). Lymphatic disorders are a relatively rare group of entities, with the most common lymphatic disorders being presented in Table 1.

Table 1. The most common lymphatic disorders

Lymphedema	Localized swelling of the tissue due to accumulation of the lymph fluid
Lymphatic filariasis	Tropical parasitic round worm infection that can lead to elephantiasis
Lymphangioleiomyomatosis	The disorder is characterized by excess growth of smooth muscle cells in the lymphatic system, lungs and kidneys
Lymphangiomatosis	Abnormal diffuse proliferation of the lymphatic vascular structures mainly involving skin, soft tissue and bone parenchyma
Lymphangioma	Localized version of lymphangiomatosis
Intestinal lymphangiectasia	Condition characterized by lymph leakage to small bowel leading to protein-losing enteropathy due to dilated intestinal lacteals.
Lymphatic cancers	Hodgkin's and Non-Hodgkin's lymphoma are cancers which develop in the lymphatic system affecting the lymphocytes

Lymphangitis	Inflammation of the lymphatic vessels
Lymphadenitis	Inflammation of the LNs in a specific region
Lymphadenopathy	Abnormal growth of LNs in size or consistency by various etiologies
Castleman's disease	The disease causes overgrowth in lymphoid tissue in the LNs. Two forms exist localized and multicentric

2.2.7 Lymphedema

It has been estimated that 200 million people worldwide suffer from lymphedema. Primary lymphedema is a rare entity usually manifesting at a young age and affecting approximately 1/100 000 people. Thus, secondary lymphedema is responsible for the vast majority of the incidence (4).

Diagnosis of primary lymphedema may be difficult and remain undiscovered. Primary forms result from gene mutations and lead to malformations or malfunctions in the lymphatic vessels. Primary lymphedema occurs twice as frequently in females than in males and more commonly affects lower extremities. Additionally, the symptoms can vary from mild to severe, which may manifest as segmental manifestation only, or as a more generalized form. Several genes behind the different forms of primary lymphedema have been discovered. However, the underlying genetic abnormality remains unknown for 70 % of patients (4,36).

While primary lymphedema results from gene mutations, secondary lymphedema is acquired through secondary means caused by internal or external disruption to the normal lymphatic system. Worldwide, the most common cause is an infection by a roundworm, Wuchereria bancrofti causing lymphatic filariasis (formerly known as elephantiasis) if left untreated (4,5,37). Filariasis is mainly encountered in sub-Saharan Africa and India. However, in the western world leading causes for lymphedema are surgeries, radiation therapy or oncological treatments. Other causes include infections, obesity and trauma. Additionally, fluid overload from

venous dysfunction and ulcers may lead to secondary lymphedema in 20 % of patients (4).

Secondary lymphedema in upper extremities is typically related to breast cancer treatments while in the lower limbs to the treatments of gynecological cancers, melanoma, lymphoma and urologic cancers (4–7). Development of secondary lymphedema varies and the first symptoms may occur as early as one month post-surgery, although in some cases symptoms may first appear years after treatment (38). However, approximately 90 % of lymphedema related to breast cancer has been estimated as becoming manifest within the first two years following the surgery (20). Axillary dissection related to breast cancer surgery is the most common nominator for upper limb lymphedema, typically affecting only the ipsilateral arm. It has been estimated in the meta-analysis that 21,4 % of breast cancer patients undergoing axillary lymph node dissection (ALND) may be affected by chronic lymphedema (39). Patients undergoing ALND compared to more conservative surgery and sentinel lymph node biopsy (SLNB) suffer more commonly from secondary lymphedema (13.5 % - 28.2 % vs. 6.1 – 7.9 %) (40) and a trend has identified between less invasive surgery and SLNB (41). Lymphedema may cause functional impairment of the affected swollen limbs as well as psychosocial pressure and diminished quality of life. The high incidence of secondary lymphedema also causes a significant economic burden on society. Recent reviews based mostly on American studies have concluded that the indirect costs range between 3325 – 5545 $ per year per patient (42). In Europe, the total cost has been shown to be 5784 € per patient per year (43).

2.3 IMAGING OF THE LYMPHATIC SYSTEM

Traditionally the golden standard for evaluating and diagnosing lymphatic disorders has been conventional lymphography. However, during the 21st century other imaging modalities and innovations have taken its place. Ultrasound (US) has retained its role in LN assessment and new US techniques have evolved to increase the sensitivity of US to detect

malignant features in LNs. Cross-sectional imaging and particularly magnetic resonance imaging (MRI) have demonstrated their capability in lymphatic imaging. Additionally, ICG-imaging is one of the newly developed techniques for lymphatic imaging, differing from more traditional radiological methods.

2.3.1 Lymphography

Lymphography has been used for many decades in radiology and the technical aspects of the procedure have remained essentially unchanged. The first step of the procedure is to inject a small amount (2 mL) of methylene blue dye (Patent Blue V dye; Guerbet Laboratories Aulnay-sous-Bois, France) into the dermis between the toes on the dorsal aspect of the foot, in order to localize the lymph vessels. The dye is taken up by the initial lymphatic vessels, coloring them blue. After the identification of the lymphatic vessels, the vessel is exposed and carefully cannulated. The patient remains in the supine position during the procedure (44). The second step is to inject non-water soluble contrast media, Ethiodol (Savage Laboratories, Melville, NY) or Lipiodol (Guerbet Laboratories) into the cannulated lymph vessels. Typically, 6 mL of contrast media is injected into each extremity. The contrast media accumulating in the LNs can often be seen for several months. Images are taken just after the injection and again 24 hours later for checking the LN status (44).

Another more recent technique for performing lymphography is the intranodal approach. Suitable inguinal LN is identified with US and a direct puncture is performed with a small (22-gauge) needle followed by slow injection of a proper contrast agent (CA) into the LN. Fluoroscopy is used to identify the efferent lymphatic vessel. This technique is used in interventional radiology to detect and repair traumatic or iatrogenic chylous leakages such as chylothorax and chylous ascites (45,46).

Kuopio University Hospital has an extensive history in lymphatic research with lymphography applied in the late 20th century by docent Sirkka Wiljasalo and Professor Mauri Wiljasalo to such topics such as

predicting malignant LNs from lymphography and research into Hodgkin's disease as well as on lymphographic studies in urological oncology by Professor Seppo Soimakallio (47–50).

2.3.2 Lymphoscintigraphy

Another older conventional lymphatic imaging method is lymphoscintigraphy, which was introduced in 1963 (51). The procedure uses ^{99m}Tc-labelled albumin solution as the radiotracer injected subdermally. As in other lymphatic imaging methods, the radiotracer is taken up by the lymphatic capillaries and travels via the larger lymphatic vessels to LNs. A gamma camera is used to detect the gamma rays emitted by the radiotracer. The procedure can offer information about many indications such as lymphedema, lymphatic dysplasia and chylous leaks (52). Even though lymphoscintigraphy enables the visualization of lymphatic flow, it has a low spatial resolution, and cannot provide detailed anatomical information. To overcome this challenge, fusion of cross sectional imaging with single positron emission computed tomography/computed tomography (SPECT/CT) has been used in the detection of SLNs (53,54). Lymphoscintigraphy has consolidated its role as a component of SLNB procedures in various cancers (55–57).

2.3.3 Computed tomography and positron emission tomography

The role of computed tomography (CT) and positron emission tomography in imaging of the lymphatic system has traditionally been to assess potential LN metastasis in various cancers, to diagnose and monitor lymphoma, to estimate the overall burden of the cancers and to provide guidance in CT-guided biopsies.

A few recent studies have investigated a novel CT-based lymphatic imaging technique to assess the central lymphatic system in the thoracic area as an alternative to MRI in animal models and in a small series with human patients. In this technique the needles are placed bilaterally into

inguinal LNs in US guidance and iodine CA is administered intranodally. CT fluoroscopy is performed intermittently 5 minutes after the CA injection at the level of upper abdomen. If the CA is detected in fluoroscopy, chest CT is performed 1 – 2 minutes later (58,59). A similar technique has been previously used successfully in lymphangiography and MRI (60).

2.3.4 Magnetic resonance imaging

MRI can also be used for the same purposes as CT. However, due to capacity, costs and the vast amount of imaging needed, MRI is reserved for selected circumstances. MRI provides far better soft tissue contrast and functional imaging in the form of diffusion weighted imaging (DWI) compared to CT.

Structural MRI features including DWI have shown promise in predicting axillary LN metastasis in patients with breast cancer (61). Additionally, a recent meta-analysis on radiomics features produced the same result. However, since sensitivity and specificity of the studies ranged between 75 – 88 % and 73 – 91 % respectively, the SLN procedures and US-guided core needle biopsies (CNB) cannot be disregarded (61–63).

Magnetic resonance lymphography (MRL) has been studied extensively during the last two decades (64). MRL has been shown to provide high spatial resolution without radiation exposure and enables the overall visualization of lymphatic anatomy overall better than other modalities. Additionally, MRL provides the means to study flow patterns and structural changes in the lymphatic system, such as dermal backflow (12,65). The method has been used to identify secondary lymphedema in the limbs in clinical practice.

Various protocols exist in clinical practice for MRL. Both 1.5 and 3.0 T magnetic resonance (MR)-devices have been used for imaging of peripheral regions and the pelvis. When gadolinium-based CA is used, the injection is typically administered into the digital webspaces. Typically, up to five ~1 mL injections are made either intradermally or subcutaneously. Injection sites are often massaged after the injection to accelerate CA

uptake into the lymphatic vessels; the same technique is also used after ultrasound contrast agent (USCA) skin injections (66). Although the MR sequences vary between studies, few sequences stand out as being heavily favored; heavily T_2-weighted 3D sequence and dynamic contrast-enhanced (CE) T_1-weighted images with maximum intensity projection reformats from each phase of enhancement. The non-contrast T_2-sequence is a fluid sensitive, fast/turbo spin echo sequence similar to those used in biliary tree imaging with a voxel size > 1 mm^3 for resolution. The T_1-weighted CE sequence used in most studies is a fat-suppressed gradient echo sequence with voxel sizes of ~1 mm^3. Examination times vary between 15 – 90 minutes, depending on the protocol (12,13).

In addition to demonstrating areas of accumulated fluid and the course of the lymphatic vessels, MRL has also identified altered speed of the lymph fluid transport on the upper limb affected by the lymphedema compared to the unaffected one; mean = 0.48 ± 0.15 cm/minute vs. 0.61 ± 0.21 cm/minute (67). MRL has also demonstrated identification rate for lymphedema in the affected limb with CE T_1-weighted images ranging from 63.3 – 100 % (12), whereas the detection rate of lymphatic vessels has varied in contralateral healthy limbs from 7.8 % to 100 % (12,68,69). A good correlation in dermal backflow has been found between MRL and lymphoscintigraphy as 92.3 % of the dermal backflow patterns detected in the MRL were confirmed by lymphoscintigraphy (70). Additionally, MRL has shown high sensitivity (92 %) and specificity (100 %) for demonstrating abnormal lymphatic drainage patterns. These results are comparable with lymphoscintigraphy having 100 % sensitivity and specificity (71).

2.3.5 Indocyanine green imaging

ICG is a tricarbocyanine dye with an affinity to bound proteins. It was introduced to the medical community in 1960s when it was used for cardiac studies (72). Classically ICG has been administered intravenously and found to be safe with only rare adverse effects (73,74). ICG has a characteristic property of absorbing and reflecting near-infrared (NIR) light,

thus enabling fluorescence-based imaging (75). The method needs a specific NIR camera system to make the ICG fluorescence visible to the human eye (76).

From a lymphatic imaging point of view, ICG has gained more popularity in the past two decades. The method was initially studied as an alternative to conventional lymphoscintigraphy localizing SLNs in breast cancer patients, with initial promising results showing a positive, 94 % identification rate of the SLN (77). With further technological advances, intraoperative NIR-systems have been developed to provide real-time color video guidance to visualize the ICG uptake in the lymphatic system during surgery procedures (78). Since the initial experience, ICG has been used for the detection of SLNs in various cancers including breast, GI-tract, skin and gynecological cancers, with a consistently high detection rate of 96 %. The same meta-analysis also reported 87 % sensitivity and 100 % specificity for ICG fluorescence guided SLNB (14). Besides the SLNB application of the method, other applications of ICG-imaging have been introduced in the field of oncology and surgery such as, lymphedema and microsurgery (79,80).

As ICG has proven useful in SLNB, the same method has been applied, since 2007, in for lymphatic mapping in secondary lymphedema, by using subcutaneous injections (81). Since then the method has been used in clinical practice to assess the severity of lymphedema, lymphatic patterns and as a guiding procedure in lymphedema-related surgery (80,82,83). In assessing the severity of lymphedema, the results of ICG lymphography have been shown to correlate strongly with those of the golden standard, lymphoscintigraphy. In a comparison between these two methods, ICG lymphography demonstrated $r > 0.83$ in the upper limbs and $r > 0.92$ in lower limbs respectively, while intra-rater agreement varied between (κ) 0.36 – 0.69, depending on the scale used (82,84).

2.3.6 Ultrasonographic techniques

Since the first medical usage of US in the late 1940s, US devices have undergone numerous technological advances (85). Nowadays, in lymphatic imaging US serves as a first line modality for assessing superficial LN areas in cases of abnormal lumps, lymphadenopathy or suspected lymphoma. Additionally, it enables US-guided LN biopsies.

Over the past few decades US has evolved such that it provides much more than the previously typical morphological gray-scale B-mode images, or vascular Doppler-based imaging. The processing power of US machines has risen exponentially, enabling complex calculations to be performed simultaneous with the imaging, thus enhancing US image quality. However, manufacturers of US devices tend to keep secret the details of their technical specifications and consequently, the processing power of current US machines is not available for comparison. New techniques in beamforming have emerged that further enhance image contrast and resolution by filtering out incoherent signals. Additionally, new algorithms have been developed to improve image quality by suppressing clutter signals, to estimate the speed of the sound more accurately and to enable aberration correction (86). Among other advances, transducer technology has evolved over the years leading to the widespread availability of higher frequency transducers (87). Recently, new clinical applications have emerged through these ultra-high frequency transducers (up to 70 MHz) and US-devices are now extensively used in the field of microsurgery and lymphaticovenous anastomosis in the detection of lymphatic vessels (88,89). Each of these advances in US technology have led to improved image quality and improved diagnostic capabilities.

2.3.7 US techniques in lymph node analysis

Where LN involvement is concerned, US is the standard additional modality for lymphatic imaging. Assessing the nodal status is a crucial prognostic factor in several different cancers. Although US and its qualities have

improved over the years, its sensitivity and specificity are at best around 90 % for detecting malignant LNs (90,91).

The most commonly documented features in US evaluation of LN are the size, shape, borders, echogenicity, hilus, intranodal necrosis, calcification, structural changes and vascular pattern and resistance index of the LN.

Nodal size and shape are more commonly measured features in characterizing LNs. The short axis diameter is used to discriminate between benign vs. malignant LN. By increasing the cut-off rate the specificity also increases although conversely, sensitivity decreases and vice versa. Malignant LNs tend to be round in shape and thus show short (S) to long (L) axial ratios (S/L) greater than 0.5. In contrast to common belief, obscure borders are not associated with metastatic LNs. Instead, metastatic LNs tend to have sharp margins, which is due to increased acoustic impedance of the intranodal growth. However, in proven malignancies ill-defined borders may indicate extracapsular growth.

Nodal echogenicity should be compared to adjacent muscles. Metastatic LNs tend to be more often hypoechoic than the benign LNs but unfortunately reactive nodes also frequently appear hypoechoic. As an exception to this, papillary carcinoma of the thyroid is usually hyperechoic which is believed to be related to deposits of tyreoglobulin inside the LNs.

In an US image, hilar structure is seen as an echogenic structure due to the acoustic interfaces of the medullary sinuses. It has been shown that about 90% of the LNs (> 5 mm in diameter) in the head and neck area represent an echogenic hilus (90). The loss of echogenic hilum is considered as a diagnostic criterion for abnormality and is more often observed with malignant LNs. However, benign LNs can also be seen without echogenic hilum while, to a lesser extent, malignant ones may also occur with echogenic hilum.

LNs can also undergo structural changes related to malignancies. Focal cortical nodules can indicate local tumor growth within the LN, although this is not a very sensitive feature. In breast cancer the cortical thickening (> 2.5 – 3.0 mm) of axillary LNs is associated with metastatic nodal

involvement (92,93). Intranodal necrosis can be seen as cystic or echogenic coagulation necrosis. Regardless of the LN size, intranodal necrosis should always be referred to as a pathologic feature. Besides the malignant LNs, necrosis is also found in tuberculous LNs. Other structural changes in the US image include reticulation, which is mostly encountered in lymphomas as fine echogenic lines. Matting (fusing) of the LNs is suggestive of malignancy and is not seen with reactive LNs. Nevertheless, matting may also be detected in tuberculous nodes or in irradiated nodes after radiation therapy. In malignancies matting also suggests extracapsular growth. Intranodal calcification has also been associated with malignancy and punctate microcalcification can be seen in different cancers including lung cancer, papillary and medullary thyroid carcinomas as well as in serous ovarian cancer. However, calcification can also be caused by benign causes such as granulomatous diseases and infections (90,91,94,95).

Color and power Doppler are used to identify different patterns of blood flow within the LN. In small LNs (< 5 mm in diameter), an absence of flow can be encountered; this phenomenon has a low specificity, typically suggesting towards benign etiology. It has been shown that in healthy volunteers ~90% of LNs with a short axis of more than 5 mm will show hilar vascularity (96). As with absence of flow, normal hilar vascularity is also associated with benign etiology. However, peripheral vascularity and mixed pattern with hilar and peripheral flow have high sensitivity (83%) and specificity (98%) in metastatic nodes. The parenchymal flow is usually seen as multiple Doppler signals scattered around the peripheral area. This is believed to be due to the angiogenetic factors released by tumor cells. The vascular resistance index (RI) can also be evaluated although its utility has been questioned (90,91,97).

Although many features of LNs evaluated with US can be suggestive of malignancy, the image characteristics cannot differentiate malignant from benign LNs. Thus, none of these features should be used as the sole criterion for nodal assessment and consequently, histopathological verifications with biopsy are needed.

2.3.8 US elastography

US elastography is an imaging method utilizing the long-established clinical awareness that malignant lesions are often stiffer than the surrounding tissues. The technique was initially introduced during the 1990's (98). The two main methods used clinically are strain and SWE. Strain elastography (SE) was developed first and it uses manually induced compression or physiological changes in tissue pressure to measure tissue deformation. SE is an indirect approach for measuring tissue stiffness based on local assessment of tissue strain. Calculating strain ratios by selecting a region of interest (ROI) in the lesion and another ROI in adjacent healthy tissue is a way of semi-quantifying the elastograms. SE has the additional benefit of being easy to learn. However, the technique is not quantitative and is thus prone to subjectivity and user dependency (99).

SWE US measures the velocity of the shear waves generated from the tissues by applying a dynamic stress to the tissue at one or multiple points. Unlike conventional SE, measurement of the shear wave velocity in this way provides both qualitative and quantitative information and is less user dependent (100,101).

Elasticity can be explained by Hooke's Law, assuming that the object is completely elastic and has no viscosity:

$$\sigma = \Gamma \cdot \varepsilon$$

where the stress (σ) represents the force per unit area in kiloPascal units (N/m^2), the strain (ε) is the change of the dimension per unit (dimensionless) and the elastic modulus (Γ) relates stress to strain in kiloPascal units. Materials that tend to resist deformation are thought to have a higher stiffness and thus a higher elastic modulus Γ.

The following equations describe static deformation of the material. Depending on the type of deformation, the elastic modulus can be described by Young's modulus (*E*), the shear modulus (*G*) or the bulk modulus (*K*).

1) Young's modulus *E* can be used when a normal stress (σ_n) produces a normal strain (ε_n); in the equation combining normal stress and normal

strain, the normal is defined as being perpendicular to the investigated surface:

$$\sigma_n = E \cdot \varepsilon_n$$

2) The shear modulus *G* is used when a shear stress (σ_s) produces a shear strain (ε_s). In this equation shear is defined as tangential to the investigated surface:

$$\sigma_s = G \cdot \varepsilon_s$$

3) Bulk modulus *K* can be used when an inward-directed force (σ_B) produces a bulk strain (ε_B) in the investigated volume:

$$\sigma_b = K \cdot \varepsilon_b$$

The elastic modulus Γ additionally characterizes the propagation speed of the waves:

$$c = \sqrt{\Gamma/\rho}$$

where c is the velocity of the wave and ρ is the density of the material. The two types of wave propagation in the US are referred to as longitudinal waves and shear waves. The conventional B-mode image of the US uses longitudinal waves, whereas shear wave imaging (SWI) in elastography utilizes the shear waves.

The particle motion in longitudinal waves is parallel to the direction of propagation and the wave speed (c_L) is approximately 1540 m/s in soft tissues. Since the differences in wave speed are relatively small in soft tissues, the bulk modulus *K* is not suitable for US elastography.

Shear waves on the other hand have particle motion perpendicular to the direction of wave propagation. Their low velocities (approximately 1 – 10 m/s) in soft tissues leads to greater differences in the shear modulus *G* between tissues, thus enabling elastography measurements. The velocity of the shear waves is defined using *G* according to the following equation:

$$c_s = \sqrt{G/\rho}$$

When comparing the relative merits of the strain and shear elastography methods, it is apparent that technological advances and studies nowadays focus mainly on SWE due to the more quantitative nature of the method and because it is less dependent on the user. During

recent years US research and development has led to the emergence of three separate technical approaches to SWI.

2.3.9 Methods of shear wave imaging

The first method to be introduced was the 1D-transient elastography system Fibroscan™ (Echosens, Paris, France) early in 21st century. The first publication assessing liver fibrosis was published in 2003 (102). Fibroscan is not capable of operating in B-mode although the device consists of an ultrasound transducer and mechanical vibrating system as in conventional US devices. The user selects the appropriate area in the liver by using time motion US (A-mode). The probe produces a mechanical stress on the body surface which generates shear waves from the tissues. Young's modulus *E* and shear wave velocity are calculated from the A-mode US. Measurement is repeated 10 times for validation, such that the interquartile range representing the variability between measurements should be < 30 % (100).

Point shear wave elastography (pSWE) is a second-generation technique using acoustic radiation force impulse (ARFI) to create tissue displacement in the direction of the propagation of the US wave at a single point. A part of the longitudinal waves induced by ARFI is converted to shear waves through the absorption of acoustic energy. Shear waves thus generated travel perpendicular to the plane of excitation and the speed of these waves is measured. Results for the shear wave velocity provide quantitative information about the elasticity of the tissue (103).

The most recent application is 2-dimensional shear wave elastography (2D-SWE) which also uses ARFI. Where pSWE uses a single focal zone, the 2D-SWE uses multiple focal zones in a cycle, faster than the shear wave velocity, generating a cylindrical cone of shear waves. This procedure enables real-time monitoring of the shear waves in 2D for measurements from quantitative elastograms superimposed on the B-mode image. Additionally, the ability to assess anatomical structures with the elastogram increases both the operator's confidence and reliability of the

measurements through the anatomical guidance and tissue elasticity information (104).

2.3.10 Challenges in US elastography

US elastography has several limitations. SE has produced highly subjective results as they rely on the operator manually inducing pressure and variability of physiological motion. Additionally, factors such as measurement depth, or operator related and internal sources of stress from the body may affect the measurements (100,105–110).

Moreover, commercially available software for processing US elastography rely on the following basic assumptions:

- linearity; strain to the tissue increases linearly as a function of incremental stress
- elasticity; the rate of the deformation is not dependent on stress rate, and tissue returns to its normal equilibrium state after the stress is removed
- isotropic; the tissue is homogenous and reacts in a similar way irrespective of the direction of applied stress
- incompressible; tissue volume remains constant despite the applied stress

However, these assumptions have been shown to hold only in specific clinical settings, such as in the assessment of liver fibrosis, but not in all scenarios, for example in patients with high body mass index (BMI) (111).

Nevertheless, SWE as well as SE have been used in many published studies assessing liver fibrosis (112–114) and more recently evaluating focal lesions in breast, prostate and LNs (115–119). Although these methods are used routinely for assessing the nature of the lesions, they have not established their place as universally trusted clinical methods. Breast cancer evaluation is however an exception to this, where elastography has been incorporated in the Breast Imaging-Reporting and Data System (BI-RADS) (120). The guidelines established by the European Federation of Societies for Ultrasound in Medicine and Biology (EFSUMB)

indicate that US elastography can be used as an additional tool to identify the most suspicious LN or suspicious areas within the LN for targeted biopsy (121). Otherwise, no recommendations nor guidelines exists in relation to LN elastography performance or interpretation. More precisely, there are no specific recommendations regarding optimal sizes, cut-off values or the number of ROIs to be used.

The size and stiffness of the investigated lesion as well as its depth affect the outcome of both SE and SWE measurements. Although elastography may be of help in differentiating between benign and malignant superficial LNs using SWE, overlapping of stiffness measurements can still occur and it remains consequently somewhat uncertain whether elastography provides further assistance to identifying the LNs with intermediate characteristics. Best results are obtained by combining SWE results with other US data available. Optimal cut-off values for benign vs. malign lesion remain unclear (115,122,123).

Depending on the choice of elastography method and the definition of cut-off values to differentiate LN malignancy, the sensitivity and specificity vary between 36 – 100 % and 35 – 100 % (115). The sensitivity of US elastography in detecting LN metastases in breast cancer has been reported as being between 60 – 90 % with a specificity between 79.6 – 89 % (124,125). The best specificity (99.3 %) was achieved by combining US B-mode characteristics with the elastogram but with very low sensitivity (26.7 %) (125). Recent meta-analysis has demonstrated that SWE improves diagnosis in the differentiation of axillary LNs resulting in a pooled sensitivity of 79 % (95 % CI: 0.71 – 0.86) and specificity of 90 % (95 % CI: 0.83 – 0.95) (119). Similar findings have been reported for malignant cervical LNs, where the meta-analysis resulted in SWE sensitivity of 81% (95 % CI: 0.72 – 0.88) and specificity of 85 % (95 % CI: 0.70 – 0.93) for diagnosing malignant cervical LNs (8). However, data for other superficial LN areas remain scarce.

2.3.11 Contrast-enhanced ultrasound

In conventional US, the LN differentiation from benign to malignant relies mainly on size and additional structural changes. CEUS is an application where USCA's such as microbubbles are used to provide an additional tool to characterize LNs.

Background research into the CEUS method started in the 1960's when it was discovered that contrast enhancement of the signal was caused by the gas core of the saline bubbles (126). After more than 20 years of development the first stable commercial USCA (Albunex®) became available (127). Since then, multiple CAs have been developed for clinical purposes. The CEUS technique provides information on the vascular pattern of the target and its perfusion. It has also been proven to improve tumor characterization and to potentially lower the number of biopsies in breast tumors (128). The method was introduced over a decade ago and it now has an established place in the international guidelines (129,130). Although the behavior of CEUS and its blood flow pattern are well documented in both normal and pathological soft tissue, knowledge about the effectiveness of CEUS in LN evaluation is still limited (131) and there are currently no clinical recommendations regarding CEUS in the guidelines (130).

USCA's are mainly microbubbles with diameters ranging from 1 to 10 μm. During the evolution of the CA's different coating materials and gases in the bubbles have been studied and used. Several microbubbles coated with phospholipids have emerged from the different options and most of the commercially available CAs use these as coating material (132), as listed in Table 2. Depending on the structure of the microbubbles different CAs may offer some advantages compared to others, for example a longer microbubble lifespan. Nevertheless, all commercially available CA's can be used for CEUS. The most widely used CA in Europe is sulphurhexafluoride (Sonovue®, Bracco, Italy) in a phospholipid shell. Administration is carried out as an intravenous bolus. The CA remains in the blood circulation without extravasation to surrounding tissues, unlike CA's used in CT or MRI

(130). Studies with even smaller bubbles, nanobubbles (400 – 800 nm), have also been carried out. Conventional microbubbles do not leave the blood circulation due to their size, but to visualize potential extravasation to tumor tissue, the smaller bubbles have been tested (133,134). Additionally, off label use of USCA's has been investigated with SLN's, mainly in breast cancer. In these studies the USCA have been seen to accumulate within lymphatic vessels of the breast and drain to the regional LNs after intradermal injections (9,131,133,135,136).

Table 2. List of commercially available ultrasound contrast agents, modified from (132)

Name	First approved for clinical use	Shell material	Gas
Optison	1998	Cross-linked serum albumin	Octafluoropropane
Sonazoid	2007	Phospholipid	Perfluorobutane
Lumason/Sonovue	2001/2004	Phospholipid	Sulphurhexafluoride
Definity/Luminity	2001/2006	Phospholipid	Octafluoropropane
Imagent/Imavist	2002, withdrawn	Phospholipid	Perfluorohexane, Nitrogen
Echovist	1991, withdrawn	Galactose microparticles	Air
Levovist	1995, withdrawn	Galactose microparticles	Air
Albunex	1993, withdrawn	Sonicated serum albumin	Air

USCAs are well tolerated as the microbubble gas is excreted by exhalation after their breakdown (130,137), while the shell material is cleared through the reticuloendothelial system, mostly through the liver and spleen. Some of the USCA's have more affinity with the reticuloendothelial system than others and intact microbubbles may also be engulfed by macrophages, as is particularly the case with

perfluorobutane (Sonazoid®), in contrast to the most widely used sulphurhexafluoride (Sonovue®). This feature of perfluorobutane enables investigation of the so-called liver specific late phase or Kupffer phase thus improving the detection of hepatic lesions (138). Additionally, USCAs can be used in patients with renal insufficiency since there is no renal clearance.

In clinical practice, CEUS is mostly used to characterize different solid lesions. An intravenously administered USCA has been used in a number of studies in the detection of thyroid cancer metastasis in the cervical region, in other head and neck -malignancies and in axillary and inguinal regions in melanoma patients (139–141). CEUS has also been utilized in axillary staging and prediction of tumor aggressiveness in patients with breast cancer (142–144). However, these preliminary studies revealed that the technique with intravenous contrast injections was of limited clinical value in breast cancer.

2.3.12 CEUS SLN procedure

Additional applications for CEUS in the localization of SLNs have been investigated. The first CEUS sentinel procedure was published in 2004 in a swine-melanoma model (145). CEUS sentinel procedure with intradermal contrast injections has shown promising results and applicability in clinical practice in breast cancer staging. For breast cancer patients, the skin injection of USCA was first introduced in 2009 (9) and later on multiple studies have shown similar results (119). In CEUS sentinel procedure the microbubble CA is used in a similar manner as with isotope injections in the traditional SLNB procedure in breast cancer. The USCA is injected intradermally at the margin of the areola and the drainage of the USCA can then be followed in real-time US via lymph vessels to axillary LNs (10,66).

The use of CEUS in off-label intradermal usage to localize SLN in breast cancer has been shown to be both safe and feasible (10,66,119,146). In comparison to traditional isotope SLNB and Patent Blue dye, which have a pooled identification rate of 94 % SLNs in breast cancer and melanomas (11), the sensitivity of CEUS in detecting SLN correctly from axillary LNs in

breast cancer was 89 % (146). The literature on CEUS-guided SLN biopsies is still limited and details such as localization methods prior to subsequent surgery remain to be determined (125,146). In each of these applications CEUS provides a minimally invasive, fast and repeatable method for the assessment of the target tissue. Despite the amount of research done on CEUS, particularly in the SLN studies, no recommendation currently exists for the usage of CEUS in LNs (130).

2.3.13 US in lymphatic vessel visualization and analysis

Conventional US has not been able to visualize lymphatic vessels until recently. Thus, publications on this matter are scarce. As a byproduct though, CEUS SLN procedures have been used in visualizing short ranges of superficial lymphatic vessels since 2004 (145). Nearly two decades later, due to a combination of technical advances and results from previous CEUS SLN studies, US has been used to visualize lymphatic vessels in microsurgery (88,89,147). More recently, CEUS has been used in conjunction with ICG fluorescent lymphography in the detection of lymphatic vessels for lymphaticovenous anastomosis surgery in secondary lymphedema. CEUS identified lymphatic vessels in all of the patients (11/11) including the patients (6/11) to whom ICG could not be performed or where it was unable to locate the lymphatic vessels (148).

2.3.14 Sentinel lymph node biopsy

According to current understanding, the cancer cells in many malignancies first spread to a draining SLN or into a group of LNs. Thus, SLN-status affects the prognosis and staging of various cancers. SLNB was developed as a less invasive technique for LN staging in order to avoid high complication rates after radical regional lymphadenectomy. SLNB was first introduced as a part of breast cancer treatment in 1994 (149). SLNB has lowered the rate of incidence of postoperative complications compared to ALND, for example arm stiffness (13.6 % vs. 23.9 %) and swelling (6.8 % vs.

30.9 %) (1). Since this method has proven to be both feasible and effective, SLNB has subsequently been adapted to other cancers treatments as well.

The first SLNB study in vulvar cancer was published in 1997 (150). Complication rates after inguinofemoral radical lymphadenectomy (IFL) in vulvar cancer remain high and are as follows; lower limb lymphedema (14 – 49 %), lymphocyst formation (11 – 40 %) and wound infections (24 %) (151–153). As in breast cancer, application of SLNB correlates with lowered complication rates in vulvar cancer (2). However, IFL still has an important place in patients not suitable for SLNB or where vulvar cancer is a recurrent disease. On the other hand re-mapping of SLN has been used in recurrent breast cancer patients after prior axillary procedures (154), whereas in vulvar cancer the issue is still under investigation (155).

Nowadays SLNB is routinely utilized in various malignancies such as breast cancer and melanoma, with high detection rates of 95 % and 98 % respectively (11). Due to the invasive nature of the IFL, SLNB has taken its place as the standard of care in selected vulvar cancer patients (tumor < 4 cm, invasion depth > 1 mm, clinically N0 stage) (156,157). In vulvar cancer, SLNB is performed ipsilaterally in lateral tumors and bilaterally in midline tumors due to the possibility of bilateral lymphatic drainage. Moreover, when only unilateral SLN is found in midline tumors, IFL is advised for the contralateral side (156,157). In vulvar cancer SLNB was shown to have a 92 % detection rate for SLN's (158).

In SLNB procedures, the SLN mapping requires no patient preparation. Usually, the SLNB procedure is performed over a 1 – 2 day protocol and the use of multiple indicators for SLN detection is advised. Therefore, in addition to traditional preoperative technetium (^{99m}Tc)-radiolabelled colloid radiotracer injection (159) a blue dye has been used as an intraoperative optical tracer. However, in recent years the use of the hybrid tracer, ICG-^{99m}Tc-nanocolloid has been introduced, thereby combining a traditional radiotracer with fluorescent material and facilitating better intraoperative SLN visualization compared to blue dye (96 % vs. 65 %) (160).

Depending on the institution, the injection of the radiotracer is done either on the day of the operation or on the day prior to the surgery and

the dose of the radiotracer is fixed accordingly. The injection is split into two to four around the tumor and the injection is preferably performed intradermally. Several minutes after the injection dynamic images of the pelvic area are acquired, followed by later static images up to two hours after the injection and markings of the SLN's on the skin are made at the sites of accumulated radiotracer. Typically, planar lymphoscintigraphy is used for the detection of the SLNs (159). However, SPECT/CT helps to pinpoint and discover more SLN's compared to planar lymphoscintigraphy (161). Furthermore, SPECT/CT enables the identification of potential abnormal drainage routes and decreases the false positive uptake of possible contaminations or other structures with uptake, thus providing more detailed SLN information (55). Fusion techniques of real-time SPECT and US for localization of the SLN have also been investigated mainly in breast cancer patients and found feasible. However, co-registration with the US was not successful in 28 % of the patients (162).

As mentioned before, blue dye has been traditionally used as an intraoperative visible optical tracer and the golden standard has been to combine blue dye with lymphoscintigraphy for better intraoperative SLN detection. When used alone it has some disadvantages, such as potential allergic reactions and a poor tissue penetration, decreasing its effectiveness in obese patients. The use of a handheld gamma camera intraoperatively is advised to help in the detection of SLNs. Occasionally the gamma probe detects more than one radioactive LN and it is not clear by using scintigraphy alone whether these truly represent additional SLN's or LN's which have collected radiotracer that has passed the SLN (53). ICG offers an alternative option as an optical tracer to replace blue dye as a safe, non-radioactive substance and has also shown promise in SLN mapping in other gynecologic cancers. Recent reviews of research into vulvar cancer showed that SLN detection rate with ICG ranged from 89.7 to 100 % depending on the study setting (163). Still, ICG also has some limitations; mandatory use of NIR camera equipment, low penetration of the NIR rays in the tissue and potential visualization of additional LN's alongside the SLN (163).

2.3.15 Role of sentinel node imaging in vulvar carcinoma

The vulva refers to all of the female external genitalia structures including mons pubis, labia minora and majora, clitoris, vulvar vestibule, vestibular bulbs, urethra, vaginal opening, perineal body and Bartholin's and Skene's glands (164,165). Lymphatic drainage of these structures is mainly concentrated in the superficial inguinal nodes (166). Superficial areas of the labia minora and majora drain to lymphatic collectors and continue via the mons pubis area towards superficial inguinal LN's, whereas the clitoris has a more complex draining system and different patterns have been described historically. The most detailed version has identified three different pathways: some groups of lymphatic vessels, including those in the distal parts of the urethra, drain into the superficial inguinal LN's; others drain into the obturator and interiliac LN's and the remaining vessels drain into the LN at the femoral annulus.

Superficial inguinal LNs are divided into four groups plus a central zone, depending on their anatomical location with respect to the great saphenous vein and the saphenous opening in the cribriform fascia (Figure 5.). Afferent lymphatic vessels mainly drain into the superomedial group and only seldom into the inferomedial or lateral groups (167,168).

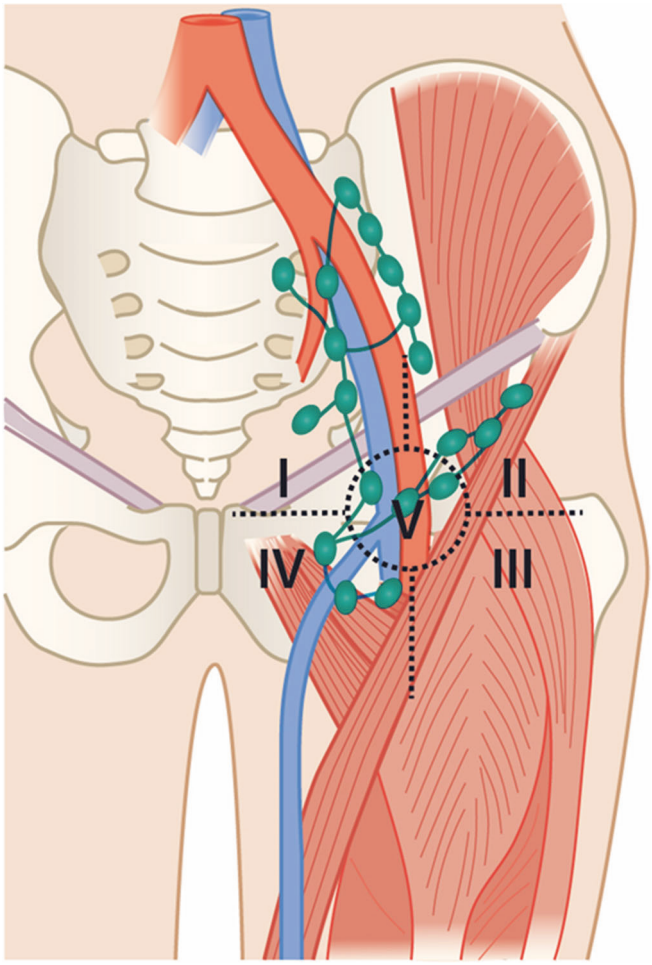

Figure 5. Superficial inguinal lymph node regions. Schematic drawing describing the superficial lymph node regions in the inguinal area. Lines alongside and perpendicular to femoral vein at the level of saphenofemoral junction divide the regions into: superomedial region (I), superolateral region (II), inferolateral region (III), inferomedial region (IV) and central zone (V).

Vulvar cancer mainly spreads via the lymphatic system, thus the regional nodal status is the most important prognostic factor. The incidence of LN metastatis increases with the depth of the tumor's stromal invasion. Superficial tumors (tumor stromal invasion < 1 mm) have less than 1 % LN involvement whereas tumors with stromal invasion > 1 mm have more

than 8 % LN involvement (169,170). Tumor size is also a predictive factor for LN metastasis, such that tumors greater than 2 cm in diameter lead to a 41.6 % chance of groin metastasis. Additionally older age, tumor differentiation and the presence of lymphovascular invasion increases the probability of LN involvement (171–173).

Cancer cells migrate via afferent lymphatic vessels and metastatic deposits can first be found in the subcapsular and cortical sections of the LN resulting in cortical thickening and bulging. As in other cancers, including breast cancer, extracapsular extension is a prognostic factor leading to a worse outcome (172).

The LN involvement is the most important prognostic factor in vulvar cancer (174) and it has been shown that pathological ultrastaging improves the detection rate of SLN metastases (175). Thus, the role of the size of SLN metastasis has also been the subject of much study (176). It has been shown that the chance of non-SLN metastases increases with size of the SLN metastases with no clear cut-off value. However, isolated tumor cells have a relatively low risk of non-SLN metastases of 4.2 %. Additionally, patients with SLN macrometastases (> 2 mm) were found to have worse disease-specific survival compared to those with SLN micrometastases < 2 mm (69.5 % vs. 94.4 %).

As with breast cancer, SLNB has gained acceptance as a less aggressive surgical approach for assessing LN status in vulvar cancer, owing to overtreatment of IFL in 65 – 75 % of patients (2). Additionally, IFL is linked to postoperative complications increasing short- and long-term morbidity, which may postpone further treatments and lower the quality of life (177). It has been shown that SLNB lowers the risk of complications such as lower limb lymphedema (1.9 % vs. 25.2 %) compared to IFL in patients with T1-T2 (< 4 cm) squamous cell carcinoma of the vulva (2). Moreover, it has been demonstrated that in selected patient groups (SLN negative, T1-T2 vulvar cancer) there was no significant difference in local groin recurrence rate and disease-free survival rate after three years. However, the SLNB procedure is strongly dependent upon the experience of the surgeon. For this reason, as well as the relative rarity of the disease, it has been

suggested that the procedure should be done in selected centers and by surgeons who routinely treat at least 5 – 10 vulvar cancer patients per year.

Surgery has been the golden standard for the treatment of the vulvar cancer. However, its nature has in recent decades shifted away from radical vulvectomy and radical IFL towards more minimally invasive surgical techniques. Palpation has in the past been the most basic diagnostic tool for assessing LN status. However, it is highly inaccurate with only 9 % accuracy preoperatively and 55 % intraoperatively. Inguinofemoral LN involvement has traditionally been confirmed with IFL covering the evacuation of Scarpa's triangle and metastases are found only in 25 – 35 % of patients (2,151,178,179).

3 AIMS OF THE STUDY

The purpose of this study was to investigate the feasibility of new ultrasonographic techniques in the assessment of the lymphatic system.

More specific aims were:

1. To evaluate the feasibility of contrast-enhanced ultrasound in identifying sentinel lymph nodes in vulvar cancer compared to lymphoscintigraphy

2. To investigate the reproducibility of shear wave elastography in inguinal lymph nodes and to define the optimal size for the region of interest for nodal status assessment

3. To investigate the feasibility of contrast-enhanced ultrasound for fast visualization of the superficial lymphatic vessels in the upper limb

4 SUBJECTS AND METHODS

All studies in this thesis were approved by the institutional review board as well as the local ethics committee. Additionally, approval from the Finnish Medicines Agency was obtained for the Sonazoid® USCA. All of the studies were prospective single center studies carried out at the Kuopio University Hospital. Written consent was obtained from all participants.

4.1 PATIENTS

Study populations consisted of three different groups; 1) The first group (study I) consisted of 12 consecutive patients (mean age 69 years) with newly diagnosed vulvar cancer scheduled for preoperative SLN study as a part of their standard treatment protocol. Altogether 20 groins were examined. 2) The second group (study II) included 21 consecutive patients (mean age 68 years, 4 males, 17 females) scheduled for inguinal US due to suspicion of abnormal LNs or who underwent inguinal US as a part of their preoperative examinations. 3) The third group (study III) consisted of 30 healthy volunteers (16 males, 14 females, mean age 41 years).

4.2 ULTRASOUND

US procedures and examinations in these studies were performed with a Logiq E9™ (GE Healthcare, Chicago, IL, USA) US-device. An ML6-15 linear array transducer was used for gray- scale imaging and for the CEUS investigations. The L9 wide band linear transducer was used for the SWE measurements. The examinations were performed by either a single radiologist (Studies I and III) or two radiologists (Study II).

4.2.1 Gray-scale ultrasound

B-mode was used to search for possible abnormal features in the inguinal LN's in studies I and II. The size, short axis, cortical thickness and shape of the LN's were registered. In addition to possible abnormal features, the distance from the suspicious LN to the femoral artery and the skin was measured. Doppler US was used to assess abnormal vascular patterns.

4.2.2 Shear wave elastography

SWE measurements were conducted on the largest inguinal LN or the one with the most abnormal features based on the gray-scale US. The patients were examined in the supine position with minimal muscle stress. To avoid excess compression from the probe to the tissues, minimal external force was applied. The probe was positioned perpendicular to the surface of the skin. SWE measurements were acquired from the longitudinal and short axis of the LN. SWE images were deemed as sufficient for analysis when the majority of the sampling box (15 x 15 mm) was color coded and no major changes occurred in the color-coded SWE-maps between the data acquisition cycles, so as to avoid the possibility of external force-related artifacts.

Two radiologists performed the SWE measurements independently and blindly, with different fixed circular ROI sizes (1, 2, 3 and 5 mm) centered on the cortex with an equal spacing to ensure that as much of the LN cortex was covered as possible. Five ROIs of each fixed size were used in both acquired planes (Figure 6). Additionally, one circular freehand ROI covering the cortex was drawn.

The US-device elastography software calculated the elasticity (E) values representing the mean value of the pixels in the ROI. Due to software problems, it was not possible to use all of the elasticity indices. Mean-E was defined as the mean of the five measurements. Min-E and Max-E represented the minimum and the maximum value of the five measurements.

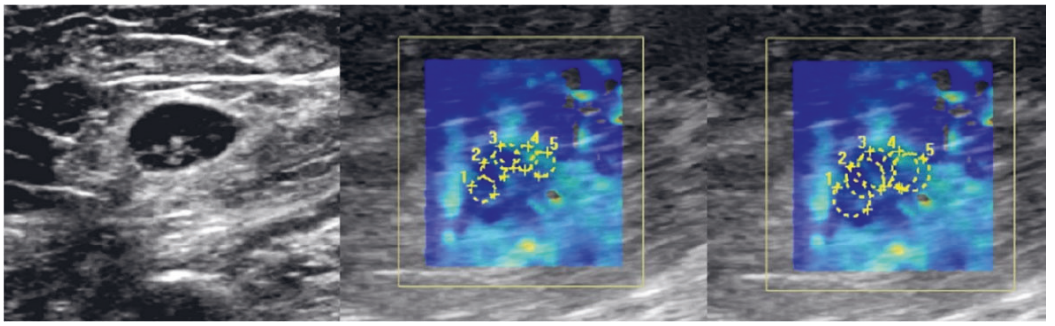

Figure 6. SWE measurements with different ROI sizes placed covering the cortex of the LN. Image on the left illustrates an inguinal LN in B-mode image. Image in the centre and right illustrate the same LN with SWE measurements done using 2 and 3 mm ROIs (Study II).

4.2.3 Contrast-enhanced ultrasound

CEUS procedures in these studies were performed with Sonovue® (study I) and Sonazoid® (Study III). The initial hypothesis was that the enhancement times for evaluation of the whole upper limb would be significantly longer than those in the SLN studies and therefore Sonazoid® was selected for Study III as potentially being more durable than Sonovue® and owing the affinity towards reticuloendothelial system. In both studies the CA powder was mixed with 2 mL of sterile saline. Injections were made with 24-gauge needle and 1.0 mL syringe. Injected volumes varied between 0.1 – 0.3 mL with the Sonazoid® and 0.3 – 0.4 mL with the Sonovue®. Injections were made to the upper lateral side of the mons pubis (study I) and the distal part of the antebrachium (Study III). If no enhancing vessels were visualized with US, the injection site was gently massaged for approximately 10 s. If no enhancing vessels were detected after the massage, the injection was repeated at a nearby site up to three times. In Study III, continuous flash was used before the next injection to help destroying residual microbubbles from previous injections. In Study III, the timer on the US-device was turned on when the whole volume was injected. CEUS-sentinel procedure and the upper limb CEUS were deemed unsuccessful if no enhancing vessels could be seen after the additional injections.

Following a successful intradermal injection an enhancing superficial lymphatic vessel or vessels were visualized in the US. In Study I, the enhancing vessels were followed with the US probe and the first enhancing LN in the inguinal area was deemed as the SLN; this was then marked with a guidewire (Somatex Medical Technologies, Berlin, Germany) under local anesthesia and US guidance. During the surgery, SLN's marked with CEUS-guidance were compared to the SLN's identified with traditional lymphoscintigraphy and/or Patent Blue dye labelled SLNs. In the Study III, the flow of the CA was observed and the enhancement time of the CA reaching the levels of antecubital fossa and axilla were registered.

4.2.4 Injection technique

To achieve intradermal administration of USCA the injections were made at low angle, almost parallel to the skin surface. The tip of the needle was positioned under the thin layer of epidermis so that it could be seen through the skin with the naked eye. The injection rate of the CA was determined by the resistance of the tissues. A small blister like spot underneath the skin was a favored outcome after the injection. The injection sites and techniques are illustrated are the Figures 7 and 8.

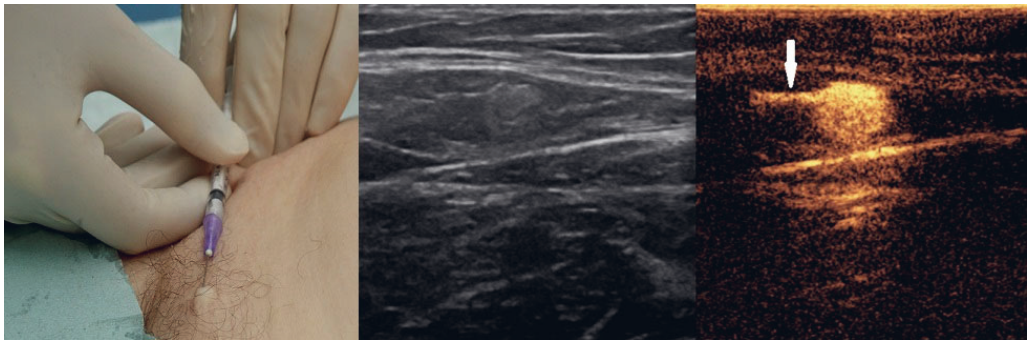

Figure 7. Panel of pictures illustrating the injection technique and the enhancing SLN in Study I. Image on the left shows the site of the injection on the upper lateral side of the mons pubis. The middle image shows the B-mode image from the SLN. Image on the right demonstrates afferent lymphatic vessel (arrow) and the enhancing SLN (Study I).

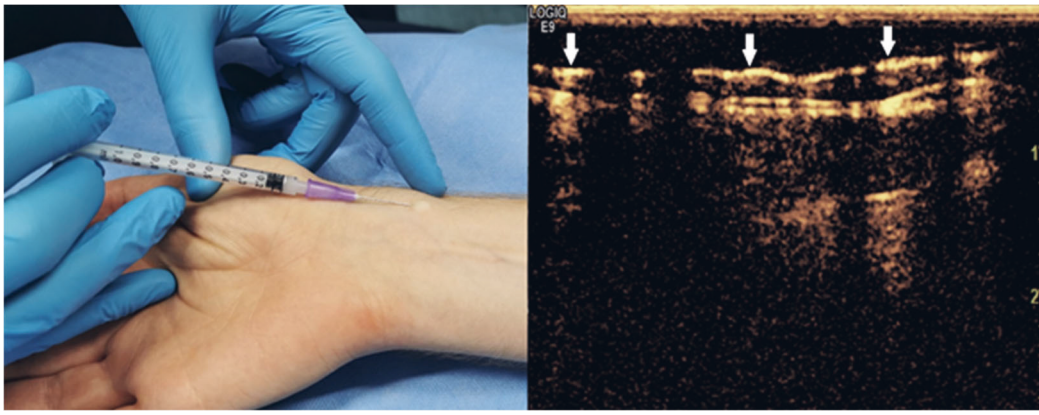

Figure 8. Injection site at the distal antebrachium in Study III and the enhancing superficial lymphatic vessel (marked with arrows) in a longitudinal CEUS image (Study III).

4.3 HISTOPATHOLOGY

CNB samples, surgical specimens and SLNs in Studies I and II were examined histopathologically in the pathology laboratory of Kuopio University Hospital as a part of the normal diagnostic procedure. After formalin fixation and paraffin embedding the samples were sectioned into 4.0 µm slices and stained with hematoxylin and eosin. Additional immunohistochemical stainings were made whenever found necessary.

4.4 TREATMENT

Regardless of the findings in the SWE or SLN studies, the patients received standard treatment and follow-up according to both the Finnish national guidelines and the European Society of Gynaecological Oncology (ESGO) guidelines, depending on the nature of their disease. All patients in the Studies I and II had histological verification of the samples through a CNB or surgical removal of the LN(s) as a part of their normal treatment.

4.5 STATISTICAL ANALYSIS

Statistical analysis for Studies II and III was performed with SPSS (Versions 22.0 and 26.0, SPSS, Chicago, Illinois). Continuous variables were reported as mean ± standard deviation for the Study II and as median and interquartile range for Study III. The sample size for statistical significance was verified for the reproducibility study with a power calculation ($\alpha = 0.05$ and power 0.80).

In Study II, optimal ROI size for differentiating benign and malignant LN was selected by area under curve (AUC) values from the receiver operating characteristic (ROC) analysis. A Delong test was used to compare the ROC curves. Additionally, diagnostic performance between different ROI sizes and types was studied with a McNemar test. Intraclass correlation (ICC) values were used to compare interrater agreement between the two readers. ICC values were classified as excellent (> 0.90), good (0.75 – 0.90), moderate (0.50 – 0.75) and poor (< 0.50).

In Study III, a Mann Whitney *U* test was performed to evaluate the statistical significance of different parameters (age, sex, BMI, strength of enhancement). The Wilcoxon related samples test was used to calculate inter-side differences on enhancement time of USCA.

Values of $P < 0.05$ were considered significant.

5 RESULTS

5.1 SENTINEL LYMPH NODE LOCALIZATION IN VULVAR CANCER WITH CEUS

After exclusion criteria 19 groins were analyzed. The CEUS identified a potential SLN in 18 of the 19 groins examined, representing a 94.7 % technical success rate, which equals the technical success rate of 94.1 % obtained for lymphoscintigraphy (16/17). When comparing cases where both lymphoscintigraphy and Patent Blue dye were performed, CEUS had a sensitivity of 81.2 % (13/16) identifying SLN. However, CEUS also found potential SLN's in two cases (2/19, 10.5 %) when traditional methods failed to do so. Histopathological analysis revealed the presence of metastatic deposits in five groins and all metastatic SLN's were identified correctly with the CEUS – sentinel procedure. Table 3 summarizes the SLN findings.

Table 3. Summary of the SLN findings in vulvar cancer patients. CEUS-procedure was compared to traditional lymphoscintigraphy and Patent Blue dye (Study I).

Patient		CEUS procedure			Patent blue dye	Gamma detector	Concordance of SLN methods	Histopathology of SLN	
Number	Side (R/L)	CEUS successful +/-	Enhancing LN short axis (mm):	Cortical thickness (mm):	+/-/not done	+/-/not done	+/-	benign/ micrometastasis/ macrometastasis	Number of metastatic LNs in LND
1.	R	+	8	3	+	+	+	macrometastasis	1/6
2.	L	+	7	3	+	+	+	benign	0/6
3.	R	+	6	1	-	-	-	benign	0/4
4.	R	+	5	1	+	+	+	benign	0/3
4.	L	+	10	10	+	+	+	micrometastasis	1/3
5	R	+	9	5	-	+	+	benign	0/5
6.	R	+	8	6	+	+	+	benign	0/3

6.	L	+	7	3	-	+	+	benign	0/6
7.	R	+	4	1	+	+	+	benign	0/12
7.	L	-	-	-	+	+	-	benign	0/5
8.	R	+	5	3	+	not done	+	macrometastasis	4/16
8.	L	+	4	3	-	not done	-	benign	0/13
9.	L	+	4	1	-	+	+	benign	0/4
10.	R	+	21	21	not done	not done	-	macrometastasis	1/4
10.	L	+	20	15	not done	not done	-	macrometastasis	1/1
11.	R	+	7	4	+	not done	+	benign	0/11
11.	L	+	7	6	+	not done	+	benign	0/11
12.	R	+	5	2	+	+	-	benign	0/3
12.	L	+	5	1	+	+	+	benign	0/2

5.2 SHEAR WAVE ELASTOGRAPHY IN THE EVALUATION OF INGUINAL LYMPH NODES

Thirty-two inguinal LN's from 21 patients were included in the final analysis. The axial plane yielded significantly better results in ICC-scores (ICC = 0.87) in the reproducibility analysis than the sagittal plane (ICC = 0.72) (*P* = 0.006). Larger Mean-E and Max-E ROI's of 3 – 5 mm diameter resulted in the highest reproducibility in the axial plane (ICC = 0.90 – 0.97). No statistical difference was found between the results of the two readers. In addition to influence due to the plane of measurements, the depth of the LN and cortical thickness > 3 mm were found to affect on the ICC-scores, resulting in better reproducibility with more superficial LN's and LN's with cortical thickness > 3 mm (P = 0.018 and 0.004, respectively). Table 4 summarizes the ICC-scores with different ROI sizes and planes between the two readers.

Table 4. Intraclass correlation coefficient values for different regions of interest (Study II)

ROI (size mm/type)	ROI plane	Mean-E (kPa) ± SD		ICC-values for Mean-E/Max-E/Min-E
		Observer 1	Observer 2	
1	Axial	9.32 ± 8.24	9.44 ± 7.08	0.87 / 0.85 / 0.61
2	Axial	9.80 ± 8.12	10.04 ± 9.93	0.91 / 0.90 / 0.70
3	Axial	9.96 ± 7.29	10.29 ± 9.50	0.90 / 0.96 / 0.82
5	Axial	9.95 ± 7.02	9.78 ± 7.80	0.97 / 0.95 / 0.91
1	Sagittal	12.32 ± 8.86	14.03 ± 10.74	0.70 / 0.42 / 0.65
2	Sagittal	12.29 ± 9.44	14.28 ± 10.98	0.77 / 0.72 / 0.91
3	Sagittal	12.28 ± 9.69	14.44 ± 11.31	0.74 / 0.74 / 0.77
5	Sagittal	12.19 ± 8.99	13.75 ± 10.25	0.79 / 0.79 / 0.80
Freehand ROI	Axial	9.61 ± 6.43	9.79 ± 6.60	0.95
Freehand ROI	Sagittal	11.46 ± 6.73	13.88 ± 10.50	0.61

When comparing benign and malignant LN's, SWE measurements values proved to be higher for malignant LN's with 3 mm Mean-E (15.81 ± 10.61 kPa; range, 3.86 – 36.45 kPa) than with benign LN's (7.68 ± 3.82 kPa; range, 3.41 – 15.40 kPa). ROI's with 2 mm and 3 mm Mean-E values in the axial plane yielded the greatest AUC-values of 0.773 in the ROC curve (Figure 9). The optimal Mean-E cut-off value for differentiating malignant LN with 3 mm axial ROI was 7.31 kPa with 88.9 % sensitivity, 60.9 % specificity, 47.0 % positive prediction value, 93.3 negative prediction value and 68.7 % accuracy. No statistical difference in diagnostic performance was found between the different ROI's for the greatest AUC-values of the highest performing Mean-E and Max-E (P = 0.250). Comparison of the 3 mm ROI

between the sagittal and longitudinal planes resulted in a significantly greater number of false negative LNs in the sagittal plane (P = 0.002).

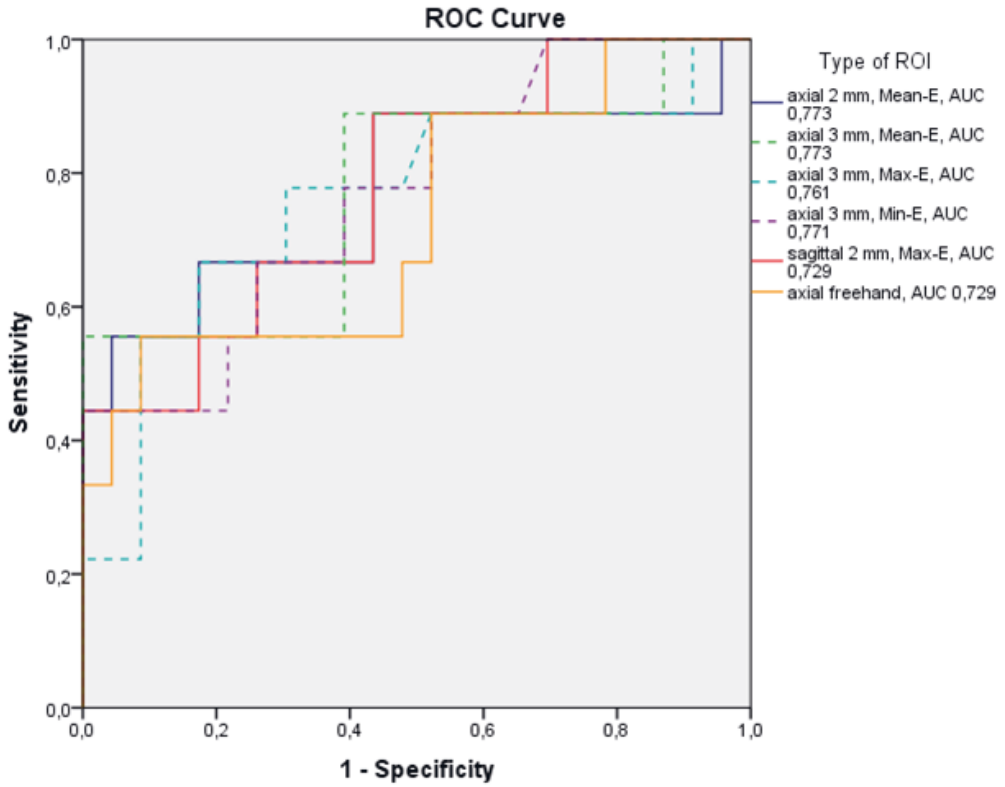

Figure 9. Receiver operating characteristic curves of the highest performing ROIs. Axially placed 2 mm and 3 mm ROIs yielded the highest results from the different ROI sizes with Mean-E and 3 mm Max-E (Study II)

5.3 IMAGING OF SUPERFICIAL LYMPHATIC VESSELS OF THE UPPER LIMB WITH CEUS

Upper limbs from 30 healthy volunteers were examined with CEUS using intradermal injection of Sonazoid® (Figure 10). The technical success rate of the intradermal injection was 98.3 % (59/60). Depending on the injection two kinds of contrast enhancement patterns were registered. In type A (n = 34), a distinct and pronounced enhancement was observed in the

superficial lymphatic vessels corresponding to fast enhancement times. Type B (n = 25) corresponded to longer enhancement times and a perceptible but somewhat weaker enhancement in the superficial lymphatic vessels.

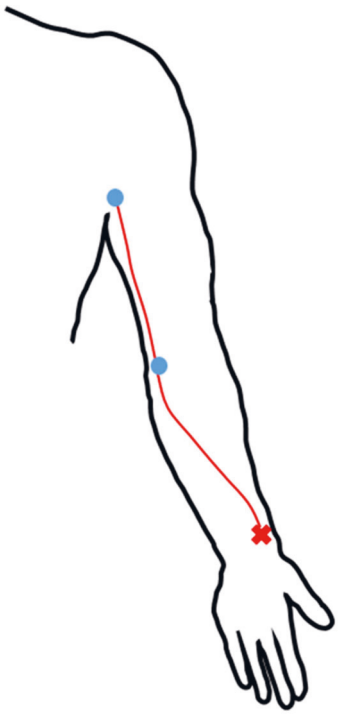

Figure 10. Schematic drawing of the enhancing lymphatic vessel route in the upper extremity. Red cross indicates the injection site in the distal antebrachium, whereas the red line demonstrates the enhancing lymphatic route assessed by CEUS. Blue dots indicate the location of enhancing LNs at the antecubital fossa and axilla (Study III).

No statistical difference was found in the enhancement times from injection site to the left and right antecubital fossa (15 sec / 18 sec, *P* = 0.863) or axilla (66 sec / 77 sec, *P* = 0.581). Neither the BMI nor the age of volunteers affected the outcome. A slight statistical difference was observed between genders in the median enhancement time in the left antecubital fossa (females 12 sec / males 20 sec, *P* = 0.029) although no

unequivocal explanation was found for this. The type of successful intradermal injection had a substantial effect on the enhancement times (Table 5).

Table 5. Effect of different parameters on the enhancement time. Enhancement type A indicates a successful intradermal injection with strong visual enhancement, whereas type B refers to a partially successful injection with moderate enhancement. Enhancement times in the Table represent median values at the antecubital fossa and axilla (Study III).

			Enhancement time (s) Median (interquartile range)			
Parameter		**Number**	**Antecubital fossa**		**Axilla**	
			Right	**Left**	**Right**	**Left**
Sex	Males	16	15 (10–31)	20 (13–25)	57 (31–120)	98 (52–133)
	Females	14	19 (12–25)	12 (9–21)	81 (42–116)	49 (31–96)
	P		0.455	0.029	0.583	0.070
Age (years)	< 40	18	18 (11–34)	19 (11–29)	77 (33–123)	92 (49–147)
	> 40	12	18 (11–25)	15 (12–24)	77 (32–109)	50 (37–95)
	P		0.929	0.484	0.825	0.086
Body mass index	< 25	16	19 (13–33)	17 (11–23)	80 (40–123)	69 (39–133)
	> 25	14	14 (11–25)	14 (12–35)	57 (28–99)	63 (44–112)
	P		0.256	0.546	0.111	0.884
		Right + Left				
Enhancement type	A	15+19 = 34	12 (9–20)	13 (10–19)	36 (29–49)	50 (32–70)
	B	14+11 = 25	25 (18–46)	25 (20–34)	118 (88–134)	126 (95–191)
	P		0.001	0.007	0.000	0.000

Additional testing with different volumes of CA (0.1 mL and 0.3 mL) and injection sites in the hand was performed with five volunteers. Superficial lymphatic vessels were visualized with both different test volumes and enhancing lymphatic vessels from other injection sites led to the same visualization of the main lymphatic pathway as from the main injection site.

No adverse effects were reported from the intradermal injection of Sonazoid® CA.

6 DISCUSSION

The lymphatic system has been poorly understood for a long time from a clinical point of view despite its important role in human tissue homeostasis. From a radiological perspective, until recently, the techniques for acquiring images and assessing the function of the lymphatic system have been limited mainly to conventional lymphography and lymphoscintigraphy. Even though new modalities are available (MRI) and imaging methods (ICG) have been developed, these are either time consuming, expensive or are demanging of human resources. Thus, the field of radiology still lacks economical and effective imaging techniques for evaluating the vast number of patients with potential problems in their lymphatic system.

Gray-scale US has traditionally been used to evaluate superficial LNs as a part of the lymphatic system. Such evaluation has been typically based on LN size, morphological features and Doppler patterns in order to differentiate between benign and malignant LN's (91,97). However, new US applications have been introduced during the last few decades, offering new techniques for exploring the lymphatic system. Numerous studies have used US SWE for identifying LN's with malignant deposits (8). In clinical practice, CEUS is mainly used for characterization of various solid lesions, for example in liver and breast tissue, as well as for US-guided interventions (128,180,181). More recently, it has been successfully used to increase diagnostic confidence in characterization of cervical LN's (182), in the detection of axillary SLN's in breast cancer and in predicting preoperative axillary status (10,136,183). Recent studies indicate that US may provide a readily available, cost-effective and fast tool in the field of lymphatic imaging. However, many aspects concerning the lymphatic system still remain unanswered. This study has focused particularly on some of the new US techniques in lymphatic imaging and on the development of new US-based methods in response to clinical demands.

6.1 US-BASED ASSESSMENT OF INGUINAL LYMPH NODES

In many disciplines of cancer surgery, it is crucial to detect and evaluate the status of SLN's for accurate staging. Lymphoscintigraphy has shown a success rate of greater than 90 % and a detection rate of 94 – 97 % of SLN's in vulvar and breast cancers (184,185). In addition, the CEUS procedure for identifying SLN's in breast cancer has shown a 89 % success rate (66). A recent meta-analysis has shown diagnostic sensitivity and specificity of 86 % and 89 %, respectively for the CEUS SLN procedure in breast cancer (186). Compared to the aforementioned diagnostic figures our preliminary results of inguinal SLN detection with CEUS in vulvar cancer are encouraging. Although only a relatively limited number of patients could be recruited, due the study being based at a single center and because of the low incidence of the disease, the procedure was successful in the detection of enhancing potential SLN's in 94.7 % of cases. The degree of concordance between CEUS-enhanced SLN's and lymphoscintigraphy and/or Patent Blue dye was 81.2 %. Additionally, CEUS found enhancing SLNs in two cases where other methods had failed to do so. Previously, it has been reported that Patent blue has a lower detection rate (69 %) of SLN's (184) than those found in the present study. Furthermore, lymphoscintigraphy was not done on all patients since SLN procedure in recurrent disease in still under investigation (155). Although further studies are warranted to confirm the results reported here for the detection of SLNs in the inguinal regions, the CEUS procedure success rate similar to that reported in breast cancer. The detection rate also approaches the detection rate of the conventional reference method, lymphoscintigraphy.

Special attention must be given in the case of midline vulvar tumors since these tumors may have a more complex lymphatic drainage than the lateral left or right sided tumors. Furthermore, lymphatics vessels may drain into deep LN's including the obturator, or to deep internal iliac LNs or to the femoral annulus in addition to the superficial inguinal LN's (166). This variation must be taken into account if an enhancing lymphatic pathway leading to deeper levels is detected and where LN's cannot be

marked preoperatively with guidewires. Since intraoperative use of CEUS may offer the same information as other imaging modalities, further studies are warranted.

The CEUS method has now proven to be feasible in the detection of SLN's in superficial regions of the body such as the axilla and inguinal region. Therefore, it could potentially be applied in the detection of SLN's in other cancers with superficially localized SLN's. Accordingly, small trials in animal melanoma models have been published (145,187). It has also been suggested that the CEUS method could offer further assistance in detecting superficial SLN's in penile cancer (188). So far however, no scientific articles on this subject have been published.

ICG alone or combined with ^{99m}Tc-nanocolloid as a hybrid tracer has emerged as a complementary or alternative method to lymphoscintigraphy for intraoperative visualization of SLN's in vulvar and other cancers (189–191). As with the CEUS procedure, ICG-imaging contrasts with lymphoscintigraphy in that it produces real-time data. Since the fluorescent light wavelength used in ICG cannot be seen with the naked eye, the method requires a special NIR-camera. ICG is injected peritumorally approximately 30 minutes before the operation. Therefore, unlike CEUS, it does not possess real time visibility or instant repeatability. Moreover, the ICG tracer may spread to multiple LN's in the lymphatic chain as in lymphoscintigraphy, obscuring the detection of the first enhancing SLN (192). Hybrid tracers also suffer from the same drawbacks as conventional lymphoscintigraphy where injections are administrated several hours before surgery. Furthermore, ICG-imaging uses wavelengths in the NIR spectrum, resulting in a limited penetration depth of 5 – 8 mm. Therefore, surgical incisions are needed to follow the course of the ICG whereas CEUS can be detected at greater depths without excessive surgery.

The next step improving US-based SLN procedures in vulvar cancer could be the intraoperative use of the method by the operating surgeons. Alternatively, intradermal perfluorobutane CA injection could potentially be made hours before the surgery. The operating surgeon is able to localize the SLN intraoperatively due to the affinity of the CA to the

reticuloendothelial system. It has been shown that perfluorobutane has prolonged enhancement (up to 4 hours) in the LN's after an intradermal injection (193). As a consequence of these results, we examined five of the enhancing LN's from the healthy volunteers 20 hours after the injection and found that the LN's were still faintly visible (unpublished observations). These results are consistent with axillary SLN's after subdermal perfluorobutane injections in the breast area with healthy volunteers (194).

To summarize, the US-based SLN procedure offers several advantages in the detection of SLN's when compared to existing traditional imaging methods. In practice, USCA's have been shown to have minimal contraindications (137). Furthermore, CEUS procedure is a minimally invasive, cost-effective, readily available, fast and repeatable technique that, unlike techniques that use radiotracers, does not need precautions.

6.2 SHEAR WAVE ELASTOGRAPHY AND SELECTION OF OPTIMAL ROI

Although recommendations concerning SWE have been published for many organs and the method has been investigated in different scenarios, SWE has thus far only been recognized as a potential additional tool for differentiating between benign and malignant LN's (130). Unlike diseases of the liver, where detailed information is available on how to perform elastography investigations (195), there are no such guidelines for the evaluation of LN's, nor has the optimal ROI size for SWE-measurements of the LN's been investigated. Numerous ROI sizes and shapes have been used to differentiate between benign and malignant masses. In most studies, a 2 – 3 mm ROI centered on the stiffest part of the lesion has been used (196,197). In this study we demonstrated that a 3 mm ROI centered on the cortex in the axial plane resulted in the best reproducibility for LN measurements. Factors like ROI size and imaging plane significantly affected the reproducibility, in contrast to the 2D-SWE with the liver, where the ROI size seemed to have only a minor effect (198).

Increase in ROI size led to higher ICC-values in axial and sagittal planes of the LN although the axial plane yielded higher ICC-values. In general, since the LN's are small, the use of five ROIs with equal spacing easily results in overlapping with larger ROI sizes, leading to higher ICC-values. The positioning of ROI should be located on the cortex of the LN; otherwise hilar fat included in the measurements decreases the SWE values and hampers discrimination between benign and malignant LN's. It has previously been reported that normal mean cortical thickness in inguinal LNs varies between 1 – 2 mm (199). We also observed that cortical thickness ≤ 3 mm or > 3 mm had a significant influence on the reproducibility (P = 0.004) and reproducibility remained good to excellent with Mean-E and Max-E (0.85 – 0.97) for all ROI sizes. However, no obvious explanation was found for the reason behind lower ICC-values of the sagittal plane. As expected, potential malignancy of the LN's had a significant impact on the SWE-values (P = 0.004). The occurance of higher ICC-values with all ROIs in the malignant LN's is probably due to the fact that malignant LN's have a thicker cortex, allowing easier placement of the ROIs and without influence the of the hilar fat in the SWE values.

Smaller ROI's in general resulted in lower ICC-values, reflecting the heterogeneity of the tissue; accordingly, avoidance of the smallest ROIs (< 2 mm) is recommended. However, previous studies with LN's and tumors have shown that a 2 – 3 mm ROI centered on the stiffest part of the investigated tissue results in the best differentiation. Our results confirmed that an ROI size of 2 – 3 mm resulted in the most consistent reproducibility of measurements (200–203). The cut-off values for differentiating between benign and malignant LN's were lower than those found in previous studies of cervical LN's (8,202,203). The observed difference may be due to the placement of the ROIs. Moreover, due to technical problems with software updates, it was not possible to apply all of the elasticity indices, including commonly used Emax.

The depth of the LN or its distance from the femoral artery did not exert a significant effect on the reproducibility of results. However, in phantom studies the reliability of the SWE has been found to be reduced, especially

with hard lesions deeper than 2 cm (109,110). Since inguinal and other superficial LN's are normally located near the skin, no reduction in reproducibility was found in the present study for LN's with a median depth of 1.5 cm.

6.3 CONTRAST-ENHANCED ULTRASOUND IN THE VISUALIZATION OF THE SUPERFICIAL LYMPHATIC VESSELS

In agreement with the SLN studies using lymphoscintigraphy and CEUS for axillary LN's (66,185,204) and the results of Study I, the technical success rate of the intradermal injections in Study III was high (98.3 %), thus demonstrating that the technique is easy to implement for the visualization of superficial lymphatics. Despite the successful intradermal injection two kinds of enhancement patterns were discovered. A fast and strong enhancement was classified as type A enhancement, whereas type B corresponded to a slower enhancement time and reduced enhancement. No indications of distinctly different enhancement patterns were found as a result of this injection technique. Sometimes the injection of the CA spread to a larger area beneath the skin surface in Type B enhancement, in contrast to a typical blister-like spot produced in Type A intradermal injection. Thus, a portion of the CA may have spread into the dermis and beneath the superficial fascia into the upper subcutis. This should be considered when interpreting different enhancement patterns. Consistent with our Type A results for faster enhancement time and strong enhancement, it has previously been found that an increase in the velocity of CA led to a better contrast-to-tissue ratio (CTR) (205). Furthermore, it has been shown that optimizing motion correction and using a higher imaging frame rate results in increased CTR (205). This approach could improve the visibility of Type B enhancement. However, the safe and minimally invasive nature of the CEUS procedure the intradermal injections means that it can be repeatedly used to achieve the Type A enhancement pattern. In future studies these different patterns could be quantified more accurately with

time-intensity curve programs such as those provided by the newest US-devices.

Nevertheless, the CEUS procedure was found to be feasible and fast for visualizing superficial lymphatic vessels in the upper limb with enhancement detected in the axillary region after a median time of 75 sec following injection. Thus, the CEUS enhancement time is remarkably rapid compared to the longer mean scan times of 81 min for CE MRI lymphangiography (206), 30 min for ICG to reach antecubital fossa (207) or up to 4 - 48 hours for lymphoscintigraphy (208). Nevertheless, the reason, why US-based CA is significantly faster than these other methods remains unknown. No common factors have been identified, such as binding of CA into albumin, which could account for the phenomenon (208–212). Although the particles applied in USCA's are small (2 – 7 µm) (213,214), they are still appreciably larger than those used in the previous techniques (215–217). It is possible that the size and coating material of the particle play a role in the velocity of the CA in lymphatic vessels. For comparison, the particle size did not affect the uptake rate of CA into the lymphatic vessels in animal studies (218). Although injection pressure did affect the uptake rate, it did not result in greater net velocity.

Further studies are needed to investigate the CEUS method in healthy volunteers and in persons with different lymphatic disorders. The ability of the method to visualize signs related to lymphedema, such as dermal backflow should be evaluated and the lymphatic routes and enhancement times should be compared between patients with lymphedema and healthy individuals. The method also has the potential to visualize and assess superficial lymphatic vessels in other regions of the body.

In the present study we used perfluorobutane as the CA since we assumed that the enhancement time would be longer and perfluorobutane could be more durable than the commonly used sulphurhexafluoride (219). Since the enhancement time of the perfluorobutane was fast, the lifespan of the sulphurhexafluoride particle should also be sufficient for visualizing superficial lymphatic vessels. Additionally, sulphurhexafluoride

has proven to be effective in visualizing the superficial lymphatic vessels in breast cancer SLN studies (66,136,186).

6.4 LIMITATIONS

The present studies do have some limitations. The vulvar cancer population in Study I is quite small due to the study having been undertaken in a single center study and also because of the rarity of the diagnosis. Despite the small population, we nevertheless considered it justified to publish these preliminary encouraging results. Further studies with a larger number of patients are clearly necessary to validate the method. Although the majority of patients had traditional lymphoscintigraphy done for the localization of the SLN, the investigation was not performed in all patients, which potentially affected the assessment between CEUS and lymphoscintigraphy.

Although reproducibility was successfully studied, Study II also had a relatively small cohort of patients. This study included patients with different background diseases. The number of patients with malignant LN's nevertheless remained small which may have affected the SWE results. Additionally, some measurements of elasticity indices were missed due to technical difficulties with the US device. This may have resulted in lower cut-off values for malignant LN's since it was not possible to include in the results the commonly used Emax, with maximum elasticity value derived from a single pixel in the ROI. Therefore, the cut-off values for differentiating benign and malignant inguinal LNs should be studied further in larger populations.

Study III was performed by one investigator and therefore the reproducibility of the results should be tested by several operators in further studies. However, since the method had previously proven to be successful in SLN studies we were confident with the results and published them after the pilot study.

6.5 FUTURE PERSPECTIVES

Study I showed that the CEUS SLN procedure is able to detect superficially located SLN's in the inguinal region, in addition to former axillary studies. Thus, the method could be used in other unexplored superficial regions as well. Additionally, avenues of intraoperative use in locating SLN in even deeper locations could be explored. Moreover, reticuloendothelial affinity of the perfluorobutane could also enable injection prior to surgery and provide location of the SLN intraoperatively.

2D-SWE provides a new noninvasive tool for more accurate assessment of LN's. Study II demonstrated the optimal ROI size of 3 mm in the axial plane for inguinal LN SWE measurements. However, at present it is not clear whether this is valid for all superficially located LN regions. Additionally, cut-off values for predicting malignant LN's in inguinal LN's should be studied further with all common elasticity indices.

CEUS with intradermal injection of the USCA proved to be effective in visualizing lymphatic vessels in the upper limbs of healthy volunteers. Accordingly, the method should be applicable for visualizing superficial lymphatic vessels in other regions although further studies are needed. The current pilot study was performed with perfluorobutane. However, due to marketing licenses this USCA is not available for general use in many countries and the more widely available sulphurhexafluoride should be studied for the same purpose. Further studies are needed to test the feasibility of the method in patients with lymphatic disorders to see if the enhancement times differ and whether the method can detect abnormal patterns, such as like dermal backflow.

7 CONCLUSIONS

Based on the results of the present study the following conclusions can be drawn:

1. Contrast-enhanced ultrasound is feasible for locating superficial sentinel lymph nodes in vulvar cancer and the method appears to be comparable to traditional lymphoscintigraphy (I).

2. Shear wave elastography is reproducible in inguinal LNs. In comparisons between different ROI sizes, a 3 mm circular ROI in the axial plane centered on the cortex proved to be optimal for LN elastography measurements (II).

3. The US-based technique with intradermal injection of the USCA is a feasible, fast and minimally invasive method for visualizing the superficial lymphatic vessels in the upper limb (III).

REFERENCES

1. Crane-Okada R, Wascher RA, Elashoff D, Giuliano AE. Long-term morbidity of sentinel node biopsy versus complete axillary dissection for unilateral breast cancer. Ann Surg Oncol. 2008 Jul;15(7):1996–2005.

2. Van Der Zee AGJ, Oonk MH, De Hullu JA, Ansink AC, Vergote I, Verheijen RH, et al. Sentinel node dissection is safe in the treatment of early-stage vulvar cancer. Journal of Clinical Oncology. 2008;26(6).

3. Liao S, Padera TP. Lymphatic Function and Immune Regulation in Health and Disease. Lymphat Res Biol. 2013 Sep;11(3):136–43.

4. Grada AA, Phillips TJ. Lymphedema: Pathophysiology and clinical manifestations. Journal of the American Academy of Dermatology. 2017;77(6).

5. Garza R, Skoracki R, Hock K, Povoski SP. A comprehensive overview on the surgical management of secondary lymphedema of the upper and lower extremities related to prior oncologic therapies. BMC Cancer. 2017;17(1).

6. Rockson SG, Keeley V, Kilbreath S, Szuba A, Towers A. Cancer-associated secondary lymphoedema. Nature Reviews Disease Primers. 2019;5(1).

7. Cormier JN, Askew RL, Mungovan KS, Xing Y, Ross MI, Armer JM. Lymphedema beyond breast cancer: a systematic review and meta-analysis of cancer-related secondary lymphedema. Cancer. 2010 Nov 15;116(22):5138–49.

8. Suh CH, Choi YJ, Baek JH, Lee JH. The diagnostic performance of shear wave elastography for malignant cervical lymph nodes: A systematic review and meta-analysis. European Radiology. 2017;27(1).

9. Sever A, Jones S, Cox K, Weeks J, Mills P, Jones P. Preoperative localization of sentinel lymph nodes using intradermal microbubbles

and contrast-enhanced ultrasonography in patients with breast cancer. British Journal of Surgery. 2009;96(11).

10. Sever AR, Mills P, Jones SE, Mali W, Jones PA. Sentinel node identification using microbubbles and contrast-enhanced ultrasonography. Clinical Radiology. 2012;67(7).

11. Niebling MG, Pleijhuis RG, Bastiaannet E, Brouwers AH, Van Dam GM, Hoekstra HJ. A systematic review and meta-analyses of sentinel lymph node identification in breast cancer and melanoma, a plea for tracer mapping. European Journal of Surgical Oncology. 2016;42(4).

12. Miseré RML, Wolfs JAGN, Lobbes MBI, van der Hulst RRWJ, Qiu SS. A systematic review of magnetic resonance lymphography for the evaluation of peripheral lymphedema. Journal of Vascular Surgery: Venous and Lymphatic Disorders. 2020;8(5).

13. Mills M, van Zanten M, Borri M, Mortimer PS, Gordon K, Ostergaard P, et al. Systematic Review of Magnetic Resonance Lymphangiography From a Technical Perspective. Journal of Magnetic Resonance Imaging. 2021;53(6).

14. Xiong L, Gazyakan E, Yang W, Engel H, Hünerbein M, Kneser U, et al. Indocyanine green fluorescence-guided sentinel node biopsy: A meta-analysis on detection rate and diagnostic performance. European Journal of Surgical Oncology. 2014;40(7).

15. Parkin J, Cohen B. An overview of the immune system. The Lancet. 2001 Jun 2;357(9270):1777–89.

16. Yatim KM, Lakkis FG. A brief journey through the immune system. Clin J Am Soc Nephrol. 2015 Jul 7;10(7):1274–81.

17. Skobe M, Detmar M. Structure, function, and molecular control of the skin lymphatic system. In: Journal of Investigative Dermatology Symposium Proceedings. 2000.

18. Hsu MC, Itkin M. Lymphatic Anatomy. Tech Vasc Interv Radiol. 2016 Dec;19(4):247–54.

19. Breslin JW, Yang Y, Scallan JP, Sweat RS, Adderley SP, Murfee WL. Lymphatic vessel network structure and physiology. Comprehensive Physiology. 2019;9(1).

20. Moore JE, Bertram CD. Lymphatic System Flows. Annual Review of Fluid Mechanics. 2018;50.

21. Polomska AK, Proulx ST. Imaging technology of the lymphatic system. Advanced Drug Delivery Reviews. 2021;170.

22. Levick JR, Michel CC. Microvascular fluid exchange and the revised Starling principle. Cardiovascular Research. 2010;87(2).

23. Santambrogio L. Chapter Four - The Lymphatic Fluid. In: Galluzzi L, editor. International Review of Cell and Molecular Biology. Academic Press; 2018. p. 111–33.

24. Hansen KC, D'Alessandro A, Clement CC, Santambrogio L. Lymph formation, composition and circulation: a proteomics perspective. International Immunology. 2015 May 1;27(5):219–27.

25. Hampton HR, Chtanova T. Lymphatic Migration of Immune Cells. Front Immunol. 2019;10:1168.

26. Morris B. The Exchange of Protein Between the Plasma and the Liver and Intestinal Lymph. Quarterly Journal of Experimental Physiology and Cognate Medical Sciences. 1956;41(3).

27. Edwards JM. Lymphatics, Lymph and the Lymphomyeloid Complex. Joseph Mendel Yoffey , Frederick Colin Courtice. The Quarterly Review of Biology. 1972;47(1).

28. Jessen NA, Munk ASF, Lundgaard I, Nedergaard M. The Glymphatic System – A Beginner's Guide. Neurochem Res. 2015 Dec;40(12):2583–99.

29. Mestre H, Mori Y, Nedergaard M. The brain's glymphatic system: current controversies. Trends in neurosciences. 2020 Jul;43(7):458.

30. Suami H, Scaglioni MF. Anatomy of the Lymphatic System and the Lymphosome Concept with Reference to Lymphedema. Seminars in Plastic Surgery. 2018;32(1).

31. Bujoreanu I, Gupta V. Anatomy, Lymph Nodes. In: StatPearls. Treasure Island (FL): StatPearls Publishing; 2022

32. Willard-Mack CL. Normal Structure, Function, and Histology of Lymph Nodes. Toxicologic Pathology. 2006;34(5).

33. Suami H. Lymphosome concept: Anatomical study of the lymphatic system. J Surg Oncol. 2017 Jan;115(1):13–7.

34. Hara H, Mihara M. Classification of the lymphatic pathways in each lymphosome based on multi-lymphosome indocyanine green lymphography: Saphenous, calf, and thigh (SCaT) classification. Journal of Plastic, Reconstructive and Aesthetic Surgery. 2021;74(11).

35. Hara H, Mihara M. Multilymphosome injection indocyanine green lymphography can detect more lymphatic vessels than lymphoscintigraphy in lymphedematous limbs. J Plast Reconstr Aesthet Surg. 2020 Jun;73(6):1025–30.

36. Brouillard P, Witte MH, Erickson RP, Damstra RJ, Becker C, Quéré I, et al. Primary lymphoedema. Nat Rev Dis Primers. 2021 Oct 21;7(1):77.

37. Warren AG, Brorson H, Borud LJ, Slavin SA. Lymphedema: A comprehensive review. Annals of Plastic Surgery. 2007;59(4).

38. Chance-Hetzler J, Armer J, Van Loo M, Anderson B, Harris R, Ewing R, et al. Prospective lymphedema surveillance in a clinic setting. Journal of Personalized Medicine. 2015;5(3).

39. Gillespie TC, Sayegh HE, Brunelle CL, Daniell KM, Taghian AG. Breast cancer-related lymphedema: Risk factors, precautionary measures, and treatments. Gland Surgery. 2018;7(4).

40. DiSipio T, Rye S, Newman B, Hayes S. Incidence of unilateral arm lymphoedema after breast cancer: A systematic review and meta-analysis. The Lancet Oncology. 2013;14(6).

41. Poodt IGM, Spronk PER, Vugts G, van Dalen T, Peeters MTFDV, Rots ML, et al. Trends on Axillary Surgery in Nondistant Metastatic Breast Cancer Patients Treated Between 2011 and 2015: A Dutch Population-based Study in the ACOSOG-Z0011 and AMAROS Era. Ann Surg. 2018 Dec;268(6):1084–90.

42. De Vrieze T, Nevelsteen I, Thomis S, De Groef A, Tjalma WAA, Gebruers N, et al. What are the economic burden and costs associated with the treatment of breast cancer-related lymphoedema? A systematic review. Support Care Cancer. 2020 Feb;28(2):439–49.

43. Gutknecht M, Herberger K, Klose K, Purwins S, Dietz D, Blome C, et al. Cost-of-illness of patients with lymphoedema. J Eur Acad Dermatol Venereol. 2017 Nov;31(11):1930–5.

44. Guermazi A, Brice P, Hennequin C, Sarfati E. Lymphography: An Old Technique Retains Its Usefulness. Radiographics. 2003;23(6).

45. Moussa AM, Maybody M, Santos E, Gonzalez-Aguirre AJ. Intranodal Lymphangiography and Lymphatic Embolization for Management of Iatrogenic Chylous Ascites in Children. Lymphat Res Biol. 2021 Dec;19(6):531–8.

46. Jardinet T, Veer HV, Nafteux P, Depypere L, Coosemans W, Maleux G. Intranodal Lymphangiography With High-Dose Ethiodized Oil Shows Efficient Results in Patients With Refractory, High-Output Postsurgical Chylothorax: A Retrospective Study. American Journal of Roentgenology. 2021 Aug;217(2):433–8.

47. Wiljasalo S. Lymphographic polymorphism in Hodgkin's disease. Correlation of lymphography to histology and duration. Acta radiologica: diagnosis. 1968;

48. Wiljasalo S. Follow up and relymphography in Hodgkin's disease. Strahlentherapie. 1974;147(3).

49. Wiljasalo M. Lymphographic differential diagnosis of neoplastic diseases. Acta radiologica: diagnosis. 1965;

50. Soimakallio S. Lymphography in Urological Oncology [Thesis]. Kuopio University Hospital; 1978.

51. Threefoot SA, Kent WT, Hatchett BF. Lymphaticovenous and lymphaticolymphatic communications demonstrated by plastic corrosion models of rats and by postmortem lymphangiography in man. The Journal of laboratory and clinical medicine. 1963;61.

52. Yoshida RY, Kariya S, Ha-Kawa S, Tanigawa N. Lymphoscintigraphy for Imaging of the Lymphatic Flow Disorders. Techniques in Vascular and Interventional Radiology. 2016;19(4).

53. Kretschmer L, Altenvoerde G, Meller J, Zutt M, Funke M, Neumann C, et al. Dynamic lymphoscintigraphy and image fusion of SPECT and pelvic CT-scans allow mapping of aberrant pelvic sentinel lymph nodes in malignant melanoma. European Journal of Cancer. 2003;39(2).

54. Koizumi M, Koyama M. Comparison between single photon emission computed tomography with computed tomography and planar scintigraphy in sentinel node biopsy in breast cancer patients. Annals of Nuclear Medicine. 2019;33(3).

55. Collarino A, Fuoco V, Garganese G, Pereira Arias-Bouda LM, Perotti G, Manca G, et al. Lymphoscintigraphy and sentinel lymph node biopsy in vulvar carcinoma: update from a European expert panel. European Journal of Nuclear Medicine and Molecular Imaging. 2020;47(5).

56. Tardelli E, Mazzarri S, Rubello D, Gennaro M, Fantechi L, Duce V, et al. Sentinel lymph node biopsy in cutaneous melanoma standard and new technical procedures and clinical advances. A systematic review of the literature. Clinical Nuclear Medicine. 2016;41(12).

57. Cheng G, Kurita S, Torigian DA, Alavi A. Current status of sentinel lymph-node biopsy in patients with breast cancer. European Journal of Nuclear Medicine and Molecular Imaging. 2011;38(3).

58. Patel S, Hur S, Khaddash T, Simpson S, Itkin M. Intranodal CT Lymphangiography with Water-soluble Iodinated Contrast Medium for Imaging of the Central Lymphatic System. Radiology. 2022;302(1).

59. Tanahashi Y, Iwasaki R, Shoda S, Kawada H, Ando T, Takasu M, et al. Dynamic contrast-enhanced computed tomography lymphangiography with intranodal injection of water-soluble iodine contrast media in microminipig: imaging protocol and feasibility. European Radiology. 2020;30(11).

60. Itkin M, Nadolski GJ. Modern Techniques of Lymphangiography and Interventions: Current Status and Future Development. CardioVascular and Interventional Radiology. 2018;41(3).

61. Rautiainen S, Könönen M, Sironen R, Masarwah A, Sudah M, Hakumäki J, et al. Preoperative axillary staging with 3.0-T breast MRI: clinical value of diffusion imaging and apparent diffusion coefficient. PLoS One. 2015;10(3):e0122516.

62. Gong X, Guo Y, Zhu T, Peng X, Xing D, Zhang M. Diagnostic performance of radiomics in predicting axillary lymph node metastasis in breast cancer: A systematic review and meta-analysis. Front Oncol. 2022;12:1046005.

63. Zhou P, Wei Y, Chen G, Guo L, Yan D, Wang Y. Axillary lymph node metastasis detection by magnetic resonance imaging in patients with breast cancer: A meta-analysis. Thorac Cancer. 2018 Aug;9(8):989–96.

64. Ruehm SG, Schroeder T, Debatin JF. Interstitial MR lymphography with gadoterate meglumine: Initial experience in humans. Radiology. 2001;220(3).

65. Arrivé L, Derhy S, Dahan B, El Mouhadi S, Monnier-Cholley L, Menu Y, et al. Primary lower limb lymphoedema: classification with non-contrast MR lymphography. European Radiology. 2018;28(1).

66. Sever AR, Mills P, Jones SE, Cox K, Weeks J, Fish D, et al. Preoperative sentinel node identification with ultrasound using microbubbles in

patients with breast cancer. American Journal of Roentgenology. 2011;196(2).

67. Rane S, Donahue PMC, Towse T, Ridner S, Chappell M, Jordi J, et al. Clinical feasibility of noninvasive visualization of lymphatic flow with principles of spin labeling MR imaging: Implications for lymphedema assessment. Radiology. 2013;269(3).

68. Zhou GX, Chen X, Zhang JH, Zhu JQ, Wang YB, Wang ZQ. MR lymphangiography at 3.0 Tesla to assess the function of inguinal lymph node in low extremity lymphedema. Journal of Magnetic Resonance Imaging. 2014;40(6).

69. Bae JS, Yoo RE, Choi SH, Park SO, Chang H, Suh M, et al. Evaluation of lymphedema in upper extremities by MR lymphangiography: Comparison with lymphoscintigraphy. Magnetic Resonance Imaging. 2018;49.

70. Strobl FF, Weiss M, Wallmichrath J, Baumeister R, Reiser MF, Notohamiprodjo M. [MR lymphangiography for assessment of focal dermal backflow for presurgical work-up in patients with peripheral lymphoedema]. Handchir Mikrochir Plast Chir. 2012;44(6).

71. Notohamiprodjo M, Weiss M, Baumeister RG, Sommer WH, Helck A, Crispin A, et al. MR lymphangiography at 3.0 T: Correlation with lymphoscintigraphy. Radiology. 2012;264(1).

72. Fox IJ, Wood EH. Indocyanine green: physical and physiologic properties. Mayo Clinic proceedings Mayo Clinic. 1960;35.

73. Carski TR, Staller BJ, Hepner G, Banka VS, Finney RA. Adverse Reactions After Administration of Indocyanine Green. JAMA: The Journal of the American Medical Association. 1978;240(7).

74. Hope-Ross M, Yannuzzi LA, Gragoudas ES, Guyer DR, Slakter JS, Sorenson JA, et al. Adverse Reactions due to Indocyanine Green. Ophthalmology. 1994;101(3).

75. Owens SL. Indocyanine green angiography. British Journal of Ophthalmology. 1996;80(3).

76. Hyvärinen L, Flower RW. Indocyanine Green Fluorescence Angiography. Acta Ophthalmologica. 1980;58(4).

77. Kitai T, Inomoto T, Miwa M, Shikayama T. Fluorescence navigation with indocyanine green for detecting sentinel lymph nodes in breast cancer. Breast Cancer. 2005;12(3).

78. Troyan SL, Kianzad V, Gibbs-Strauss SL, Gioux S, Matsui A, Oketokoun R, et al. The FLARE™ intraoperative near-infrared fluorescence imaging system: A first-in-human clinical trial in breast cancer sentinel lymph node mapping. Annals of Surgical Oncology. 2009;16(10).

79. Zelken JA, Tufaro AP. Current Trends and Emerging Future of Indocyanine Green Usage in Surgery and Oncology: An Update. Annals of Surgical Oncology. 2015;22.

80. Ito R, Wu CT, Lin MCY, Cheng MH. Successful treatment of early-stage lower extremity lymphedema with side-to-end lymphovenous anastomosis with indocyanine green lymphography assisted. Microsurgery. 2016;36(4).

81. Unno N, Inuzuka K, Suzuki M, Yamamoto N, Sagara D, Nishiyama M, et al. Preliminary experience with a novel fluorescence lymphography using indocyanine green in patients with secondary lymphedema. Journal of Vascular Surgery. 2007;45(5).

82. Yoon JA, Shin MJ, Shin YB, Kim K, Park H, Kang T, et al. Correlation of ICG lymphography and lymphoscintigraphy severity stage in secondary upper limb lymphedema. Journal of Plastic, Reconstructive and Aesthetic Surgery. 2020;73(11).

83. Akita S, Mitsukawa N, Kazama T, Kuriyama M, Kubota Y, Omori N, et al. Comparison of lymphoscintigraphy and indocyanine green lymphography for the diagnosis of extremity lymphoedema. Journal of Plastic, Reconstructive and Aesthetic Surgery. 2013;66(6).

84. Yoon JA, Shin MJ, Kim JH. Indocyanine green lymphography and lymphoscintigraphy severity stage showed strong correlation in lower limb lymphedema. Lymphatic Research and Biology. 2021;19(1).

85. Kaproth-Joslin KA, Nicola R, Dogra VS. The history of US: From bats and boats to the bedside and beyond. Radiographics. 2015;35(3).

86. Hasegawa H. Advances in ultrasonography: image formation and quality assessment. Journal of Medical Ultrasonics. 2021;48(4).

87. Li J, Ma Y, Zhang T, Shung KK, Zhu B. Recent Advancements in Ultrasound Transducer: From Material Strategies to Biomedical Applications. BME Frontiers. 2022 May 12;2022:1–19.

88. Hayashi A, Visconti G, Giacalone G, Hayashi N, Yoshimatsu H. Recent Advances in Ultrasound Technology: Ultra-High Frequency Ultrasound for Reconstructive Supermicrosurgery. Journal of Reconstructive Microsurgery. 2022;38(3).

89. Izzetti R, Vitali S, Aringhieri G, Nisi M, Oranges T, Dini V, et al. Ultra-High Frequency Ultrasound, A Promising Diagnostic Technique: Review of the Literature and Single-Center Experience. Canadian Association of Radiologists Journal. 2021;72(3).

90. Ahuja AT, Ying M, Ho SY, Antonio G, Lee YP, King AD, et al. Ultrasound of malignant cervical lymph nodes. Cancer Imaging. 2008;8(1).

91. Dudea SM, Lenghel M, Botar-Jid C, Vasilescu D, Duma M. Ultrasonography of superficial lymph nodes: Benign vs. malignant. Medical Ultrasonography. 2012;14(4).

92. Stachs A, Thi ATH, Dieterich M, Stubert J, Hartmann S, Glass Ä, et al. Assessment of Ultrasound Features Predicting Axillary Nodal Metastasis in Breast Cancer: The Impact of Cortical Thickness. Ultrasound Int Open. 2015 Jul;1(1):E19–24.

93. Humphrey KL, Saksena MA, Freer PE, Smith BL, Rafferty EA. To Do or Not to Do: Axillary Nodal Evaluation after ACOSOG Z0011 Trial. RadioGraphics. 2014 Nov;34(7):1807–16.

94. Singer C, Blankstein E, Koenigsberg T, Mercado C, Pile-Spellman E, Smith SJ. Mammographic Appearance of Axillary Lymph Node Calcification in Patients with Metastatic Ovarian Carcinoma. American Journal of Roentgenology. 2001 Jun;176(6):1437–40.

95. Eisenkraft BL, Som PM. The spectrum of benign and malignant etiologies of cervical node calcification. American Journal of Roentgenology. 1999 May;172(5):1433–7.

96. Ying M, Ahuja A, Brook F, Metreweli C. Vascularity and grey-scale sonographic features of normal cervical lymph nodes: variations with nodal size. Clin Radiol. 2001 May;56(5):416–9.

97. Dudea SM, Botar-Jid C, Dumitriu D, Vasilescu D, Manole S, Lenghel ML. Differentiating benign from malignant superficial lymph nodes with sonoelastography. Medical Ultrasonography. 2013;15(2).

98. Sarvazyan AP, Skovoroda AR, Emelianov SY, Fowlkes JB, Pipe JG, Adler RS, et al. Biophysical Bases of Elasticity Imaging. In 1995.

99. Wang B, Guo Q, Wang JY, Yu Y, Yi AJ, Cui XW, et al. Ultrasound Elastography for the Evaluation of Lymph Nodes. Frontiers in Oncology. 2021;11.

100. Sigrist RMS, Liau J, Kaffas AE, Chammas MC, Willmann JK. Ultrasound elastography: Review of techniques and clinical applications. Theranostics. 2017;7(5).

101. Gennisson JL, Deffieux T, Fink M, Tanter M. Ultrasound elastography: Principles and techniques. Diagnostic and Interventional Imaging. 2013;94(5).

102. Sandrin L, Fourquet B, Hasquenoph JM, Yon S, Fournier C, Mal F, et al. Transient elastography: A new noninvasive method for assessment of hepatic fibrosis. Ultrasound in Medicine and Biology. 2003;29(12).

103. Nightingale K. Acoustic Radiation Force Impulse (ARFI) Imaging: A Review. Current Medical Imaging Reviews. 2011;7(4).

104. Ferraioli G, Tinelli C, Dal Bello B, Zicchetti M, Filice G, Filice C. Accuracy of real-time shear wave elastography for assessing liver fibrosis in chronic hepatitis C: A pilot study. Hepatology. 2012;56(6).

105. Korta Martiartu N, Nambiar S, Nascimento Kirchner I, Paverd C, Cester D, Frauenfelder T, et al. Sources of Variability in Shear Wave Speed and Dispersion Quantification with Ultrasound Elastography: A Phantom Study. Ultrasound in Medicine and Biology. 2021;47(12).

106. Romano A, Staber D, Grimm A, Kronlage C, Marquetand J. Limitations of muscle ultrasound shear wave elastography for clinical routine—positioning and muscle selection. Sensors. 2021;21(24).

107. Dighe M, Hippe DS, Thiel J. Artifacts in Shear Wave Elastography Images of Thyroid Nodules. Ultrasound in Medicine and Biology. 2018;44(6).

108. Bruce M, Kolokythas O, Ferraioli G, Filice C, O'Donnell M. Limitations and artifacts in shear-wave elastography of the liver. Biomedical Engineering Letters. 2017;7(2).

109. Lee HY, Lee JH, Shin JH, Kim SY, Shin HJ, Park JS, et al. Shear wave elastography using ultrasound: Effects of anisotropy and stretch stress on a tissue phantom and in vivo reactive lymph nodes in the neck. Ultrasonography. 2017;36(1).

110. Carlsen JF, Pedersen MR, Ewertsen C, Săftoiu A, Lönn L, Rafaelsen SR, et al. A comparative study of strain and shear-wave elastography in an elasticity phantom. American Journal of Roentgenology. 2015;204(3).

111. Palmeri ML, Nightingale KR. What challenges must be overcome before ultrasound elasticity imaging is ready for the clinic? Imaging in Medicine. 2011;3(4).

112. Wei H, Jiang HY, Li M, Zhang T, Song B. Two-dimensional shear wave elastography for significant liver fibrosis in patients with chronic hepatitis B: A systematic review and meta-analysis. European Journal of Radiology. 2020;124.

113. Kim JR, Suh CH, Yoon HM, Lee JS, Cho YA, Jung AY. The diagnostic performance of shear-wave elastography for liver fibrosis in children and adolescents: A systematic review and diagnostic meta-analysis. European Radiology. 2018;28(3).

114. Dong B, Chen Y, Chen Y, Wang H, Lyu G. Diagnostic accuracy of liver stiffness on two-dimensional shear wave elastography for detecting clinically significant portal hypertension: a meta-analysis. Expert Rev Med Devices. 2022 May 19;1–9.

115. Chiorean L, Barr RG, Braden B, Jenssen C, Cui XW, Hocke M, et al. Transcutaneous Ultrasound: Elastographic Lymph Node Evaluation. Current Clinical Applications and Literature Review. Ultrasound in Medicine and Biology. 2016;42(1).

116. Pillai A, Voruganti T, Barr R, Langdon J. Diagnostic Accuracy of Shear-Wave Elastography for Breast Lesion Characterization in Women: A Systematic Review and Meta-Analysis. Journal of the American College of Radiology. 2022;19(5).

117. Pulappadi VP, Paul S, Hari S, Dhamija E, Manchanda S, Kataria K, et al. Role of shear wave elastography as an adjunct to axillary ultrasonography in predicting nodal metastasis in breast cancer patients with suspicious nodes. British Journal of Radiology. 2022;95(1134).

118. Anbarasan T, Wei C, Bamber JC, Barr RG, Nabi G. Characterisation of prostate lesions using transrectal shear wave elastography (SWE) ultrasound imaging: A systematic review. Cancers. 2021;13(1).

119. Tang GX, Xiao XY, Xu XL, Yang HY, Cai YC, Liu XD, et al. Diagnostic value of ultrasound elastography for differentiation of benign and malignant axillary lymph nodes: a meta-analysis. Clinical Radiology. 2020;75(6).

120. Spak DA, Plaxco JS, Santiago L, Dryden MJ, Dogan BE. BI-RADS® fifth edition: A summary of changes. Diagnostic and Interventional Imaging. 2017 Mar 1;98(3):179–90.

121. Săftoiu A, Gilja OH, Sidhu PS, Dietrich CF, Cantisani V, Amy D, et al. The EFSUMB Guidelines and Recommendations for the Clinical Practice of Elastography in Non-Hepatic Applications: Update 2018. Ultraschall in der Medizin. 2019;40(4).

122. Okasha HH, Mansour M, Attia KA, Khattab HM, Sakr AY, Naguib M, et al. Role of high resolution ultrasound/endosonography and elastography in predicting lymph node malignancy. Endoscopic Ultrasound. 2014;3(1).

123. Cui XW, Jenssen C, Saftoiu A, Ignee A, Dietrich CF. New ultrasound techniques for lymph node evaluation. World Journal of Gastroenterology. 2013;19(30).

124. Taylor K, O'Keeffe S, Britton PD, Wallis MG, Treece GM, Housden J, et al. Ultrasound elastography as an adjuvant to conventional ultrasound in the preoperative assessment of axillary lymph nodes in suspected breast cancer: A pilot study. Clinical Radiology. 2011;66(11).

125. Wojcinski S, Dupont J, Schmidt W, Cassel M, Hillemanns P. Real-time ultrasound elastography in 180 axillary lymph nodes: Elasticity distribution in healthy lymph nodes and prediction of breast cancer metastases. BMC Medical Imaging. 2012;12.

126. Gramiak R, Shah PM. Echocardiography of the aortic root. Invest Radiol. 1968 Oct;3(5):356–66.

127. Feinstein SB, Cheirif J, Ten Cate FJ, Silverman PR, Heidenreich PA, Dick C, et al. Safety and efficacy of a new transpulmonary ultrasound contrast agent: Initial multicenter clinical results. Journal of the American College of Cardiology. 1990;16(2).

128. Janu E, Krikavova L, Little J, Dvorak K, Brancikova D, Jandakova E, et al. Prospective evaluation of contrast-enhanced ultrasound of breast BI-RADS 3-5 lesions. BMC Medical Imaging. 2020;20(1).

129. Dietrich CF, Nolsoe CP, Barr RG, Berzigotti A, Burns PN, Cantisani V, et al. Guidelines and good clinical practice recommendations for contrast enhanced ultrasound (CEUS) in the liver - Update 2020 -

WFUMB in cooperation with EFSUMB, AFSUMB, AIUM, and FLAUS. Ultraschall in der Medizin. 2020;41(5).

130. Sidhu PS, Cantisani V, Dietrich CF, Gilja OH, Saftoiu A, Bartels E, et al. The EFSUMB guidelines and recommendations for the clinical practice of contrast-enhanced ultrasound (CEUS) in Non-Hepatic Applications: Update 2017 (Long Version). Ultraschall in der Medizin. 2018;39(2).

131. Rubaltelli L, Beltrame V, Scagliori E, Bezzon E, Frigo AC, Rastrelli M, et al. Potential use of contrast-enhanced ultrasound (CEUS) in the detection of metastatic superficial lymph nodes in melanoma patients. Ultraschall in der Medizin. 2014;35(1).

132. Paefgen V, Doleschel D, Kiessling F. Evolution of contrast agents for ultrasound imaging and ultrasound-mediated drug delivery. Frontiers in Pharmacology. 2015;6(SEP).

133. Oeffinger BE, Wheatley MA. Development and characterization of a nano-scale contrast agent. In: Ultrasonics. 2004.

134. Yin T, Wang P, Zheng R, Zheng B, Cheng D, Zhang X, et al. Nanobubbles for enhanced ultrasound imaging of tumors. International Journal of Nanomedicine. 2012;7.

135. Toki A, Niikura H, Mori N, Shigeta S, Nagai T, Tokunaga H, et al. Establishment of a Diagnostic Method for Pelvic Sentinel Lymph Node Metastasis by Contrast-Enhanced Ultrasound in Uterine Cancer. Ultrasound in Medicine and Biology. 2021;47(8).

136. Rautiainen S, Sudah M, Joukainen S, Sironen R, Vanninen R, Sutela A. Contrast-enhanced ultrasound -guided axillary lymph node core biopsy: Diagnostic accuracy in preoperative staging of invasive breast cancer. European Journal of Radiology. 2015;84(11).

137. Tang C, Fang K, Guo Y, Li R, Fan X, Chen P, et al. Safety of Sulfur Hexafluoride Microbubbles in Sonography of Abdominal and Superficial Organs: Retrospective Analysis of 30,222 Cases. Journal of Ultrasound in Medicine. 2017;36(3).

138. Moriyasu F, Itoh K. Efficacy of perflubutane microbubble-enhanced ultrasound in the characterization and detection of focal liver lesions: Phase 3 multicenter clinical trial. American Journal of Roentgenology. 2009;193(1).

139. Rubaltelli L, Beltrame V, Tregnaghi A, Scagliori E, Frigo AC, Stramare R. Contrast-enhanced ultrasound for characterizing lymph nodes with focal cortical thickening in patients with cutaneous melanoma. American Journal of Roentgenology. 2011;196(1).

140. Xiang D, Hong Y, Zhang B, Huang P, Li G, Wang P, et al. Contrast-enhanced ultrasound (CEUS) facilitated US in detecting lateral neck lymph node metastasis of thyroid cancer patients: diagnosis value and enhancement patterns of malignant lymph nodes. European Radiology. 2014;24(10).

141. Poanta L, Serban O, Pascu I, pop S, Cosgarea M, Fodor D. The place of CEUS in distinguishing benign from malignant cervical lymph nodes: A prospective study. Medical Ultrasonography. 2014;16(1).

142. Matsuzawa F, Einama T, Abe H, Suzuki T, Hamaguchi J, Kaga T, et al. Accurate diagnosis of axillary lymph node metastasis using contrast-enhanced ultrasonography with Sonazoid. Molecular and Clinical Oncology. 2015;3(2).

143. Ouyang Q, Chen L, Zhao H, Xu R, Lin Q. Detecting metastasis of lymph nodes and predicting aggressiveness in patients with breast carcinomas. Journal of Ultrasound in Medicine. 2010;29(3).

144. Szabó BK, Saracco A, Tánczos E, Aspelin P, Leifland K, Wilczek B, et al. Correlation of contrast-enhanced ultrasound kinetics with prognostic factors in invasive breast cancer. European Radiology. 2013;23(12).

145. Goldberg BB, Merton DA, Liu JB, Thakur M, Murphy GF, Needleman L, et al. Sentinel Lymph Nodes in a Swine Model with Melanoma: Contrast-enhanced Lymphatic US. Radiology. 2004;230(3).

146. Sever AR, Mills P, Weeks J, Jones SE, Fish D, Jones PA, et al. Preoperative needle biopsy of sentinel lymph nodes using intradermal

microbubbles and contrast-enhanced ultrasound in patients with breast cancer. American Journal of Roentgenology. 2012;199(2).

147. Hayashi A, Giacalone G, Yamamoto T, Belva F, Visconti G, Hayashi N, et al. Ultra High-frequency Ultrasonographic Imaging with 70 MHz Scanner for Visualization of the Lymphatic Vessels. Plast Reconstr Surg Glob Open. 2019 Jan;7(1):e2086.

148. Jang S, Lee CU, Hesley GK, Knudsen JM, Brinkman NJ, Tran NV. Lymphatic Mapping Using US Microbubbles before Lymphaticovenous Anastomosis Surgery for Lymphedema. Radiology. 2022 Jul;304(1):218–24.

149. Giuliano AE, Kirgan DM, Guenther JM, Morton DL. Lymphatic mapping and sentinel lymphadenectomy for breast cancer. Ann Surg. 1994 Sep;220(3):391–401.

150. Decesare SL, Fiorica JV, Roberts WS, Reintgen D, Arango H, Hoffman MS, et al. A Pilot Study Utilizing Intraoperative Lymphoscintigraphy for Identification of the Sentinel Lymph Nodes in Vulvar Cancer. Gynecologic Oncology. 1997 Sep 1;66(3):425–8.

151. Merlo S. Modern treatment of vulvar cancer. Radiology and Oncology. 2020;54(4).

152. Huang J, Yu N, Wang X, Long X. Incidence of lower limb lymphedema after vulvar cancer. Medicine (Baltimore). 2017 Nov 17;96(46):e8722.

153. Soliman AA, Heubner M, Kimmig R, Wimberger P. Morbidity of Inguinofemoral Lymphadenectomy in Vulval Cancer. ScientificWorldJournal. 2012 Jan 4;2012:341253.

154. Tokmak H, Kaban K, Muslumanoglu M, Demirel M, Aktan S. Management of sentinel node re-mapping in patients who have second or recurrent breast cancer and had previous axillary procedures. World Journal of Surgical Oncology. 2014 Jul 12;12(1):205.

155. van Doorn HC, Oonk MHM, Fons G, Gaarenstroom KN, de Hullu J, van Rosmalen J, et al. Sentinel lymph node procedure in patients with

recurrent vulvar squamous cell carcinoma: a proposed protocol for a multicentre observational study. BMC Cancer. 2022 Apr 23;22(1):445.

156. Koh WJ, Greer BE, Abu-Rustum NR, Campos SM, Cho KR, Chon HS, et al. Vulvar cancer, version 1.2017: Clinical practice guidelines in oncology. JNCCN Journal of the National Comprehensive Cancer Network. 2017;15(1).

157. Oonk MHM, Planchamp F, Baldwin P, Bidzinski M, Brännström M, Landoni F, et al. European society of gynaecological oncology guidelines for the management of patients with Vulvar cancer. International Journal of Gynecological Cancer. 2017;27(4).

158. Levenback CF, Ali S, Coleman RL, Gold MA, Fowler JM, Judson PL, et al. Lymphatic mapping and sentinel lymph node biopsy in women with squamous cell carcinoma of the vulva: A gynecologic oncology group study. Journal of Clinical Oncology. 2012;30(31).

159. Giammarile F, Bozkurt MF, Cibula D, Pahisa J, Oyen WJ, Paredes P, et al. The EANM clinical and technical guidelines for lymphoscintigraphy and sentinel node localization in gynaecological cancers. European Journal of Nuclear Medicine and Molecular Imaging. 2014;41(7).

160. Mathéron HM, Van Den Berg NS, Brouwer OR, Kleinjan GH, Van Driel WJ, Trum JW, et al. Multimodal surgical guidance towards the sentinel node in vulvar cancer. Gynecologic Oncology. 2013;131(3).

161. Klapdor R, Länger F, Gratz KF, Hillemanns P, Hertel H. SPECT/CT for SLN dissection in vulvar cancer: Improved SLN detection and dissection by preoperative three-dimensional anatomical localisation. Gynecologic Oncology. 2015;138(3).

162. Bluemel C, Safak G, Cramer A, Wöckel A, Gesierich A, Hartmann E, et al. Fusion of freehand SPECT and ultrasound: First experience in preoperative localization of sentinel lymph nodes. European Journal of Nuclear Medicine and Molecular Imaging. 2016;43(13).

163. Koual M, Benoit L, Nguyen-Xuan HT, Bentivegna E, Azaïs H, Bats AS. Diagnostic value of indocyanine green fluorescence guided sentinel

lymph node biopsy in vulvar cancer: A systematic review. Gynecologic Oncology. 2021;161(2).

164. Nguyen J, Duong H. Anatomy, Abdomen and Pelvis, Female External Genitalia. StatPearls. 2020.

165. Chow L, Tsui BQ, Bahrami S, Masamed R, Memarzadeh S, Raman SS, et al. Gynecologic tumor board: a radiologist's guide to vulvar and vaginal malignancies. Abdominal Radiology. 2021;46(12).

166. Iversen T, Aas M. Lymph drainage from the vulva. Gynecologic Oncology. 1983;16(2).

167. Pavlista D, Eliska O. Superficial lymphatic drainage of the vulva and its relation to the regional nodes: An experimental study. Folia Morphologica. 2021;

168. Fischerova D, Garganese G, Reina H, Fragomeni SM, Cibula D, Nanka O, et al. Terms, definitions and measurements to describe sonographic features of lymph nodes: consensus opinion from the Vulvar International Tumor Analysis (VITA) group. Ultrasound in Obstetrics and Gynecology. 2021;57(6).

169. National Cancer Institute. SEER Cancer Stat Facts: Vulvar Cancer. Surveillance, Epidemiology and End Results (SEER) Program. 2020.

170. Tan A, Bieber AK, Stein JA, Pomeranz MK. Diagnosis and management of vulvar cancer: A review. Journal of the American Academy of Dermatology. 2019;81(6).

171. Homesley HD, Bundy BN, Sedlis A, Yordan E, Berek JS, Jahshan A, et al. Prognostic factors for groin node metastasis in squamous cell carcinoma of the vulva (a gynecologic oncology group study). Gynecologic Oncology. 1993;49(3).

172. Luchini C, Nottegar A, Solmi M, Sergi G, Manzato E, Capelli P, et al. Prognostic implications of extranodal extension in node-positive squamous cell carcinoma of the vulva: A systematic review and meta-analysis. Surgical Oncology. 2016;25(1).

173. Klapdor R, Wölber L, Hanker L, Schmalfeldt B, Canzler U, Fehm T, et al. Predictive factors for lymph node metastases in vulvar cancer. An analysis of the AGO-CaRE-1 multicenter study. Gynecologic Oncology. 2019;154(3).

174. Homesley HD, Bundy BN, Sedlis A, Yordan E, Berek JS, Jahshan A, et al. Assessment of current International Federation of Gynecology and Obstetrics staging of vulvar carcinoma relative to prognostic factors for survival (A Gynecologic Oncology Group Study). American Journal of Obstetrics and Gynecology. 1991;164(4).

175. Weaver DL, Le UP, Dupuis SL, Weaver KAE, Harlow SP, Ashikaga T, et al. Metastasis detection in sentinel lymph nodes: Comparison of a limited widely spaced (NSABP Protocol B-32) and a comprehensive narrowly spaced paraffin block sectioning strategy. American Journal of Surgical Pathology. 2009;33(11).

176. Oonk MH, van Hemel BM, Hollema H, de Hullu JA, Ansink AC, Vergote I, et al. Size of sentinel-node metastasis and chances of non-sentinel-node involvement and survival in early stage vulvar cancer: Results from GROINSS-V, a multicentre observational study. The Lancet Oncology. 2010;11(7).

177. Gaarenstroom KN, Kenter GG, Trimbos JB, Agous I, Amant F, Peters AAW, et al. Postoperative complications after vulvectomy and inguinofemoral lymphadenectomy using separate groin incisions. International Journal of Gynecological Cancer. 2003;13(4).

178. Levenback C, Morris M, Burke TW, Gershenson DM, Wolf JK, Wharton JT. Groin dissection practices among gynecologic oncologists treating early vulvar cancer. Gynecologic Oncology. 1996;62(1).

179. Gu HF, Liu GC, Chen JP, Li JY, Zhang XK, Liu ZM, et al. Proposal for modified inguinofemoral lymphadenectomy derived from investigation of anatomic distribution of sentinel and metastatic nodes in vulvar cancer. Journal of Surgical Oncology. 2021;123(2).

180. Kim TK, Noh SY, Wilson SR, Kono Y, Piscaglia F, Jang HJ, et al. Contrast-enhanced ultrasound (CEUS) liver imaging reporting and data system

(LI-RADS) 2017 – A review of important differences compared to the CT/MRI system. Clinical and Molecular Hepatology. 2017;23(4).

181. Huang DY, Yusuf GT, Daneshi M, Ramnarine R, Deganello A, Sellars ME, et al. Contrast-enhanced ultrasound (CEUS) in abdominal intervention. Abdominal Radiology. 2018;43(4).

182. Spiesecke P, Neumann K, Wakonig K, Lerchbaumer MH. Contrast-enhanced ultrasound (CEUS) in characterization of inconclusive cervical lymph nodes: a meta-analysis and systematic review. Scientific Reports. 2022 Dec 12;12(1):7804.

183. Cox K, Weeks J, Mills P, Chalmers R, Devalia H, Fish D, et al. Contrast-Enhanced Ultrasound Biopsy of Sentinel Lymph Nodes in Patients with Breast Cancer: Implications for Axillary Metastases and Conservation. Annals of Surgical Oncology. 2016;23(1).

184. Covens A, Vella ET, Kennedy EB, Reade CJ, Jimenez W, Le T. Sentinel lymph node biopsy in vulvar cancer: Systematic review, meta-analysis and guideline recommendations. Gynecologic Oncology. 2015;137(2).

185. Lin KM, Patel TH, Ray A, Ota M, Jacobs L, Kuvshinoff B, et al. Intradermal radioisotope is superior to peritumoral blue dye or radioisotope in identifying breast cancer sentinel nodes. Journal of the American College of Surgeons. 2004;199(4).

186. Deng H, Lei J, Jin L, Shi H. Diagnostic efficacy of sentinel lymph node in breast cancer under percutaneous contrast-enhanced ultrasound: An updated meta-analysis. Thoracic Cancer. 2021;12(21).

187. Bertelsen C, King KG, Swanson M, Duddalwar V, Pepper JP. Contrast-Enhanced Ultrasound With Perflubutane for Sentinel Lymph Node Mapping in Cutaneous Melanoma: A Pilot Study. Laryngoscope. 2019;129(5).

188. Gkegkes ID, Iavazzo C. Advantages by using the intradermal microbubbles for sentinel lymph node detection in penile cancer. Hellenic Journal of Nuclear Medicine. 2016;19(3).

189. Crane LMA, Themelis G, Arts HJG, Buddingh KT, Brouwers AH, Ntziachristos V, et al. Intraoperative near-infrared fluorescence imaging for sentinel lymph node detection in vulvar cancer: First clinical results. Gynecologic Oncology. 2011;120(2).

190. Deken MM, van Doorn HC, Verver D, Boogerd LSF, de Valk KS, Rietbergen DDD, et al. Near-infrared fluorescence imaging compared to standard sentinel lymph node detection with blue dye in patients with vulvar cancer – a randomized controlled trial. Gynecologic Oncology. 2020;159(3).

191. KleinJan GH, van Werkhoven E, van den Berg NS, Karakullukcu MB, Zijlmans HJMAA, van der Hage JA, et al. The best of both worlds: a hybrid approach for optimal pre- and intraoperative identification of sentinel lymph nodes. European Journal of Nuclear Medicine and Molecular Imaging. 2018;45(11).

192. Kuo YL, Yao WJ, Chang TW. Which hottest nodes can predict sentinel lymph node metastasis in breast cancer? Journal of Surgical Research. 2011;168(2).

193. Goldberg BB, Merton DA, Liu JB, Forsberg F, Zhang K, Thakur M, et al. Contrast-enhanced ultrasound imaging of sentinel lymph nodes after peritumoral administration of sonazoid in a melanoma tumor animal model. Journal of Ultrasound in Medicine. 2011;30(4).

194. Machado P, Stanczak M, Liu JB, Moore JN, Eisenbrey JR, Needleman L, et al. Subdermal Ultrasound Contrast Agent Injection for Sentinel Lymph Node Identification: An Analysis of Safety and Contrast Agent Dose in Healthy Volunteers. J Ultrasound Med. 2018 Jul;37(7):1611–20.

195. Dietrich CF, Bamber J, Berzigotti A, Bota S, Cantisani V, Castera L, et al. EFSUMB Guidelines and Recommendations on the Clinical Use of Liver Ultrasound Elastography, Update 2017 (Long Version). Ultraschall in der Medizin. 2017;38(4).

196. Sun YM, Dong H, Du ZY, Yang ZL, Zhao C, Chong J, et al. The effect of regions-of-interest and elasticity modulus selection on differentiating

benign and malignant cervical lymph nodes with shear wave elastography. Clinics. 2020;75.

197. Blank MAB, Antaki JF. Breast Lesion Elastography Region of Interest Selection and Quantitative Heterogeneity: A Systematic Review and Meta-Analysis. Ultrasound in Medicine and Biology. 2017;43(2).

198. Schellhaas B, Strobel D, Wildner D, Goertz RS, Neurath MF, Pfeifer L. Two-dimensional shear-wave elastography: A new method comparable to acoustic radiation force impulse imaging? European Journal of Gastroenterology and Hepatology. 2017;29(6).

199. Solivetti FM, Elia F, Graceffa D, Di Carlo A. Ultrasound morphology of inguinal lymph nodes may not herald an associated pathology. Journal of Experimental and Clinical Cancer Research. 2012;31(1).

200. Moon JH, Hwang JY, Park JS, Koh SH, Park SY. Impact of region of interest (ROI) size on the diagnostic performance of shear wave elastography in differentiating solid breast lesions. Acta Radiologica. 2018;59(6).

201. Youk JH, Son EJ, Han K, Gweon HM, Kim JA. Performance of shear-wave elastography for breast masses using different region-of-interest (ROI) settings. Acta Radiologica. 2018;59(7).

202. Azizi G, Keller JM, Mayo ML, Piper K, Puett D, Earp KM, et al. Shear Wave Elastography and Cervical Lymph Nodes: Predicting Malignancy. Ultrasound in Medicine and Biology. 2016;42(6).

203. Li T, Li H, Xue J, Miao J, Kang C. Shear wave elastography combined with gray-scale ultrasound for predicting central lymph node metastasis of papillary thyroid carcinoma. Surgical Oncology. 2021;36.

204. Nielsen Moody A, Bull J, Culpan AM, Munyombwe T, Sharma N, Whitaker M, et al. Preoperative sentinel lymph node identification, biopsy and localisation using contrast enhanced ultrasound (CEUS) in patients with breast cancer: a systematic review and meta-analysis. Clin Radiol. 2017 Nov;72(11):959–71.

205. Zhu J, Lin S, Leow CH, Rowland EM, Riemer K, Harput S, et al. High Frame Rate Contrast-Enhanced Ultrasound Imaging for Slow Lymphatic Flow: Influence of Ultrasound Pressure and Flow Rate on Bubble Disruption and Image Persistence. Ultrasound in Medicine and Biology. 2019;45(9).

206. Wolfs JAGN, Qiu SS, Lobbes MBI, Bijkerk E, Van Der Hulst RRWJ, Keuter XHA. Visualization of Both the Superficial and Deep Lymphatic System of the Upper Extremity Using Magnetic Resonance Lymphography. Lymphatic Research and Biology. 2022;20(3).

207. Farias-Cisneros E, Chilton PM, Palazzo MD, Ozyurekoglu T, Hoying JB, Williams SK, et al. Infrared imaging of lymphatic function in the upper extremity of normal controls and hand transplant recipients via subcutaneous indocyanine green injection. SAGE Open Medicine. 2019;7.

208. Villa G, Campisi CC, Ryan M, Boccardo F, Di Summa P, Frascio M, et al. Procedural Recommendations for Lymphoscintigraphy in the Diagnosis of Peripheral Lymphedema: the Genoa Protocol. Nuclear Medicine and Molecular Imaging. 2019;53(1).

209. Kraft JC, Ho RJY. Interactions of Indocyanine Green and Lipid in Enhancing Near-Infrared Fluorescence Properties: The Basis for Near-Infrared Imaging in Vivo. Biochemistry. 2014 Mar 4;53(8):1275–83.

210. PubChem. Indocyanine green [Internet]. Available from: https://pubchem.ncbi.nlm.nih.gov/compound/5282412

211. Laurent S, Elst LV, Muller RN. Comparative study of the physicochemical properties of six clinical low molecular weight gadolinium contrast agents. Contrast Media & Molecular Imaging. 2006;1(3):128–37.

212. Xiao YD, Paudel R, Liu J, Ma C, Zhang ZS, Zhou SK. MRI contrast agents: Classification and application (Review). Int J Mol Med. 2016 Nov;38(5):1319–26.

213. Tu J, Guan J, Qiu Y, Matula TJ. Estimating the shell parameters of SonoVue ® microbubbles using light scattering. The Journal of the Acoustical Society of America. 2009;126(6).

214. Sontum PC. Physicochemical Characteristics of Sonazoid™, A New Contrast Agent for Ultrasound Imaging. Ultrasound in Medicine and Biology. 2008;34(5).

215. Jimenez IR, Roca M, Vega E, García ML, Benitez A, Bajén M, et al. Particle sizes of colloids to be used in sentinel lymph node radiolocalization. Nucl Med Commun. 2008 Feb;29(2):166–72.

216. Yon M, Billotey C, Marty JD. Gadolinium-based contrast agents: From gadolinium complexes to colloidal systems. Int J Pharm. 2019 Oct 5;569:118577.

217. Bar-David S, Larush L, Goder N, Aizic A, Zigmond E, Varol C, et al. Size and lipid modification determine liposomal Indocyanine green performance for tumor imaging in a model of rectal cancer. Sci Rep. 2019 Jun 12;9(1):8566.

218. Swartz MA, Berk DA, Jain RK. Transport in lymphatic capillaries. I. Macroscopic measurements using residence time distribution theory. American Journal of Physiology - Heart and Circulatory Physiology. 1996;270(1 39-1).

219. Alter J, Sennoga CA, Lopes DM, Eckersley RJ, Wells DJ. Microbubble Stability is a Major Determinant of the Efficiency of Ultrasound and Microbubble Mediated in vivo Gene Transfer. Ultrasound in Medicine & Biology. 2009 Jun 1;35(6):976–84.

ORIGINAL PUBLICATIONS (I – III)

I

Preoperative sentinel lymph node localization in vulvar cancer: preliminary experience with inguinal intradermal contrast-enhanced ultrasound.

Lahtinen O, Eloranta M, Anttila M, Kärkkäinen H, Sironen R, Vanninen R, Rautiainen S.

Eur Radiol. 2018 May;28(5): 2089-295. doi: 10.1007/s00330-017-5155-7

II

2D-shear wave elastography in the evaluation of suspicious superficial inguinal lymph nodes: Reproducibility and region of interest selection.

Lahtinen O, Pulkkinen M, Sironen R, Vanninen R, Rautiainen S.
PLoS One. 2022 Mar 28;17(3):e0265802. doi: 10.1371/journal.pone.0265802

PLOS ONE

RESEARCH ARTICLE

2D-shear wave elastography in the evaluation of suspicious superficial inguinal lymph nodes: Reproducibility and region of interest selection

Olli Lahtinen[1,2]*, **Mika Pulkkinen**[1], **Reijo Sironen**[3,4,5,6], **Ritva Vanninen**[1,2], **Suvi Rautiainen**[1]

1 Diagnostic Imaging Centre, Department of Clinical Radiology, Kuopio University Hospital, Kuopio, Finland, **2** Institute of Clinical Medicine, Unit of Radiology, University of Eastern Finland, Kuopio, Finland, **3** Institute of Clinical Medicine, Clinical Pathology, University of Eastern Finland, Kuopio, Finland, **4** Department of Clinical Pathology, Kuopio University Hospital, Kuopio, Finland, **5** Institute of Clinical Medicine/Clinical Pathology, University of Eastern Finland, Kuopio, Finland, **6** Cancer Centre of Eastern Finland, Kuopio, Finland

* olli.lahtinen@kuh.fi

Citation: Lahtinen O, Pulkkinen M, Sironen R, Vanninen R, Rautiainen S (2022) 2D-shear wave elastography in the evaluation of suspicious superficial inguinal lymph nodes: Reproducibility and region of interest selection. PLoS ONE 17(3): e0265802. https://doi.org/10.1371/journal.pone.0265802

Editor: Giovanni Delli Carpini, Universita Politecnica delle Marche, ITALY

Received: April 7, 2020

Accepted: March 8, 2022

Published: March 28, 2022

Data Availability Statement: All relevant data are within the paper.

Funding: O.L has received funding by Wiljasalo foundation (grant), Pohjois-Savo cancer association (grant) and Kuopio University Hospital Science Foundation (grant). The funders had no role in study design, data collection and analysis, decision to publish, or preparation of the manuscript.

Abstract

Purpose

To assess the ability of 2D-Shear wave elastography (2D-SWE) to evaluate its reproducibility, to define the optimal orientation and size of the region of interest (ROI), and to differentiate benign from malignant inguinal lymph nodes (LNs).

Method

Thirty-two suspicious inguinal LNs from 21 patients were evaluated with 2D-SWE. SWE measurements were obtained in two orthogonal planes. To investigate reproducibility, sensitivity and specificity, circular ROIs with a diameter of 1 mm, 2 mm, 3 mm and 5 mm were placed on the cortex of the LNs. Additionally, one freehand ROI was drawn covering majority of the LN. Two observers performed five sets of SWE measurements for each ROI size. All LNs underwent core needle biopsy or were surgically removed.

Results

The 3 mm ROI for Mean-E in axial plane showed high interrater agreement [intraclass correlation coefficient (ICC) 0.899] with the cut-off value of 7.31 kPa resulting in 88.9% sensitivity and 60.9% specificity for differentiating malignant from benign LNs. In benign LNs, mean elasticity of the ROI was lower (7.68 ± 3.82 kPa; range, 3.41–15.40 kPa) compared to the malignant LNs (15.81 ± 10.61 kPa; range, 3.86–36.45 kPa).

Conclusions

The most reproducible way to measure stiffness in inguinal LNs is a 3 mm circular ROI centered on the cortex of the LN in axial plane. Elasticity values were higher in the malignant

Competing interests: The authors have declared that no competing interests exist.

Abbreviations: CNB, core needle biopsy; E, elasticity; ICC, intraclass correlation coefficient; LN, lymph node; ROI, region of interest; SWE, shear wave elastography; US, ultrasound.

LNs reflecting the stiffer nature of the metastatic LNs. 2D-SWE offers a noninvasive ultrasonographic tool to assess superficial inguinal lymph nodes with high reproducibility.

Introduction

When a malignancy is detected, accurate assessment of the regional lymph nodes (LNs) is crucial for the management and prognosis of the patient. Superficial LNs are easily detected and evaluated with ultrasound (US). US B-mode alone has sensitivity of 61.4–98.0% and specificity of 31.4–97.0% in the differentiation of malignant and benign LNs in superficial lymph node regions [1–6]. Despite its high resolution in superficial areas none of the US criterions can be used as a sole predictor of malignancy and LN biopsy remains to be the golden standard for the characterization of the LNs [7–11].

US elastography has been available since 1990s [12, 13]. Currently, there are two kinds of elastography methods: strain and shear wave elastography (SWE). SWE using mechanical shear waves improves the reproducibility of the tissue elasticity measurements, since the measurement of the velocity of the shear waves gives quantitative and qualitative results from the elasticity of the tissues [7, 12, 13]. Newest application of shear wave imaging is the 2D-SWE. Unlike the older shear wave imaging methods, the 2D-SWE uses acoustic radiation force in multiple points allowing real time monitoring of shear wave propagation. Promising results to differentiate malignant from benign superficial LNs have been reported using SWE [7, 9, 14, 15].

Like conventional B-mode US, elastography has its limitations. Anisotrophy, depth of the measurement, tissue interfaces, attenuation of the signal, tissue pulsations due to blood pulsation, breathing and operator dependent high contact force may affect the reliability of SWE [13, 16–19].

Different sizes and shapes of regions of interest (ROIs) have been investigated mostly in elastography of breast lesions. Yet, there is no consensus on the optimal type, size or plane of the ROI for the SWE measurements. Typically, a small 2–3 mm circular ROI is placed over the stiffest part of the lesion on the axial plane. In contrast, also larger ROIs covering the whole lesion and two orthogonal planes have been used [20–27]. Thus far, no recommendations exist for ROI types in LN assessment with SWE.

The aims of the present validation study were to evaluate the reproducibility of 2D-SWE and to define the optimal ROI size for inguinal LNs. As a secondary endpoint, we wanted to study whether the depth, anisotrophy of the tissue or vicinity of the femoral artery would affect the repeatability of the measurements. Additionally, we wanted to assess the ability of 2D-SWE to differentiate benign and malignant inguinal LNs.

Materials and methods

Patients and study design

Approval of institutional review board, local ethics committee and written informed consent of the patients were obtained for this prospective single center study.

All consecutive patients who were scheduled for inguinal US as part of their preoperative staging examinations or had otherwise a suspicion of abnormal LNs in the inguinal region were invited to participate in this study between November 2016 and September 2018. Exclusion criteria were as follows: 1) patient could not provide informed consent 2) inguinal LNs less than 5 mm on their short axis to avoid surrounding tissues to be included in larger SWE

ROIs 3) inguinal LNs without further histopathological confirmation. Biopsies were performed, when necessary depending on the clinical setting and were taken after the SWE examinations to avoid effects of possible hemorrhage on the measurements.

Inguinal US and elastography

The US examinations were performed independently by one of two radiologists with 5 and 15 years of experience in conventional US and 3 years of experience in SWE. All studies were performed with Logiq E9™ US-device (GE Healthcare, Chicago, USA) with ML6-15 (4–15 MHz) linear array transducer for grey scale imaging. SWE was performed with 2D wide band linear transducer, 9L (2–8 MHz).

During the US studies, the patients rested in supine position on the examination table. Inguinal region and the LNs were first examined with traditional grey scale US. The size, short axis, cortical thickness, shape and vascular pattern of the LNs were registered. A LN was considered abnormal if it showed rounded shape, no hilar fat, cortical thickness greater than 3 mm or lobular cortical thickening, mixed or cortical vascularity, or the short axis $>$ 1 cm. If a LN greater than 5 mm in short axis was found in the grey scale US, 2D-SWE was performed. Furthermore, the distance between the SWE measured LN and femoral artery and skin were measured.

Based on the grey scale US, SWE was conducted on each inguinal side to the largest LN or to the LN with most abnormal features if a suitable LN was found. A thick layer of gel was put on the skin and the probe was placed on a perpendicular plane to the skin. A minimal external force was applied to the probe avoiding too high compression against the tissue. SWE measurements were acquired and registered in two perpendicular planes to the LN. First a longitudinal view along the LN's long axis was acquired (called axial plane in further text), followed by the probe rotation of 90 degrees to have a transverse image (called sagittal plane in further text).

The more detailed SWE measurements with several ROI types were later performed blindly and independently by two radiologists with 5-year experience in US and 3 years of experience in SWE. SWE sampling box was fixed to 15 x 15 mm. Color-coded elastography maps showed stiff areas (high kPa) as red and soft areas (low kPa) as blue. The color-coded SWE image was superimposed onto the conventional grey scale B-mode image and displayed in a split screen together with normal B-mode image (Fig 1). Circular ROI was centered to cover the cortex of the LN or the cortex and the hilum if the ROI did not fit purely in the cortex. ROI diameters of 1, 2, 3 and 5 mm were used in the analysis (Fig 2). The US device provided a fixed ROI size of 5 mm, smaller ROIs were calculated individually from the surface area given by the device to

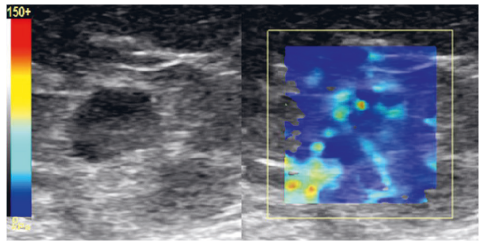

Fig 1. B-mode and elastography images in axial plane of an inguinal lymph node (LN) from a 68-year old patient with vulvar cancer. Although the B-mode image shows a slightly rounded LN, elastography shows the LN as blue (soft) indicating benign etiology. In histopathology, the inguinal lymph nodes proved to be benign.

https://doi.org/10.1371/journal.pone.0265802.g001

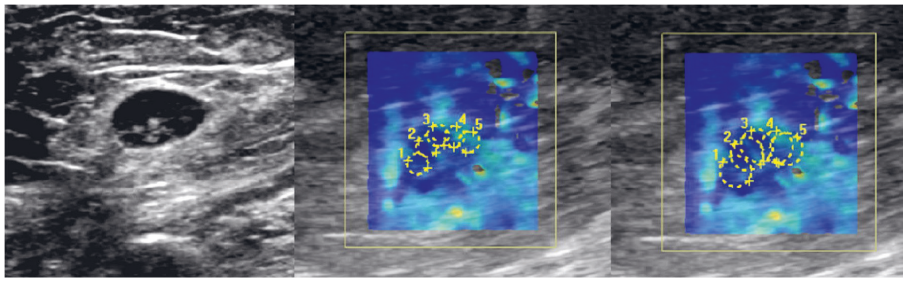

Fig 2. SWE measurements with different ROI sizes in axial plane. A 7 mm inguinal LN of a 70-year old woman with vulvar cancer is shown in B-mode image (left). The same LN is illustrated with five 2 mm (middle image) and 3 mm (right image) SWE ROIs. ROIs are centered evenly on the 4 mm cortex to cover majority of it. The Mean-E values were 7.8 kPa and 7.0 kPa with 2 mm and 3 mm ROIs accordingly. The LN proved to be histopathologically benign.

https://doi.org/10.1371/journal.pone.0265802.g002

match the smaller ROI sizes. A total of five ROIs with diameters of each predefined size were placed with even spacing to cover the cortex in both perpendicular planes. In addition, a manual freehand circular ROI, covering most of the LN, was also drawn once. SWE data was deemed sufficient when majority of the color box was color-coded (>75%) and the cycles remained constant to avoid excess use of pressure on the probe. Approximately five images were taken with each orientation. The elasticity (E) of the ROI was calculated by the system representing the average elasticity value of the pixels in the ROI. Mean elasticity (Mean-E) was defined as the mean value of the five measurements. Additionally maximum (Max-E) and minimum (Min-E) elasticity out of the five ROI measurements were registered. Due to software update of the US device during the study all of the elasticity indices were not automatically included in the measurements after the update. Thus, to keep the data homogeneous some of the elasticity indices could not be used.

Patient treatments

All patients received standard treatment according to national and local guidelines regardless of the findings in SWE. All patients in this study had histological verification through a core needle biopsy (CNB) or surgical removal of LN(s) as a part of their normal treatment. CNB was performed using a 16 or 14 gauge needle (Temno Evolution™). A total of 3–7 biopsies were obtained depending on the clinical setting. At least six samples were taken if lymphoma was suspected. Clinical 6-month follow up period was included in the study setting.

Histopathology

CNB samples and surgical specimens were examined histopathologically in pathology laboratory as a part of the normal diagnostic procedure. The samples were sectioned into 4 μm thick slices after formalin fixation and paraffin embedding. Standard hematoxylin and eosin (HE) staining was done to all LNs. Additionally, immunohistochemical stainings (cytokeratins) were performed whenever found necessary (Fig 3).

Statistical analysis

Statistical analysis was performed using statistical software (SPSS Version 22.0, SPSS, Chicago, Illinois). Continuous variables with normal distribution are reported as mean ± standard deviation. A power calculation was used to verify statistically significant sample size for this

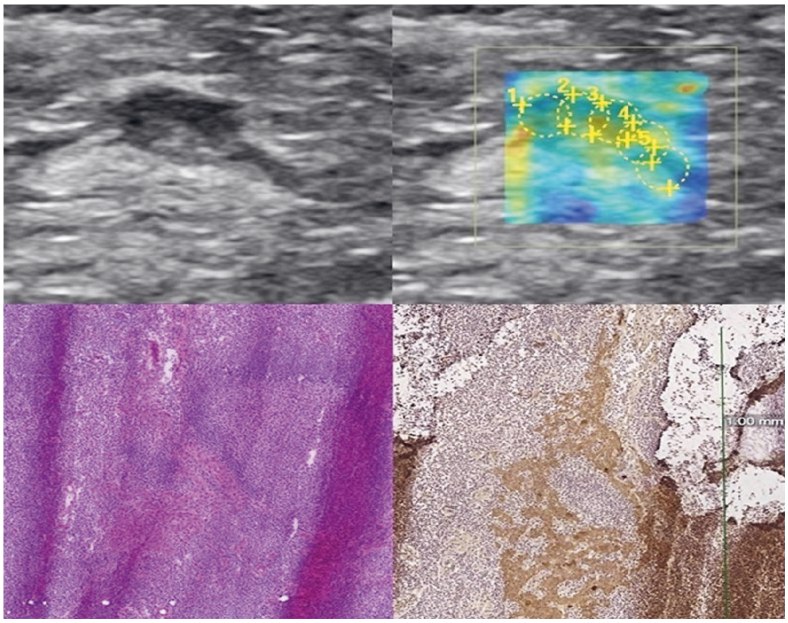

Fig 3. Ultrasound images and histopathology of a micrometastatic inguinal LN of a 67-year old woman with vulvar cancer. B-mode and elastography images (upper images) illustrate a superficial inguinal LN with abnormal focal cortical thickening. SWE demonstrated Mean-E value of 9.68 kPa and Max-E value of 11.46 kPa with 3 mm ROI in the axial plane. Histopathological analysis revealed a micrometastatic 1 mm deposit of squamocellular carcinoma. HE and cytokeratin stainings are illustrated in the lower row. atypical nuclei show variation in their size and shape. Additionally metastatic cell nuclei stain positive (brown) in cytokeratin staining (scale bar 1 mm).

https://doi.org/10.1371/journal.pone.0265802.g003

reproducibility study ($\alpha = 0.05$, power 0.80). The ROI size to best differentiate benign LNs from the malignant LNs was selected by using the areas under the curve (AUC) values from the receiver operating characteristic (ROC) curve analysis. Delong test was used to compare the ROC curves. McNemar test was applied to compare the diagnostic performance of the different ROI types.

Interrater agreement between the two readers was assessed by intraclass correlation coefficient (ICC), using the mean value of the five measurements of each observer. The ICC values were considered excellent (> 0.90), good (0.75–0.90), moderate (0.50–0.75) or poor (< 0.50). *P* values for the ICCs of the different ROIs were calculated by using the bootstrap method. Paired samples t-test was used to calculate statistical significances for the ICC values, $P < 0.05$ was considered statistically significant.

Results

Altogether 27 consecutive patients with 39 inguinal LNs were initially recruited to this study. Data from 5 LNs was lost due to US device software updates. Additionally, one LN with measurements in only one plane and one LN with no histopathological verification were excluded. After exclusion criteria, altogether 32 inguinal lymph nodes from 21 patients were included in the statistical analysis. Mean age of the patients was 68 years (range 27–85 years). Majority of the patients had a malignant disease treated (19/21, 90.5%) of which vulvar cancer was the

Table 1. Patient demographics and lymph node (LN) characteristics.

Patients and characteristics	N (%)	Mean (range)
N	21	
Gender	Male 4 (19.0) Female 17 (81.0)	
Age (years)		68 (27–85)
BMI		33.9 (19.1–44.6)
Number of LNs evaluated/patient		
1	10 (47.6)	
2	11 (52.4)	
LN		**Median, (range) in mm**
Number	32	
Cortical thickness		4 (1–59)
Short axis		7 (5–59)
Depth		15 (3–27)
Distance from femoral artery		11 (2–21)

https://doi.org/10.1371/journal.pone.0265802.t001

most common (16/20, 80.0%). No malignancy was detected after 6-month follow up in patients who had no malignancy in the final histopathology of the inguinal LN. Patient demographics and LN characteristics from grey scale US are presented in Table 1.

Majority (24/32, 75.0%) of the LNs were surgically removed while CNB was performed in 25.0% (8/32) of the LNs. Altogether, nine out of thirty-two (28.1%) of the LNs were malignant in final histopathology. Detailed histopathological findings are presented in Table 2. All malignant LNs expressed cortical thickness $\geq$ 5 mm is US.

Reproducibility

The reproducibility of the SWE measurements was highest in larger ROIs measured in axial plane; 5 mm ROI in Mean-E and 3 mm and 5 mm ROIs in Max-E ($P = 0.003$ and 0.006, respectively). In addition, the ICC scores were good to excellent (0.85–0.97) for Mean-E and Max-E measurements in axial plane (Table 3). In sagittal plane the ICC scores varied from poor to good (0.42–0.79).

In the reproducibility analysis the SWE measurements in axial plane yielded greater ICC-values than in sagittal plane ($P = 0.006$). Paired samples t-test showed no significant difference in the elastography analysis between the two observers. In addition, the distance from the LN to the femoral artery had no significant effect on reproducibility. However, depth of the LN had an influence on the ICC-values resulting in better reproducibility for more superficial LNs. Moreover, LNs with a cortical thickness greater than 3 mm had higher ICC values. Reproducibility in the subgroups is presented in Table 4.

Table 2. Histopathology of the core biopsy samples or removed inguinal lymph nodes (N = 32).

Histopathology	N (%)
Squamous cell carcinoma (SCC)	6 (18.7)
Serous ovarian cancer	1 (3.1)
Lymphoma	2 (6.3)
Reactive lymphoid tissue	2 (6.3)
Lymphoid tissue, no abnormal features	21 (65.6)

https://doi.org/10.1371/journal.pone.0265802.t002

Table 3. Intraclass correlation coefficient (ICC) for different regions of interest (ROIs).

ROI (size mm/type)	ROI plane	Mean-E (kPa) ± SD		Max-E (kPa) ± SD		Min-E (kPa) ± SD		ICC-values for Mean-E/Max-E/Min-E
		Observer 1	Observer 2	Observer 1	Observer 2	Observer 1	Observer 2	
1	Axial	9.32 ± 8.24	9.44 ± 7.08	18.63 ± 22.44	18.22 ± 17.46	4.49 ± 4.07	3.84 ± 2.66	0.87 / 0.85 / 0.61
2	Axial	9.80 ± 8.12	10.04 ± 9.93	17.10 ± 17.73	18.57 ± 23.88	5.01 ± 3.58	4.82 ± 4.15	0.91 / 0.90 / 0.70
3	Axial	9.96 ± 7.29	10.29 ± 9.50	16.84 ± 18.20	17.18 ± 20.59	5.82 ± 4.13	5.52 ± 5.04	0.90 / 0.96 / 0.82
5	Axial	9.95 ± 7.02	9.78 ± 7.80	14.20 ± 11.43	14.17 ± 14.06	6.69 ± 3.97	6.21 ± 4.47	0.97 / 0.95 / 0.91
1	Sagittal	12.32 ± 8.86	14.03 ± 10.74	21.15 ± 18.01	24.12 ± 19.40	6.08 ± 6.49	6.41 ± 5.43	0.70 / 0.42 / 0.65
2	Sagittal	12.29 ± 9.44	14.28 ± 10.98	21.57 ± 20.27	24.01 ± 19.32	6.24 ± 6.33	7.14 ± 6.77	0.77 / 0.72 / 0.91
3	Sagittal	12.28 ± 9.69	14.44 ± 11.31	19.76 ± 17.60	21.97 ± 19.15	7.01 ± 6.66	8.50 ± 6.29	0.74 / 0.74 / 0.77
5	Sagittal	12.19 ± 8.99	13.75 ± 10.25	16.58 ± 12.77	17.55 ± 13.24	8.58 ± 7.13	10.36 ± 8.15	0.79 / 0.79 / 0.80
Freehand ROI	Axial	9.61 ± 6.43	9.79 ± 6.60	-		-		0.95
Freehand ROI	Sagittal	11.46 ± 6.73	13.88 ± 10.50	-		-		0.61

https://doi.org/10.1371/journal.pone.0265802.t003

Differentiation of benign and malignant LNs using SWE data

When the SWE data was used to differentiate benign from malignant LNs, 2 mm and 3 mm Mean-E ROIs in axial plane yielded both the highest AUC value of 0.773 in the ROC-curve, 2 mm ROI ($P = 0.018$, 95% CI 0.559–0.987) and 3 mm ROI ($P = 0.018$, 95% CI 0.568–0.978) (Fig 4). Optimal Mean-E cut-off values differentiating benign from malignant inguinal LNs from the ROC-curve analysis was 7.31 kPa when measured from 3 mm axial ROI and 6.6 kPa with 2 mm axial ROI. These results corresponded to 88.9% sensitivity, 60.9% specificity, 47.0% PPV, 93.3% NPV and 68.7% accuracy for the detection of a malignant LN with 3 mm axial ROI and 88.9%, 56.5%, 44.4%, 92.8%, 65.6% with 2 mm ROI, respectively. No statistical significance was found in the diagnostic performance between 2 mm and 3 mm ROI ($P = 1,000$).

Mean-E with 3 mm ROI proved to be higher (15.81 ± 10.61 kPa; range, 3.86–36.45 kPa) in malignant LNs compared to benign LNs (7.68 ± 3.82 kPa; range, 3.41–15.40 kPa). Between the different ROIs with highest AUC-values, there was no significant difference in the diagnostic

Table 4. Effect of different parameters on reproducibility of SWE elastography, assessed by intraclass correlation coefficient (ICC) values.

Parameter	n	Mean-E ± SD Observer A	Mean-E ± SD Observer B	ICC-values	P-value
All LNs	32	10.92 ± 8.08	11.97 ± 9.47	0.80	0.971
Plane					0.006
Axial	32	9.73 ± 7.42	9.87 ± 8.18	0.87	
Sagittal	32	12.11 ± 8.74	14.07 ± 10.76	0.72	
Distance from the femoral artery					0.529
< 10 mm	16	12.98 ± 8.67	13.99 ± 9.54	0.77	
≥ 10 mm	16	8.86 ± 6.39	9.96 ± 8.59	0.81	
Cortical thickness					0.004
≤ 3 mm	14	8.85 ± 4.34	11.12 ± 8.08	0.57	
> 3 mm	18	12.53 ± 9.87	12.64 ± 10.40	0.93	
Depth					0.018
< 15 mm	14	14.23 ± 10.44	14.50 ± 11.63	0.92	
≥ 15 mm	18	8.35 ± 4.31	10.01 ± 6.61	0.61	
Benign	23	8.85 ± 4.44	10.44 ± 6.87	0.63	0.004
Malignant	9	16.20 ± 12.35	15.88 ± 13.63	0.93	

$P < .05$ of the t-test was considered statistically significant. ICC-values are calculated from the averages of all ROI sizes and planes.

https://doi.org/10.1371/journal.pone.0265802.t004

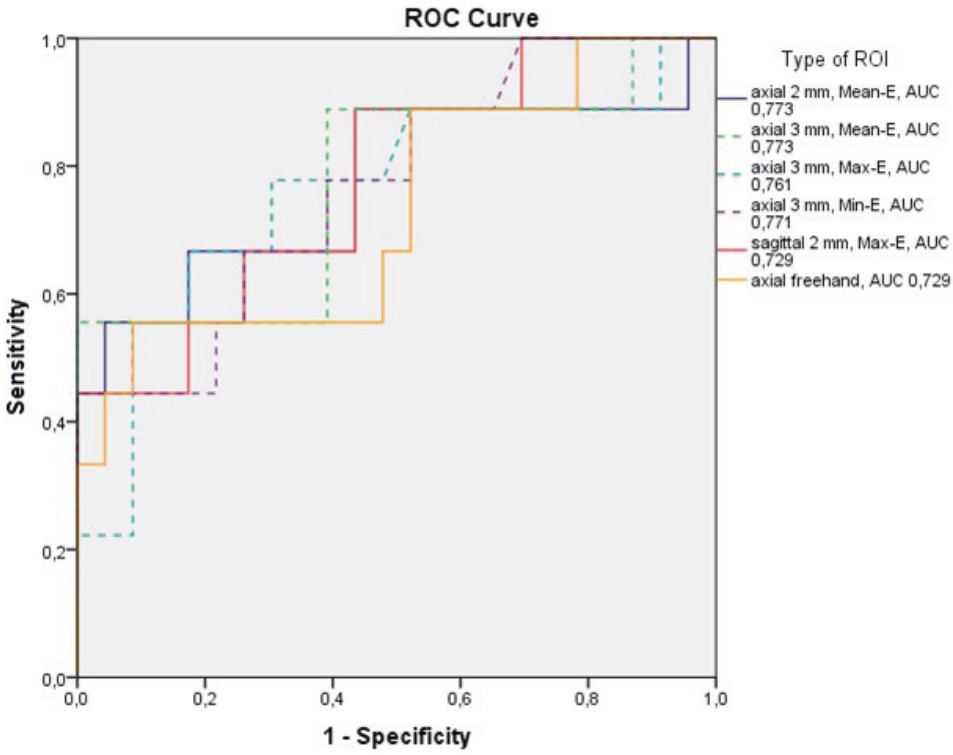

Fig 4. Receiver operating characteristic (ROC) curves of SWE ROIs with the highest AUC values. Axially placed 2 mm and 3 mm ROIs yielded the best results with Mean-E (88.9% sensitivity, 56.5% specificity and 88.9%, 60.9% respectively) and 3 mm Max-E (77.8% sensitivity and 69.4% specificity).

https://doi.org/10.1371/journal.pone.0265802.g004

performance of Mean-E and Max-E ($P = 0.250$). When the diagnostic performance of 3 mm axial and sagittal ROIs were compared, the sagittal ROIs resulted in larger number of false negatives compared to the axial ROIs *($P = 0.002$)*. Box plots of the Mean-E values in the benign vs. malignant LNs are shown in Fig 5.

Discussion

The current study demonstrates that SWE measurements in inguinal lymph nodes are reproducible between different observers. This is in congruence with the results from earlier publications where reproducibility and ICC have been found good to excellent in phantom studies and in studies related to SWE in liver and cervical LNs [28–30].

Previously SWE has been mainly used to evaluate axillary and cervical LN regions [2, 3, 7, 15, 31–34]. The first report where SWE was used solely to investigate inguinal LNs was published by Kawahara et al. in patients with metastatic skin cancer [26]. When evaluating suspicious LNs with traditional US, multiple indicators should be assessed. As an adjunct to

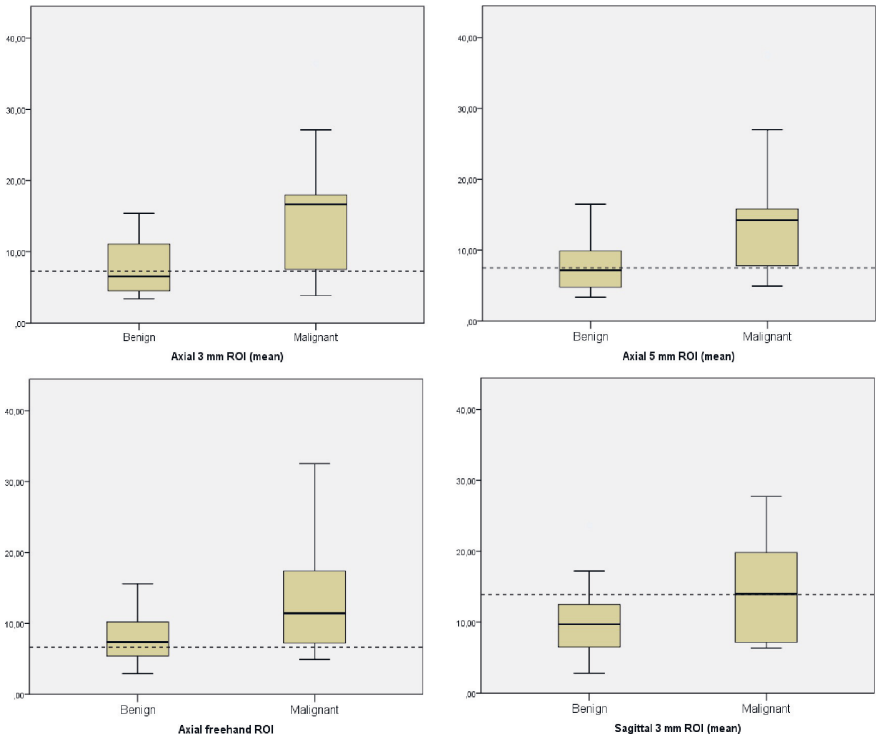

Fig 5. Boxplots of several different types of ROIs. Boxplots of axial 3 mm, 5 mm and freehand ROI and sagittal 3 mm ROIs in benign vs. malignant lymph nodes with the elasticity cut off values (kPa) from the ROC-curve (black dotted line). Axial ROIs demonstrated better diagnostic performance than sagittal ROIs.

https://doi.org/10.1371/journal.pone.0265802.g005

morphology and vascularity, SWE now provides a new possibility to differentiate malignant from benign LNs. The cut-off value of 7.31 kPa with the 3 mm cortical axially placed ROI resulted in 88.9% sensitivity and 60.9% specificity for differentiating malignancy. The Mean-E values proved to be significantly lower in the benign LNs compared to the malignant LNs. Similar findings of elasticity indices being lower in benign LNs have also been reported axillary and cervical LNs [15, 35]. The result presumably reflects the stiffer nature of the highly cellular metastatic LNs compared to the more loose lymphatic structure of the benign LNs.

Optimal size of ROI for LNs has not been previously investigated. Various ROI sizes and placements have been mostly used in breast masses and cervical LNs. Usually a small 2–3 mm ROI is placed centered in the stiffest part of the lesion [20, 21, 23, 24, 27]. Additionally, placing the ROI to cover the whole suspected lesion has been studied [20, 21, 26]. Since the normal mean cortical thickness in inguinal LNs has been reported to be 1–2 mm [36], we placed ROIs of different sizes to cover majority of the cortex to define the most reproducible ROI size in the inguinal LNs instead of one ROI. In this study, with patients with preoperative US for vulvar cancer, ovarian cancer, lymphoma or patients with otherwise suspected LN enlargement, the mean cortical thickness was 4 mm and the optimal ROI size found to be 3 mm in axial plane.

Smallest ROIs showed more variation in the SWE results than a larger ROIs reflecting the heterogeneity of the tissue. In suspicious LNs, a larger cortical thickness can often be detected in clinical work, allowing use of larger cortical ROI size for SWE. This in turn may average the results, especially with benign LNs consisting of stiffer cortex but also hilar fat leading to lower elasticity values. Due to averaging, our results in inguinal LNs' Mean-E values differ from breast tissue studies where the mean elasticity remained unchanged between different ROI sizes in benign breast tissue masses [21].

Interrater agreement was good to excellent for Mean-E and Max-E measurements with different ROI sizes. However, if only one ROI size were to be selected for clinical practice, the 3 mm ROI in axial plane proved to be most reliable according to our results. This finding is in line with previous breast tissue findings [20, 21, 24]. ROIs placed on the sagittal plane constantly yielded lower ICC values, reason behind the result remains unclear and further studies are needed to verify this result. The interrater agreement was also better with larger ROIs compared to smaller ones; large 5 mm ROIs resulted in even better ICC-values than 3 mm ROI. The finding can be mainly explained by overlapping and averaging large ROIs in smaller LNs. However, the large 5 mm ROIs yielded a lower sensitivity and specificity since medullar fat might also be included in the larger ROI.

Vicinity of the femoral artery did not affect the results of the elasticity measurements in our cohort. Similar findings have been published regarding the carotid artery and the depth of the LN in neck area [30]. However, in this study superficial LNs resulted in higher reproducibility than the deep LNs. In our cohort the median depth of the superficial inguinal LNs was 15 mm, but with obese patients the measurements may have limited reproducibility. Similar depth dependence has been shown in phantom studies, where it has been shown that the reliability of SWE is reduced especially in hard lesions with depths greater than 2 cm [16, 17]. Although muscle tension and stress from stretching has been found to affect the elastography measurements, they had no effect on the two perpendicular planes in the groin area. Unlike in the neck region where muscle tension may be high, the inguinal region will stay in a relaxed state when the patient is studied in supine position.

In literature the studies of SWE in head & neck and axillary LNs report a sensitivity of 81.0–95.0% and specificity of 80–95% to identify malignant LNs [7, 10, 14, 15, 31]. The results of the present study with suspicious inguinal LNs yielded similar sensitivity but a lower specificity. However, the relatively low number (9 cases) of malignant LNs and heterogenous patient material in this study may influence the result. Only one small study has been conducted solely on inguinal LNs. However, due to its small study population no sensitivity or specificity numbers were given [26]. Other previous studies have had superficial LNs from different areas [33]. On the other hand, this is also the case in clinical setting with suspicious inguinal LNs.

In this study the Mean-E cut-off value for malignant LNs was 7.31 kPa when using the 3 mm ROI. The earlier reports for SWE in inguinal LN diagnosis are scarce, but in head & neck and axillary LN studies the cut-off values have been reported to be higher, between 20 to 56 kPa [31, 32, 35, 37, 38]. None of these LN SWE studies were conducted with similar US equipment as the present study and it is evident that the elasticity values may differ between the US manufacturers. Furthermore, the higher elasticity values in the previous studies are based on a single ROI placed in the stiffest part of the LN which leads to higher elasticity values. This may be due to the finding that placing a ROI over the stiffest lesion seems to increase the specificity of the measurements [7, 10, 14, 31].

Our study has some limitations. As a single center study, the cohort was small and had relatively low number of malignant LNs. Additionally patients had various background diseases which might affect the SWE results. Multicenter studies with a larger cohort and malignant LNs are needed to confirm the results of the present preliminary study. Our results on the

usefulness of ROI selection are based only on the Logiq E9 ™ US-device. Since the SWE results may differ between US devices, further studies with different manufacturers' US devices are needed to verify the results. Furthermore, although the SWE technique might be reproducible in patients with low and normal weight, the inguinal region with obese people is challenging due to skinfolds and may lead to excess pressure of the US probe against skin thus potentially influencing the result of the elasticity measurement. Due to software issues some elasticity indices, including maximum elasticity in the ROI, were not automatically included in all of the measurements. Thus, maximum elasticity index could not be used. In the future, a study with the maximum elasticity index may improve the results and help to better set the optimal cut off values for better differentiation between benign and malignant inguinal LNs.

Conclusion

This prospective study shows that 2D-SWE provides a reproducible tool for multiparametric, noninvasive US assessment in inguinal LNs. The most reproducible way to measure 2D-shear wave elastography in inguinal LNs is a 3 mm circular ROI centered on the cortex of the LN in axial plane. Further studies, with larger populations with benign and malignant LNs, are needed to evaluate the cut-off values for SWE lymph node elasticity measurements.

Acknowledgments

Special thanks to Tuomas Selander who provided help with the statistical analysis.

Author Contributions

Formal analysis: Olli Lahtinen.

Funding acquisition: Olli Lahtinen.

Investigation: Olli Lahtinen, Mika Pulkkinen.

Methodology: Olli Lahtinen, Suvi Rautiainen.

Supervision: Ritva Vanninen, Suvi Rautiainen.

Writing – original draft: Olli Lahtinen.

Writing – review & editing: Olli Lahtinen, Reijo Sironen, Ritva Vanninen, Suvi Rautiainen.

References

1. Rautiainen S, Masarwah A, Sudah M, Sutela A, Pelkonen O, Joukainen S, et al. Axillary lymph node biopsy in newly diagnosed invasive breast cancer: comparative accuracy of fine-needle aspiration biopsy versus core-needle biopsy. Radiology. 2013 Oct; 269(1):54–60. https://doi.org/10.1148/radiol.13122637 PMID: 23771915
2. Choi JJ, Kang BJ, Kim SH, Lee JH, Jeong SH, Yim HW, et al. Role of Sonographic Elastography in the Differential Diagnosis of Axillary Lymph Nodes in Breast Cancer. J Ultrasound Med. 2011 Apr; 30 (4):429–36. https://doi.org/10.7863/jum.2011.30.4.429 PMID: 21460142
3. Alam F, Naito K, Horiguchi J, Fukuda H, Tachikake T, Ito K. Accuracy of sonographic elastography in the differential diagnosis of enlarged cervical lymph nodes: comparison with conventional B-mode sonography. AJR Am J Roentgenol. 2008 Aug; 191(2):604–10. https://doi.org/10.2214/AJR.07.3401 PMID: 18647939
4. Acu L, Oktar SÖ, Acu R, Yücel C, Cebeci S. Value of Ultrasound Elastography in the Differential Diagnosis of Cervical Lymph Nodes: A Comparative Study With B-mode and Color Doppler Sonography. J Ultrasound Med. 2016 Nov; 35(11):2491–2499. https://doi.org/10.7863/ultra.15.09019 PMID: 27794132

5. Gregorio N, Ebner F, Schwenter L, Fierdl TW, Deniz M, Látó K, et al. The role of preoperative ultrasound evaluation of inguinal lymph nodes in patients with vulvar malignancy. Gynecol Oncol. 2013 Oct; 131(1):113–7. https://doi.org/10.1016/j.ygyno.2013.07.103 PMID: 23932893

6. Krishna RP, Sistla SC, Smile R, Krishnan R. Sonography: an underutilized diagnostic tool in the assessment of metastatic groin nodes. J Clin Ultrasound. 2008 May; 36(4):212–7. https://doi.org/10.1002/jcu.20420 PMID: 17960822

7. Suh CH, Choi YJ, Baek JH, Lee JH. The diagnostic performance of shear wave elastography for malignant cervical lymph nodes: A systematic review and meta-analysis. Eur Radiol. 2017 Jan; 27(1):222–230. https://doi.org/10.1007/s00330-016-4378-3 PMID: 27147221

8. Białek EJ, Jakubowski W. Mistakes in ultrasound diagnosis of superficial lymph nodes. J Ultrason. 2017 Mar; 17(68):59–65. https://doi.org/10.15557/JoU.2017.0008 PMID: 28439430

9. Dudea SM, Botar-Jid C, Dumitriu D, Vasilescu D, Manole S, Lenghel ML. Differentiating benign from malignant superficial lymph nodes with sonoelastography. Med Ultrason. 2013 Jun; 15(2):132–9. https://doi.org/10.11152/mu.2013.2066.152.smd1cbj2 PMID: 23702503

10. Zhang F, Zhao X, Ji X, Han R, Li P, Du M. Diagnostic value of acoustic radiation force impulse imaging for assessing superficial lymph nodes: A diagnostic accuracy study. Medicine (Baltimore). 2017 Oct; 96 (43):e8125. https://doi.org/10.1097/MD.0000000000008125 PMID: 29068984

11. Chiorean L, Barr RG, Braden B, Jenssen C, Cui XW, Hocke M, et al. Transcutaneous Ultrasound: Elastographic Lymph Node Evaluation. Current Clinical Applications and Literature Review. Ultrasound Med Biol. 2016 Jan; 42(1):16–30. https://doi.org/10.1016/j.ultrasmedbio.2015.09.005 PMID: 26489365

12. Sigrist RMS, Liau J, Kaffas AE, Chammas MC, Willmann JK. Ultrasound Elastography: Review of Techniques and Clinical Applications. Theranostics. 2017 Mar 7; 7(5):1303–1329. https://doi.org/10.7150/thno.18650 PMID: 28435467

13. Garra BS. Elastography: history, principles, and technique comparison. Abdom Imaging. 2015 Apr; 40 (4):680–97. https://doi.org/10.1007/s00261-014-0305-8 PMID: 25637125

14. Tan S, Miao LY, Cui LG, Sun PF, Qian LX. Value of Shear Wave Elastography Versus Contrast-Enhanced Sonography for Differentiating Benign and Malignant Superficial Lymphadenopathy Unexplained by Conventional Sonography. J Ultrasound Med. 2017 Jan; 36(1):189–199. https://doi.org/10.7863/ultra.16.01014 PMID: 27925679

15. Youk JH, Son EJ, Kim JA, Gweon HM. Pre-operative Evaluation of Axillary Lymph Node Status in Patients with Suspected Breast Cancer Using Shear Wave. Ultrasound Med Biol. 2017 Aug; 43 (8):1581–1586. https://doi.org/10.1016/j.ultrasmedbio.2017.03.016 PMID: 28511961

16. Carlsen JF, Pedersen MR, Ewertsen C, Săftoiu A, Lönn L, Rafaelsen SR, et al. A comparative study of strain and shear-wave elastography in an elasticity phantom. AJR Am J Roentgenol. 2015 Mar; 204(3): W236–42. https://doi.org/10.2214/AJR.14.13076 PMID: 25714307

17. Lee HY, Lee JH, Shin JH, Kim SY, Shin HJ, Park JS, et al. Shear wave elastography using ultrasound: effects of anisotropy and stretch stress on a tissue phantom and *in vivo* reactive lymph nodes in the neck. Ultrasonography. 2017 Jan; 36(1):25–32. https://doi.org/10.14366/usg.16003 PMID: 27459989

18. Aubry S, Nueffer JP, Carrié M. Evaluation of the Effect of an Anisotropic Medium on Shear Wave Velocities of Intra-Muscular Gelatinous Inclusions. Ultrasound Med Biol. 2017 Jan; 43(1):301–308. https://doi.org/10.1016/j.ultrasmedbio.2016.09.006 PMID: 27742141

19. Barr RG, Zhang Z. Effects of precompression on elasticity imaging of the breast: development of a clinically useful semiquantitative method of precompression assessment. J Ultrasound Med. 2012 Jun; 31 (6):895–902. https://doi.org/10.7863/jum.2012.31.6.895 PMID: 22644686

20. Moon JH, Hwang JY, Park JS, Koh SH, Park SY. Impact of region of interest (ROI) size on the diagnostic performance of shear wave elastography in differentiating solid breast lesions. Acta Radiol. 2018 Jun; 59(6):657–663. https://doi.org/10.1177/0284185117732097 PMID: 28899126

21. Youk JH, Son EJ, Han K, Gweon HM, Kim JA. Performance of shear-wave elastography for breast masses using different region-of-interest (ROI) settings. Acta Radiol. 2018 Jul; 59(7):789–797. https://doi.org/10.1177/0284185117735562 PMID: 29058962

22. Ko KH, Jung HK, Kim SJ, Kim H, Yoon JH. Potential role of shear-wave ultrasound elastography for the differential diagnosis of breast non-mass lesions: preliminary report. Eur Radiol. 2014 Feb; 24(2):305–11. https://doi.org/10.1007/s00330-013-3034-4 PMID: 24081648

23. Azizi G, Keller JM, Mayo ML, Piper K, Puett D, Earp KM, et al. Shear Wave Elastography and Cervical Lymph Nodes: Predicting Malignancy. Ultrasound Med Biol. 2016 Jun; 42(6):1273–81. https://doi.org/10.1016/j.ultrasmedbio.2016.01.012 PMID: 26976785

24. Skerl K, Vinnicombe S, Giannotti E, Thomson K, Evans A. Influence of region of interest size and ultrasound lesion size on the performance of 2D shear wave elastography (SWE) in solid breast masses. Clin Radiol. 2015 Dec; 70(12):1421–7. https://doi.org/10.1016/j.crad.2015.08.010 PMID: 26455652

25. Blank MAB, Antaki JF. Breast Lesion Elastography Region of Interest Selection and Quantitative Heterogeneity: A Systematic Review and Meta-Analysis. Ultrasound Med Biol. 2017 Feb; 43(2):387–397. https://doi.org/10.1016/j.ultrasmedbio.2016.09.002 PMID: 27746010

26. Kawahara Y, Togawa Y, Yamamoto Y, Wakabayashi S, Matsue H, Kazuhiro I. Usefulness of 2-D shear wave elastography for the diagnosis of inguinal lymph node metastasis of malignant melanoma and squamous cell carcinoma. J Dermatol. 2020 Nov; 47(11):1312–1316. https://doi.org/10.1111/1346-8138.15545 PMID: 32794264

27. Li T, Li H, Xue J, Miao J, Kang C. Shear wave elastography combined with gray-scale ultrasound for predicting central lymph node metastasis of papillary thyroid carcinoma. Surg Oncol. 2021 Mar; 36:1–6. https://doi.org/10.1016/j.suronc.2020.11.004 PMID: 33271464

28. Seliger G, Chaoui K, Kunze C, Dridi Y, Jenderka KV, Wienke A, et al. Intra- and inter-observer variation and accuracy using different shear wave elastography methods to assess circumscribed objects–a phantom study. Med Ultrason. 2017 Nov 29; 19(4):357–365. https://doi.org/10.11152/mu-1080 PMID: 29197911

29. Mancini M, Salomone Megna A, Ragucci M, De Luca M, Marino Marsilia G, Nardone G, et al. Reproducibility of shear wave elastography (SWE) in patients with chronic liver disease. PLoS One. 2017 Oct 12; 12(10):e0185391. https://doi.org/10.1371/journal.pone.0185391 PMID: 29023554

30. Park JE, Choi YJ, Lee SS, Lee JH, Baek JH. Assessment of Measurement Repeatability and Reliability With Virtual Touch Tissue Quantification Imaging in Cervical Lymphadenopathy. J Ultrasound Med. 2016 May; 35(5):927–32. https://doi.org/10.7863/ultra.15.06067 PMID: 27022174

31. Seo M, Sohn YM. Differentiation of benign and metastatic axillary lymph nodes in breast cancer: additive value of shear wave elastography to B-mode ultrasound. Clin Imaging. 2018 Jul–Aug; 50:258–263. https://doi.org/10.1016/j.clinimag.2018.04.013 PMID: 29704810

32. Youk JH, Son EJ, Kim JA, Gweon HM. Pre-operative Evaluation of Axillary Lymph Node Status in Patients with Suspected Breast Cancer Using Shear Wave. Ultrasound Med Biol. 2017 Aug; 43(8):1581–1586. https://doi.org/10.1016/j.ultrasmedbio.2017.03.016 PMID: 28511961

33. Ben Z, Gao S, Wu W, Chen S, Fu S, Zhang J, et al. Clinical value of the VTIQ technology in the differential diagnosis of superficially enlarged lymph nodes. Acta Radiol. 2018 Jul; 59(7):836–844. https://doi.org/10.1177/0284185117732601 PMID: 28927297

34. Wang RY, Zhang YW, Gao ZM, Wang XM. Role of sonoelastography in assessment of axillary lymph nodes in breast cancer: a systematic review and meta-analysis. Clin Radiol. 2019 Dec 28. pii: S0009-9260(19)30674-9. https://doi.org/10.1016/j.crad.2019.11.016 PMID: 31892406

35. Jung WS, Kim JA, Son EJ, Youk JH, Park CS. Shear wave elastography in evaluation of cervical lymph node metastasis of papillary thyroid carcinoma: elasticity index as a prognostic implication. Ann Surg Oncol. 2015 Jan; 22(1):111–6. https://doi.org/10.1245/s10434-014-3627-4 PMID: 24740830

36. Solivetti FM, Elia F, Graceffa D, Di Carlo A. Ultrasound morphology of inguinal lymph nodes may not herald an associated pathology. J Exp Clin Cancer Res. 2012 Oct 18; 31:88. https://doi.org/10.1186/1756-9966-31-88 PMID: 23078807

37. Chen BB, Li J, Guan Y, Xiao WW, Zhao C, Lu TX, et al. The value of shear wave elastography in predicting for undiagnosed small cervical lymph node metastasis in nasopharyngeal carcinoma: A preliminary study. Eur J Radiol. 2018 Jun; 103:19–24. https://doi.org/10.1016/j.ejrad.2018.03.006 PMID: 29803380

38. Bae SJ, Park JT, Park AY, Youk JH, Lim JW, Lee HW, et al. *Ex Vivo* Shear-Wave Elastography of Axillary Lymph Nodes to Predict Nodal Metastasis in Patients with Primary Breast Cancer. J Breast Cancer. 2018 Jun; 21(2):190–196. https://doi.org/10.4048/jbc.2018.21.2.190 PMID: 29963115

III

Contrast-enhanced ultrasound: a new tool for imaging the superficial lymphatic vessels of the upper limb.

Lahtinen O, Vanninen R, Rautiainen S.
Eur Radiol Exp. 2022 Apr 12;6(1):18. doi: 10.1186/s41747-022-00270-4

Lahtinen et al. European Radiology Experimental (2022) 6:18
https://doi.org/10.1186/s41747-022-00270-4

European Radiology Experimental

ORIGINAL ARTICLE Open Access

Contrast-enhanced ultrasound: a new tool for imaging the superficial lymphatic vessels of the upper limb

Olli Lahtinen[1,2*], Ritva Vanninen[1,2], Suvi Rautiainen[1]

Abstract

Background: Despite the new lymphatic imaging methods, there is still a need for a straightforward method of detecting lymphatic abnormalities. Our goal was to investigate the feasibility of applying a contrast enhanced ultrasound (CEUS) procedure as a new approach for visualising the superficial lymphatic vessels of the upper limb.

Methods: Thirty healthy volunteers were examined with CEUS after bilateral intradermal injection of Sonazoid® contrast agent in distal antebrachium. We registered factors affecting intradermal injections, imaging of the superficial lymphatic vessels and the enhancement time of contrast agent reaching the levels of elbow and axilla.

Results: CEUS imaging of superficial lymphatic vessels was successful in 59 of 60 upper limbs (98.3%). Median [interquartile ranges] enhancement times of contrast agent to reach the elbow (right 18 s [11–25], left 15 s [12–25]) and axilla (right 77 s [33–118], left 66 s [42–115]) were equally fast. Successful intradermal injections were found to result in two types of contrast enhancement (strong or moderate), while the enhancement time depended on the type of the successful injection. No major differences in enhancement times were observed related to sex, body mass index, age, or side of the arm.

Conclusions: The superficial lymphatic pathways of the upper limb can be visualised with CEUS imaging. Since enhancement time is dependent on the success of intradermal injections, one must pay attention to the injection technique. Further studies are needed to evaluate the method in patients with lymphatic function disorders such as breast cancer therapy related lymphoedema.

Keywords: Contrast media, Injections (intradermal), Lymphatic vessels, Sonazoid, Ultrasonography

Key points

- Superficial lymphatic vessels of the upper limbs can be visualised with contrast-enhanced ultrasound.
- Successful intradermal Sonazoid® injections were followed by fast lymphatic drainage.
- Contrast enhancement in the axillary area was detected with a median time of 75 s after the injection.

* Correspondence: olli.lahtinen@kuh.fi
[1]Diagnostic Imaging Centre, Department of Clinical Radiology, Kuopio University Hospital, Kuopio, Finland
[2]Institute of Clinical Medicine, Unit of Radiology, University of Eastern Finland, Kuopio, Finland

Background

Despite the important role of the lymphatic system in human health and diseases, this system is still poorly understood. After the pioneering work of Mascagni [1] and Sappey [2] using a mercury injection method, recent studies with radiopaque lead oxide mixtures in cadavers have led to a re-evaluation of the anatomical details of the lymphatic pathways [3, 4]. Similar to the situation with the vascular system, the anatomy of the lymphatic system consists of a complex network of small vessels. The lymphatic network is composed of the initial lymphatics or lymphatic capillaries, precollectors and collecting vessels [5–7]. The lymphatic capillaries are blind-ended vessels containing a single layer of endothelial

cells. The diameter of the initial lymphatic vessels typically o ranges from 20 to 70 μm. Unlike the lymphatic capillaries, precollectors and collecting vessels contain valves to prevent a backflow of lymph fluid. The walls of collecting vessels have smooth muscle cells and collagen fibres that maintain efficient lymph drainage [7]. However, unlike the vascular system the lymph drainage through lymphatic vessels is not propelled by pulsatile blood circulation.

Traditionally, lymphoscintigraphy has been the method of choice for diagnosing lymphatic disorders such as lymphoedema [8]. Recently, new lymphatic imaging methods have developed such as magnetic resonance (MR) lymphangiography and indocyanine green (ICG) fluorescence imaging [9–11]. However, all these imaging techniques are either time consuming, need to expose the patient to radioactive tracer or are not cost effective on a large scale. Therefore, there is a need for a quick, easy and readily available tool with which to assess common lymphatic abnormalities such as secondary lymphoedema after lymphadenectomies of breast cancer surgery [12–14].

Ultrasound (US) might possess some of these advantages since the contrast agent used for contrast-enhanced ultrasound (CEUS) is a water-based solution like ICG which is known to travel faster in lymphatics than is the case with non-water based solutions. Ultrasound has been applied in imaging of the lymphatic system as is in the case of evaluation of lymph nodes (LN) [15]. In breast cancer-related lymphoedema, US can assess the response to physical therapy [16]. Recently, ultra-high frequency US has been applied as an intraoperative planning tool in lymphatic microsurgery [17]. Additionally, the sentinel lymph nodes (SLNs) and related afferent lymphatic vessels have been successfully visualised with CEUS in breast and vulvar cancers [18–22].

CEUS is one of the new US approaches using microbubbles such as those of perflubutane (Sonazoid®, GE Healthcare, Oslo, Norway) used in this study. Perflubutane is a relatively new, second generation US contrast agent with some additional characteristics over the more commonly used sulfur hexafluoride (Sonovue®, Bracco, Milan, Italy) such as its affinity for reticuloendothelial cells [23, 24]. Like sulfur hexafluoride, it is well tolerated and has no major contraindications or severe known adverse effects when administered by intravenous or subdermal injections [25, 26].

In the present study, our aim was to investigate the feasibility of applying CEUS to achieve a fast visualisation of the superficial lymphatic vessels of the upper limbs in healthy volunteers. In addition, we registered possible confounding factors related to the intradermal injection technique to be applied with the microbubble contrast agent.

Methods

Patients and study design

Approvals from our institutional review board, local ethics committee and Finnish Medicines Agency (FIMEA) were obtained for this prospective single-centre study and all of the participants provided written informed consent.

Thirty healthy volunteers were recruited to the study. Both upper limbs were independently evaluated in each subject. Exclusion criteria were (1) egg protein allergy; (2) pregnancy; (3) breastfeeding; (4) prior axillary lymphadenectomy. To allow us to evaluate age dependence, the volunteers were further divided into two groups: a younger group of persons less than 40 years of age and an older group equal or greater than 40 years of age. When studying the possible effect of body mass index (BMI), the volunteers were divided into two groups: subjects with BMI < 25 and subjects with BMI > 25.

Upper limb US and CEUS

The US procedures were performed by a single radiologist with 6 years of experience with CEUS. A Logiq E9^{TM} US-device (General Electric Healthcare, Chicago, USA) with a broad spectrum ML6-15 (6–15 MHz) linear array transducer. Participants were examined in supine position relaxed with no muscle stress. The applied CEUS procedure was performed similar to US studies for the identification of SLNs [18, 20].

Microbubble contrast agent injection

We hypothesised that the required enhancement times for the evaluation of the whole upper limb would be longer compared to those required in SLN studies. Therefore, the contrast agent Sonazoid® was selected for the study as potentially being more durable compared to the more commonly used Sonovue®. The contrast agent powder, Sonazoid® was mixed with 2.0 mL of sterile saline producing a microbubble solution with a mean particle diameter of 2.6 μm. The Sonazoid® particles were injected intradermally with a 1.0-mL syringe and a 24-gauge needle laterally on the volar side of the distal antebrachium (Fig. 1). The injection was made with a low angle, typically less than 5° from the skin. The tip of the needle was positioned so that it could be seen through the thin layer of epidermis. Injection was made as a fast bolus. However, the injection rate depended on the resistance from the tissues. The timer was started after the whole volume was injected. The injected volume of the contrast agent solution was 0.2-mL for the whole study population. If an enhancing lymphatic vessel was not detected after injection or only minimal enhancement was seen near the injection site in the CEUS image, the injection site was gently massaged for approximately 10 s. The injection was repeated up to three times at a nearby skin site within 1 cm from the first injection site if no

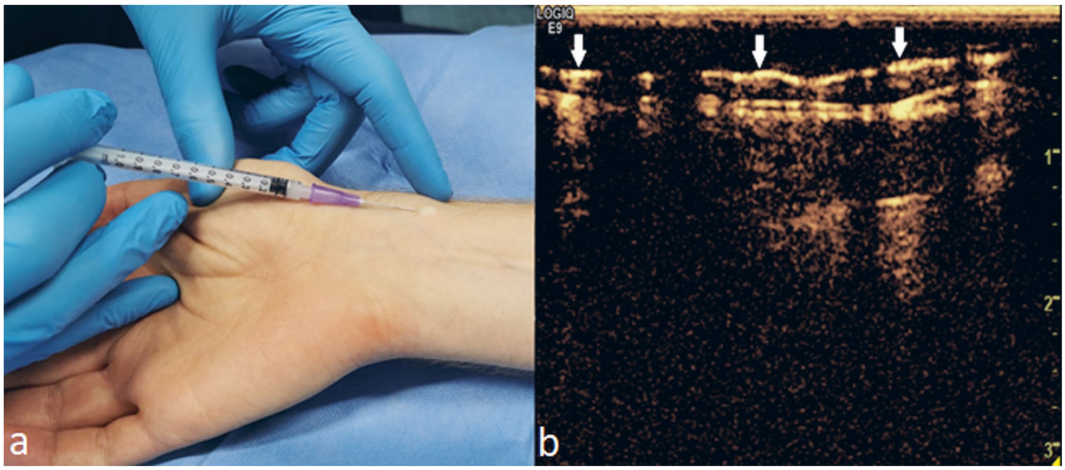

Fig. 1 **a** Injection site in the distal antebrachium and intradermal injection technique. A small blister-like spot beneath the skin in addition to resistance to injection are probable indicators of a successful injection. Contrast agent (Sonazoid®, white arrows) can be seen in the superficial lymphatic vessel in **b**

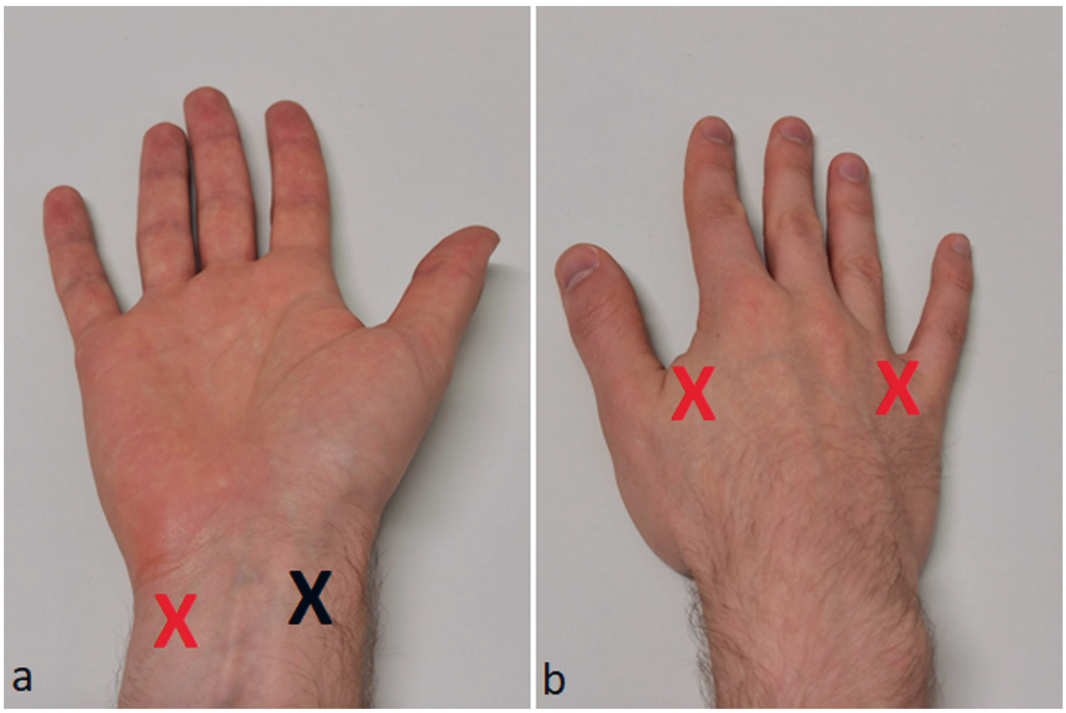

Fig. 2 The black X in **a** marks the primary injection site in the distal antebrachium. Additional injection sites are marked with a red X in **a** and **b**

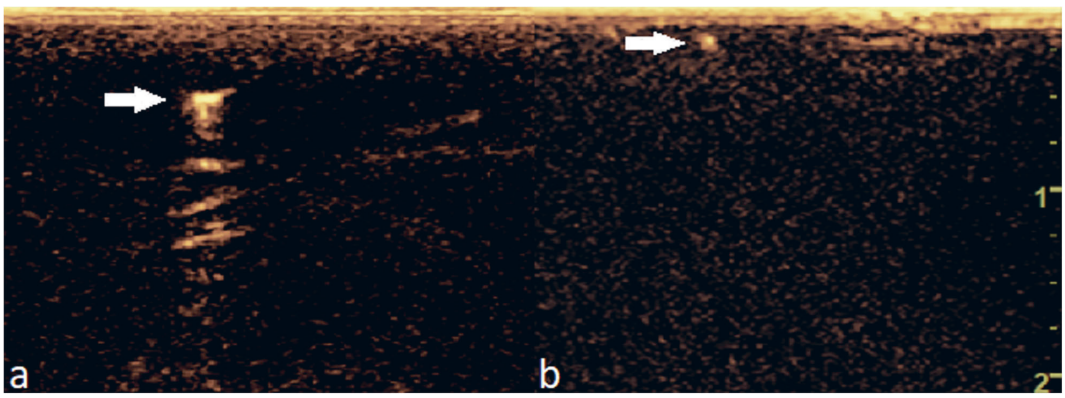

Fig. 3 The CEUS image in **a** correlates with a type A (strong enhancement) in the superficial lymphatic vessel, whereas the CEUS image in **b** corresponds to type B (moderate enhancement), which is clearly seen from the background but is clearly more faint than type A. White arrows mark the enhancing superficial lymphatic vessels

additional enhancement was seen after the massage. In addition, three other injection sites (Fig. 2) similar to those used by Suami et al. [11] were tested in each upper limb. Injected volumes of 0.1, 0.2, and 0.3 mL were tested in five volunteers after a successful injection to the primary site. Additional injections were made when no residual enhancement was seen from the previous injections. Continuous flash was used before the next injection to help to destroy the microbubbles. Thus, the additional test volumes in the five volunteers were used to test: (1) the feasibility with a lower dose; and (2) whether a stronger enhancement type would follow with the larger dose. Besides feasibility assessment, no detailed evaluation of the different enhancement patterns or times from other injection sites was performed.

The flow of contrast agent was followed using a standard low (< 0.10) mechanical index, as recommended by the manufacturer of Sonazoid®. The CEUS program allows the user to distinguish the echoes emitted by the microbubbles from tissue background and optimise the visualisation of the contrast agent in the US image. The enhancement time from contrast agent injection to the detection of the contrast agent in antecubital fossa and axilla was registered and major lymphatic pathways and the number of enhanced lymphatic vessels were documented. The strength of the enhancement was divided into two categories by the observer, depending on the visual appearance of the contrast enhancement. Category A corresponded to strong enhancement in the superficial lymphatic vessel while category B referred to moderate enhancement (Fig. 3).

Follow-up

Participants were followed up for any possible acute onset of adverse effects for one hour after the administration of the contrast agent. In addition, the participants were told to contact the main investigator should any late onset symptoms develop within 72 h after the contrast agent injection.

Statistical analysis

Variables are reported as median and interquartile range. Statistical analysis was performed with SPSS (Version 26.0, SPSS, Chicago, IL, USA). The Mann-Whitney *U* test was used to calculate statistical significance between the different variables (dichotomised age, sex, BMI, strength of the enhancement). Wilcoxon-related samples test was used to calculate inter-side differences between right and left upper limbs of the appearance time of the contrast agent in antecubital fossa and axilla. Values of p lower than 0.05 were considered significant.

Results

Thirty healthy volunteers (16 males and 14 females, aged 41 ± 11.2 years, mean ± standard deviation, range 27–69 years) were recruited between October 2020 and January 2021. Both upper limbs were evaluated in each subject. The BMI was 25.8 ± 4.8 (mean ± standard deviation, range 19.2–39.3). The right arm was dominant in 29 persons.

Intradermal contrast agent injections were successful in 59/60 (98.3%) of the upper limbs evaluated. A mean of 3.1 injections were needed to visualise the lymphatic collector vessels from upper arms combined. A clear indicator of a failed injection was the lack of resistance during the administration of contrast agent. The number of enhanced lymphatic collectors varied between 1 and 4 with a mean of 1.5 vessels per upper limb that were

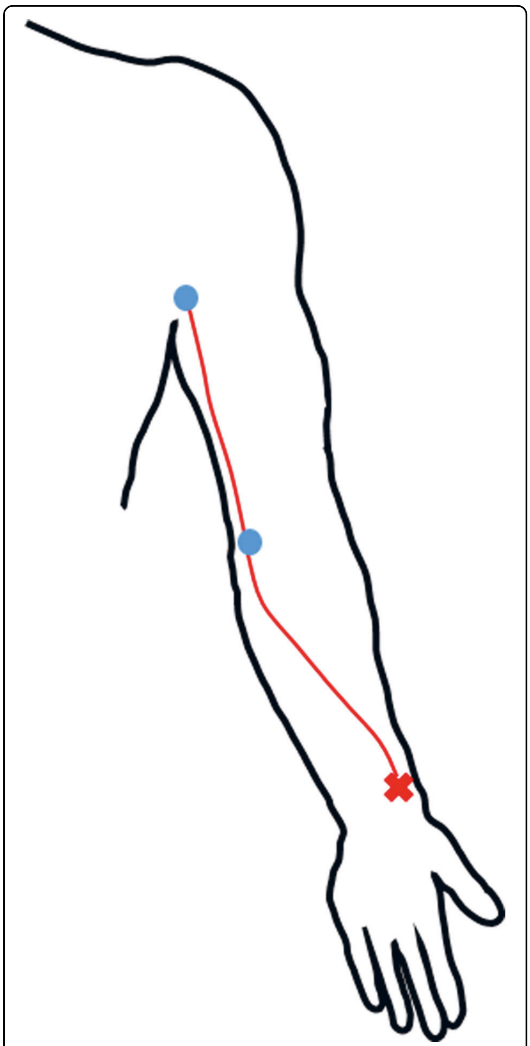

Fig. 4 The red X marks the injection site of the contrast agent. Blue dots demonstrate the location of the enhancing lymph nodes in the antecubital fossa and axilla. The red line illustrates roughly the enhancing superficial lymphatic route seen in all of the successful injections

located in parallel. In all volunteers, the contrast agent followed the same lymphatic pathway (Fig. 4).

The enhancement time of the contrast agent depended on the success of intradermal injections. Typically, a successful intradermal injection produced a blister-like spot with a diameter of about 5 mm. None or only minimal visualisation of the lymphatics was registered if the injection of contrast agent had occurred subcutaneously. Successful intradermal injections resulted into two types of contrast enhancement. In type A (n = 34), a high concentration enhancement and a fast enhancement time of contrast agent in lymphatics were observed. Type B (n = 25) enhancements demonstrated less noticeable visualisation of the lymphatics with a longer enhancement time in antecubital fossa and axillar area (Fig. 5). In some injections resulting in type B enhancements, the contrast agent was found to have spread into a larger area beneath the skin surface compared to the typical intradermal injections producing a blister-like spot. Thus, type A enhancement pattern could be characterised as being associated with a successful intradermal injection, and a type B enhancement pattern as related to a partially successful intradermal injection. Table 1 summarises the enhancement times of the contrast agent.

There was no statistically significant difference in median enhancement times to reach right antecubital fossa (18 s) and left antecubital fossa (15 s) (p = 0.863) or axilla (77 s and 66 s, respectively) (p= 0.581). BMI or younger *versus* older age of volunteers had no significant effect on enhancement times. A slight difference was found between genders in the enhancement time in the left antecubital fossa, where females had 28% faster mean enhancement time compared to males (females 18 s *versus* males 23 s, p = 0.029). More detailed information is presented in Table 2.

Additional test volumes were used in five volunteers. These demonstrated that in addition to a standard test dose of 0.2 mL, lymphatic vessels could also be visualised with doses of 0.1 mL and 0.3 mL. Furthermore, injections of contrast agent into one additional volar site and into two sites in dorsal aspects on back of the hand were also feasible to visualise the superficial lymphatic routes. The lymph drainage from these additional sites followed the same pathway as with the main injection site on the volar aspect of the distal antebrachium. The alternative lymphatic pathways passing on the lateral aspect of the upper arm following the cephalic vein and connecting straight to the supraclavicular lymph nodes were not visualised in this study. In two subjects, an enhancing lymph node following the main pathway was found in the medial aspect of the elbow (Fig. 4).

No adverse effects were reported related to the intradermal injections or CEUS microbubble contrast agent.

Discussion

The present study demonstrates that the CEUS method can be used to visualise the anatomy and function of the superficial lymphatics in the upper limbs, offering a feasible radiological tool for the assessment of diseases and conditions affecting the normal lymphatic function such as in patients suffering from problems after breast

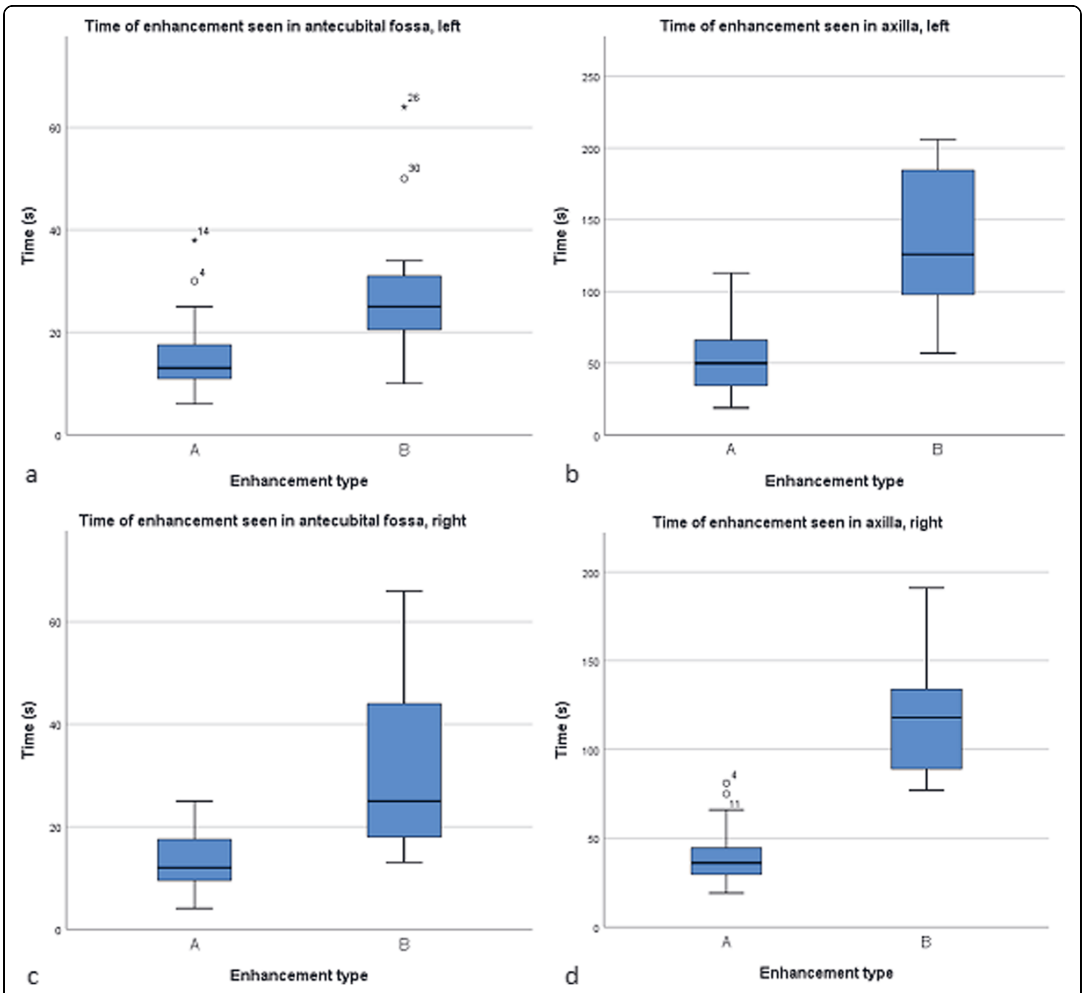

Fig. 5 Enhancement times in antecubital fossa (**a**, **c**) and axilla (**b**, **d**) displayed variance according to the two US enhancement categories (type A = strong, type B = moderate) in the right and left arms

Table 1 Enhancement times in the antecubital fossa and axilla after intradermal injections

Assessment site	Enhancement time (s) Median (interquartile range)
Right antecubital fossa	18 (11–25)
Left antecubital fossa	15 (12–25)
Right axilla	77 (33–118)
Left axilla	66 (42–115)

cancer therapy. Visualisation of lymphatic pathways agrees with previous studies using microbubble contrast agent imaging for the sentinel lymph nodes and animal studies with cutaneous melanoma [18, 20, 22, 27]. The anatomical information on the lymphatic pathways is in agreement with findings from traditional lymphoscintigraphy and MR lymphangiography [8, 28].

CEUS microbubble technology

Previously, studies with CEUS have been mainly limited to the imaging of the SLNs in breast cancer and vulvar cancer following intradermal injection of contrast agent [22, 18–20]. To the best of our knowledge, the current

Table 2 Effect of different parameters on the enhancement time after successful intradermal injections

Parameter		Number	Enhancement time (s) Median (interquartile range)			
			Antecubital fossa		Axilla	
			Right	Left	Right	Left
Sex	Males	16	15 (10–31)	20 (13–25)	57 (31–120)	98 (52–133)
	Females	14	19 (12–25)	12 (9–21)	81 (42–116)	49 (31–96)
	p		0.455	0.029	0.583	0.070
Age (years)	< 40	18	18 (11–34)	19 (11–29)	77 (33–123)	92 (49–147)
	> 40	12	18 (11–25)	15 (12–24)	77 (32–109)	50 (37–95)
	p		0.929	0.484	0.825	0.086
Body mass index	< 25	16	19 (13–33)	17 (11–23)	80 (40–123)	69 (39–133)
	> 25	14	14 (11–25)	14 (12–35)	57 (28–99)	63 (44–112)
	p		0.256	0.546	0.111	0.884
		Right+ left				
Enhancement type	A	15 + 19 = 34	12 (9–20)	13 (10–19)	36 (29–49)	50 (32–70)
	B	14 + 11 = 25	25 (18–46)	25 (20–34)	118 (88–134)	126 (95–191)
	p		0.001	0.007	0.000	0.000

Enhancement type A indicates a successful intradermal injection with strong visual enhancement, whereas type B refers to a partially successful injection with moderate enhancement. Enhancement times in the table represent median enhancement times at the antecubital fossa and axilla

study is the first to explore the potential of CEUS as a tool for mapping superficial lymphatics in humans. Although several other means for visualising and diagnosing possible lymphatic problems such as ICG and MR lymphangiography are nowadays available [9–11], there is a lack of a quick and cost-effective screening tool.

This study demonstrated in healthy volunteers that the CEUS procedure can be technically successful in 98.3% of upper limbs for visualising the pathways of the superficial lymphatics. The method proved to be quick since contrast agent enhancement in the axillar area was detected with a median time of 75 s after injection. These enhancement times are much faster than those necessary with ICG, which are about 30 min in the antecubital fossa [29]. The early enhancement time is evidently due to the small particle size of the microbubbles and the water-based solution of contrast agent. Due to the fast enhancement times, the contrast agent was seen in the superficial lymphatic vessels for a few minutes after the initial enhancement. Thus, these results could probably be achieved with the more commonly used contrast agent Sonovue® since it shares same kind of qualities as the Sonazoid® and the lifespan of the microbubbles exceeds the enhancement times shown in this study. Furthermore, it has been previously successfully used in the SLN studies to visualise lymphatic vessels [18–20, 30].

Factors related to intradermal injections

The intradermal injection technique is a procedure with a learning curve. In our study, a mean of 3.1 injections were needed in order to visualise the lymphatic collector vessels of both upper limbs. Successful intradermal injections were followed by fast lymphatic drainage and good visualisation of the contrast agent in lymphatic vessels (Table 2). However, successful injections could also result in slight-to-moderate visualisation of the lymphatics and longer enhancement times in elbow and axillar area. In some of the slower type B enhancements, the contrast agent was observed to be spreading into a larger area beneath the skin surface whereas more typically, intradermal injections produced a blister-like spot with a diameter of about 5 mm. Thus, the type B enhancements might be related to injections partly into dermis and partly into the upper subcutis and these injections could thus be defined as partially successful. In contrast, an indicator of a failed injection was the lack of resistance during the administration of contrast agent. If no enhancement was detected in the lymphatic vessels, it was evident that the injection had been totally subcutaneous.

In both type A (strong) and type B (moderate) enhancement patterns, the route of contrast agent was found to be identical and corresponded to the major pathways detailed in previous cadaver and ICG studies [7, 11]. Even the partially successful injections could thus also provide valuable information on the anatomy and function of the lymphatic drainage. The enhancement time results were registered from the first successful injection regardless of its enhancement type, leading to a relatively large variation in the enhancement times in our relatively small study population.

In our study, the alternative lymphatic pathways passing on the lateral aspect of the upper arm following the cephalic vein and connecting straight to supraclavicular lymph nodes were not visualised. Injections from secondary peripheral injection sites (Fig. 2), similar to those used by Suami et al. [11], only produced findings that the ipsilateral axilla drainage pathway was the major pathway of contrast agent; results are in agreement with those obtained with ICG fluorescence lymphography.

Initial findings in healthy volunteers

By dividing our group of volunteers according to gender, BMI, or into subjects young or older ages, we attempted to assess possible individual factors affecting the enhancement time of the contrast agent. If one considers gender-related differences, females displayed a 28% faster mean enhancement time than males in left antecubital fossa (18 s *versus* 23 s) with a slight statistically significant association. However, no clear reason for this phenomenon was identified and it might be affected by variables not included in the study such as arm length. Participants lay on the examination table and no muscle stress was induced voluntary that could affect the result. As massaging the injection site in the SLN studies to expedite the lymphatic flow [18, 20], the muscle contractions increase the lymph flow in skeletal muscle [6] and involuntary upper limb movement could potentially result in faster enhancement time. Otherwise no statistical differences were detected.

This microbubble contrast agent method proved to be feasible in mapping the superficial lymphatics of the upper limbs in healthy volunteers. The method needs to be further tested in patients with lymphatic disorders such as breast cancer-related lymphoedema associated with an abnormal distribution of lymph fluid into dermis. Studies planned for the future should help us to fully understand differences in CEUS lymphatic imaging between the upper limbs of healthy volunteers and patients with lymphoedema. Moreover, since lymphatic anatomy after breast cancer surgery may totally differ from normal lymphatic anatomy [31], benefits, and limitations of the CEUS for imaging the routes of abnormal lymphatic drainage in sites with dermal backflow need to be investigated. Furthermore, lymphatic CEUS studies in patients with breast cancer-related lymphoedema are therefore warranted since dermal backflow is considered as the most reliable indicator for lymphoedema [32] and US devices are widely available in healthcare units.

Study limitations

The present study has several limitations. Enhancement times were registered quantitatively, but the division into two different enhancement types was done subjectively as whether the intradermal injection was successful, leading to a type A (strong) enhancement or partially successful leading to a relatively large number of type B (moderate) enhancements. Classification into these two types was subjective although the difference could be seen on the live display. The use of time intensity curve analysis, not available for this study, could provide more quantitative results of these types in the future.

Another limitation is the lack of multiple observers, also adding subjectivity to our results. However, a similar injection technique has been used in SLN studies and has shown to be reproducible both in patients with breast cancer and vulvar cancer [20, 21]. Since enhancement time is dependent on the success of intradermal injections, the injection technique demands special care to avoid unsuccessful injection. A reproducible injection technique is crucial if one is to differentiate real lymphatic disorders from injection-induced effects. Further studies investigating the CEUS technique in the longer range of the whole upper limb are warranted to fully clarify the differences between normal and abnormal lymphatic anatomy.

Conclusions

From this preliminary study, we conclude that the CEUS method following intradermal injections was able to identify the superficial lymphatic pathways in the upper arms of healthy volunteers. CEUS represents a potential minimally invasive tool with which to assess the kinetics of lymph fluid and allow the imaging of abnormal lymphatic anatomy.

Abbreviations

BMI: Body mass index; CEUS: Contrast-enhanced ultrasound; ICG: Indocyanine green; MR: Magnetic resonance; SLN: Sentinel lymph node; US: Ultrasound

Authors' contributions

OL was the main investigator. He analysed, interpreted the data, and was the writer of the manuscript. RV and SR contributed to writing of the manuscript. All authors read and approved the final manuscript.

Funding

This study has received funding from the Paavo Koistinen foundation (grant number 20200021) and Kuopio University Hospital Science Foundation (grant).

Availability of data and materials

The datasets used and/or analysed during the current study are available from the corresponding author on reasonable request.

Declarations

Ethics approval and consent to participate

Approvals from our institutional review board, local ethics committee (Kuopio University Hospital) and Finnish Medicines Agency (FIMEA) were obtained for this prospective single-center study and all of the participants provided written informed consent.

Consent for publication

All the participants in the study have given written consent to use the data collected in the study as a part of the manuscript.

Competing interests
The authors declare that they have no competing interests.

Received: 17 December 2021 Accepted: 9 March 2022
Published online: 12 April 2022

References

1. Sappey PC (1874) Anatomie, physiologie, pathologie de vaisseaux lymphatiques. Adrien Delahaye, Paris
2. Mascagni P (1787) Vasorum lymphaticorum corporis humani. Historia & iconographia. P. Carli Edit, Senis
3. Suami H, Taylor GI, Wei-Ren P (2007) The lymphatic territories of the upper limb: anatomical study and clinical implications. Plast Reconstr Surg 119: 1813–1822. https://doi.org/10.1097/01.prs.0000246516.64780.61
4. Wei-Ren P, Suami H, Taylor GI (2008) Lymphatic drainage of the superficial tissues of the head and neck: anatomical study and clinical implications. Plast Reconstr Surg 121:1614–1624. https://doi.org/10.1097/PRS.0b013e31816aa072
5. Hsu M, Itkin M (2016) Lymphatic anatomy. Tech Vasc Interv Radiol 19:247–254. https://doi.org/10.1053/j.tvir.2016.10.003
6. Breslin J, Yang Y, Scallan J, Sweat RS, Adderley SP, Murfee WL (2018) Lymphatic vessel network structure and physiology. Compr Physiol 9:207–299. https://doi.org/10.1002/cphy.c180015
7. Suami H, Scaglioni M (2018) Anatomy of the lymphatic system and the lymphosome concept with reference to lymphedema. Semin Plast Surg 32: 5–11. https://doi.org/10.1055/s-0038-1635118
8. Szuba A, Shin W, Strauss H, Rockson S (2003) The third circulation: radionuclide lymphoscintigraphy in the evaluation of lymphedema. J Nucl Med 44:43–57
9. Dori Y (2016) Novel lymphatic imaging techniques. Tech Vasc Interv Radiol 19:255–261. https://doi.org/10.1053/j.tvir.2016.10.002
10. Notohamiprodjo M, Weiss M, Baumeister R et al (2012) MR lymphangiography at 3.0 T: correlation with lymphoscintigraphy. Radiology 264:78–87. https://doi.org/10.1148/radiol.12110229
11. Suami H, Heydon-White A, Mackie H, Czerniec S, Koelmeyer L, Boyages J (2019) A new indocyanine green fluorescence lymphography protocol for identification of the lymphatic drainage pathway for patients with breast cancer-related lymphedema. BMC Cancer 19:985. https://doi.org/10.1186/s12885-019-6192-1
12. Gillespie T, Sayegh H, Brunelle C, Daniell K, Taghian A (2018) Breast cancer-related lymphedema: risk factors, precautionary measures, and treatments. Gland Surg 7:379–403. https://doi.org/10.21037/gs.2017.11.04
13. DiSipio T, Rye S, Newman B, Hayes S (2013) Incidence of unilateral arm lymphoedema after breast cancer: a systematic review and meta-analysis. Lancet Oncol 14:500–515. https://doi.org/10.1016/S1470-2045(13)70076-7
14. Zou L, Liu F, Shen P, et al (2018) The incidence and risk factors of related lymphedema for breast cancer survivors post-operation: a 2-year follow-up prospective cohort study. Breast Cancer 25:309–314. https://doi.org/10.1007/s12282-018-0830-3
15. Dudea S, Lenghel M, Botar-Jid C, Vasilescu D, Duma M (2012) Ultrasonography of superficial lymph nodes: benign vs. malignant. Med Ultrason 14:294–306
16. Jeon Y, Beom J, Ahn S, Bok S (2017) Ultrasonographic evaluation of breast cancer-related lymphedema. J Vis Exp:54996. https://doi.org/10.3791/54996
17. Hayashi A, Visconti G, Yamamoto T, et al (2018) Intraoperative imaging of lymphatic vessel using ultra high-frequency ultrasound. J Plast Reconstr Aesthet Surg 71:778–780. https://doi.org/10.1016/j.bjps.2018.01.013
18. Sever A, Broillet A, Schneider M, et al (2010) Dynamic visualization of lymphatic channels and sentinel lymph nodes using intradermal microbubbles and contrast-enhanced ultrasound in a swine model and patients with breast cancer. J Ultrasound Med 29:1699–1704. https://doi.org/10.7863/jum.2010.29.12.1699
19. Sever A, Mills P, Jones S et al (2011) Preoperative sentinel node identification with ultrasound using microbubbles in patients with breast cancer. AJR Am J Roentgenol 196:251–256. https://doi.org/10.2214/AJR.10.4865
20. Lahtinen O, Eloranta M, Anttila M, et al (2018) Preoperative sentinel lymph node localization in vulvar cancer: preliminary experience with inguinal intradermal contrast-enhanced ultrasound. Eur Radiol 28:2089–2095. https://doi.org/10.1007/s00330-017-5155-7
21. Moody A, Bull J, Culpan A-M et al (2017) Preoperative sentinel lymph node identification, biopsy and localisation using contrast enhanced ultrasound (CEUS) in patients with breast cancer: a systematic review and meta-analysis. Clin Radiol 72:959–971. https://doi.org/10.1016/j.crad.2017.06.121
22. Wang Y, Zhou W, Li C, et al (2017) Variation of sentinel lymphatic channels (SLCs) and sentinel lymph nodes (SLNs) assessed by contrast-enhanced ultrasound (CEUS) in breast cancer patients. World J Surg Oncol 15:127. https://doi.org/10.1186/s12957-017-1195-3
23. Cheu Y, Liang J, Wang S et al (2019) Safety of perfluorobutane (Sonazoid) in characterizing focal liver lesions. J Med Ultrasound 27:81–85. https://doi.org/10.4103/JMU.JMU_44_19
24. Machado P, Stanczak M, Liu J et al (2018) Subdermal ultrasound contrast agent injection for sentinel lymph node identification: an analysis of safety and contrast agent dose in healthy volunteers. J Ultrasound Med 37:1611–1620. https://doi.org/10.1002/jum.14502
25. Sontum P (2008) Physicochemical characteristics of Sonazoid™, a new contrast agent for ultrasound imaging. Ultrasound Med Biol 34:824–833. https://doi.org/10.1016/j.ultrasmedbio.2007.11.006
26. Bertelsen C, King K, Swanson M, Duddalwar V, Pepper J-P (2019) Contrast-enhanced ultrasound with perflubutane for sentinel lymph node mapping in cutaneous melanoma: a pilot study. Laryngoscope 129:1117–1122. https://doi.org/10.1002/lary.27397
27. Goldberg B, Merton D, Liu J-B, Murphy G, Forsberg F (2005) Contrast-enhanced sonographic imaging of lymphatic channels and sentinel lymph nodes. J Ultrasound Med 24:953–965. https://doi.org/10.7863/jum.2005.24.7.953
28. Bae J, Yoo R, Choi S et al (2018) Evaluation of lymphedema in upper extremities by MR lymphangiography: comparison with lymphoscintigraphy. Magn Reson Imaging 49:63–70. https://doi.org/10.1016/j.mri.2017.12.024
29. Farias-Cisneros E, Chilton P, Palazzo M et al (2019) Infrared imaging of lymphatic function in the upper extremity of normal controls and hand transplant recipients via subcutaneous indocyanine green injection. SAGE Open Med 7:2050312119862670. https://doi.org/10.1177/2050312119862670
30. Rautiainen S, Sudah M, Joukainen S, Sironen R, Vanninen R, Sutela A (2015) Contrast-enhanced ultrasound -guided axillary lymph node core biopsy: Diagnostic accuracy in preoperative staging of invasive breast cancer. Eur J Radiol 84:2130–2136. https://doi.org/10.1016/j.ejrad.2015.08.006
31. Suami H, Koelmeyer L, Mackie H, Boyages J (2018) Patterns of lymphatic drainage after axillary node dissection impact arm lymphoedema severity: a review of animal and clinical imaging studies. Surg Oncol 27:743–750. https://doi.org/10.1016/j.suronc.2018.10.006
32. Akita S, Nakamura R, Yamamoto N, et al (2016) Early detection of lymphatic disorder and treatment for lymphedema following breast cancer. Plast Reconstr Surg 138:192e–202e. https://doi.org/10.1097/PRS.0000000000002337

Publisher's Note

OLLI LAHTINEN

The aim of this thesis was to study new ultrasound (US) techniques in the assessment of the lymphatic system. More precisely, to assess the feasibility of contrast-enhanced ultrasound (CEUS) as a sentinel lymph node procedure in patients with vulvar cancer, to evaluate the reproducibility and to define the optimal region of interest for US elastography in inguinal lymph nodes (LNs) and to investigate the suitability of CEUS for visualizing superficial lymphatic vessels. In conclusion, new US techniques provide added value in the assessment of inguinal LNs and superficial lymphatic vessels.

UNIVERSITY OF
EASTERN FINLAND

uef.fi

**PUBLICATIONS OF
THE UNIVERSITY OF EASTERN FINLAND**
Dissertations in Health Sciences

ISBN 978-952-61-5086-4
ISSN 1798-5706